Republic of Iraq
Ministry of Higher Education
and Scientific Research
University of Babylon
College of Engineering
Civil Engineering Department

A Comparative Study of the Structural Performance Between Steel and Glass Fiber Reinforced Polymer Bars for Reinforced Concrete Elements.

A Thesis
Submitted to the College of Engineering at University of Babylon
inPartial Fulfillment of the Requirements for the Degree of Master science in Engineering/ Civil Engineering /Structures

By

Zahraa Luay Azeez Shubbar

Supervised by

Prof. Dr. Haitham H. Muteb Al-Daami

2023A.D **1444 A.H**

بِسْمِ اللَّهِ الرَّحْمَٰنِ الرَّحِيمِ

وَأَنْ لَيْسَ لِلْإِنسَانِ إِلَّا مَا سَعَىٰ ﴿٣٩﴾

وَأَنَّ سَعْيَهُ سَوْفَ يُرَىٰ ﴿٤٠﴾

ثُمَّ يُجْزَاهُ الْجَزَاءَ الْأَوْفَىٰ ﴿٤١﴾

(صدق الله العلي العظيم)

سورة النجم - الايات (٣٩-٤١)

Dedication

On behalf of the times that I faltered and then upraised...

On behalf of the times that I bewildered and then perceived...

On behalf of the calls Yaa Zahraa when be at one's wit's end…

On behalf of my father's hopes and mother's prayers…

On my behalf, my sire...

I inscribed this insignificant work...

waiting for Al-Faraj

Acknowledgments

In the name of Allah, the most gracious, the most merciful

All thanks and praise to Allah who enabled me to achieve this research work. Firstly, I would like to express my sincerest gratitude to my supervising professor, Dr. Haitham H. Muteb Al-Daami, for his invaluable insight, wisdom, and guidance,

I would like to thank the support staff of the Department of Civil Engineering of Karbalaa University to the technical staff of the structural laboratories for their assistance during the undertaking of my experimental program.

I would like to acknowledge the friendly support and assistance of my fellow graduate students who made my overall experience more gratifying.

Finally, a special thanks and gratitude to my family for their care, and patience, in particular: my parents, my brother, and my sisters who have been by my side throughout this entire endeavor. Without their love, encouragement, and support I would not have been able to complete this academic achievement.

Zahraa Luay Azeez Shubbar

2023

Abstract

Corrosion of the reinforcing steel is the most common cause of reinforced concrete structure deterioration. Glass fiber reinforced polymer (GFRP) was utilized in place of steel rebar. It has high strength, is lightweight, and corrosion resistance. With a good mechanical performance. The experimental program including many experimental tests the concrete specimens were classified into two groups of different element types for beams, and two-way slabs were test. Also, the mechanical properties for the alternative reinforcement, three beams under a two-point loading system. Four two-way slab specimens were also placed and tested until they failed under concentric loading. Additionally, the bond slip is studied here by testing six specimens three of them for steel rebars and three for GFRP bars.

The beam group was reinforced by steel rebars and GFRP bars separately in this group the behavior of the alternative reinforcement was studied under the effects of shear and bending behavior. All the beams have a rectangular cross-section of 150×200 mm, and the span between the supports was 1200 mm. To avoid shear failure, steel stirrups were used with an adequate amount Ø6 @100mm, two nominal 6mm rebars were used as top reinforcement. The main parameters investigated were the type and amount of reinforcement. The findings show that flexure failure occurs from tensile rupture of the bars at the midsection or under the applied point load. The data indicated that RC beams with GFRP bars deflect more than beams made of steel, while the GFRP beam has a wider crack width than a steel RC beam.

The slab group includes the first and second slabs, which consist of 7-Ø6 bars in two-way from GFRP and steel with a reinforcement ratio of 4.5% and 3.8%, respectively, for GFRP and steel. The third and fourth slabs consist of 14Ø6 bars from GFRP and steel with a reinforcement ratio of 9% and 7.5% of

GFRP and steel bars, respectively. The main parameters studied were the type of reinforcement and the effect of flexural reinforcement spacing on the flat slab. The specimens were squares with a clear span of 1000 mm and a depth of 70 mm. Simple support was used for all specimens acting on all four edges. According to the failure modes, high reinforcement ratio slabs fail by punching shear, whereas low reinforcement ratio slabs fail by flexural failure. When compared between the slabs reinforced with steel and GFRP bars that failed due to punching shearing and flexural failure, the resistance of the slabs with steel rebar increased by 34% and 30%, respectively.

The bond group includes only GFRP and only steel cubes. The main variables studied in pull-out cubes were embedment length, GFRP bar, and steel bar (5, 7.5, and 10 times bar diameter). The pull-out cube's geometric dimensions were 200 x 200 x 200 mm. Helical wrapping was used to test the surface texture of GFRP bars for pull-out. The bar was centered in the concrete cube. The specimens that contained GFRP bars failed due to bar pull-out from the concrete cube because of slippage between the GFRP bar and concrete. This is a result of weak bonding between GFRP bars and concrete. The specimens contained steel bars that failed due to bar cutting in different places. The cutting point is the point where the reinforcing steel and concrete connection, the end of the concrete cube, or the point where the holding arm and the bar connection. This is a result of the steel bars and concrete's good bond.

Notation

A = cross-sectional area, mm2

Af = area of fiber-reinforced polymer (FRP) reinforcement, (mm^2)

a = depth of equivalent rectangular stress block, (mm)

b = width of rectangular cross section, in. (mm)

b_o = perimeter of critical section for slabs and footings, in. (mm)

b_w = width of the web, in. (mm)

c = distance from extreme compression fiber to the neutral axis, in. (mm)

c_b = distance from extreme compression fiber to neutral axis at balanced strain condition, (mm)

d = distance from extreme compression fiber to centroid of tension reinforcement, (mm)

d_b = diameter of reinforcing bar, (mm)

ρ =steel reinforcement ratio

ρ_b = steel reinforcement ratio producing balanced strain conditions

ρ_f = fiber-reinforced polymer reinforcement ratio

ρ_{fb} = fiber-reinforced polymer reinforcement ratio producing balanced strain conditions

ε_c = strain in concrete

ε_{cu} = ultimate strain in concrete

εf = strain in FRP reinforcement

ε_{fu} = design rupture strain of FRP reinforcement, defined as the guaranteed tensile rupture strain multiplied by the environmental reduction factor.

Ec= modulus of elasticity of concrete, (MPa)

Ef = modulus of elasticity of FRP (MPa)

Es= modulus of elasticity of steel, (MPa)

fc' = specified compressive strength of concrete, (MPa)

f_f = stress in FRP reinforcement in tension, (MPa)

f_{fu} = design tensile strength of FRP, (MPa)

fy = specified yield stress of non-prestressed steel reinforcement, (MPa)

h = overall height of flexural member, (mm)

k = stiffness (kN/mm)

ℓ = span length of member, (mm)

ℓe = embedded length of reinforcing bar, in. (mm)

Mn = nominal moment capacity, (N-mm)

Vc =nominal shear strength provided by concrete, (N)

Vn =nominal shear strength at section, (N)

Vs =shear resistance provided by steel stirrups, (N)

β = ratio of distance from neutral axis to extreme tension fiber to distance from neutral axis to center of tensile reinforcement

β1 = factor taken as 0.85 for concrete strength fc' (30 MPa).

τ = average bond stress, MPa

F = tensile load, N

C_b = equivalent circumference of FRP bar, mm

l = bonded length, mm

Sc= elastic elongation, mm

L_C = length from the top of the embedded bar to the point of the attachment of the measuring device mm

E_L = longitudinal modulus of elasticity of GFRP bar, MPa

Abbreviations

ABNT	Brazilian Association of Technical Standards
ACI	American Concrete Institute
ASTM	American Society for Testing and Material
BS	British Standards
DAQ	data acquisition
FRP	Fiber Reinforced Polymer
GFRP	Glass Fiber Reinforced Polymer
IQ.S	Iraqi Specification
LVDT	linear variable differential transformer
MRI	Magnetic Resonance Imaging
N.A	Neutral Axis
RC	Reinforced Concrete
Rebar	Reinforcing Bar
TBM	Tunnel Boring Machine

Chapter One

CHAPTER ONE

INTRODUCTION

1.1 Introduction:

Through the last 100 years, reinforced concrete (RC) has been widely used in construction sectors. Reinforced concrete offers superior strength and stiffness. Although RC has these properties, drawbacks are observed such as steel reinforcements are susceptible to corrosion, as shown in Figure (1-1), which can cause deterioration in the RC strength and performance.

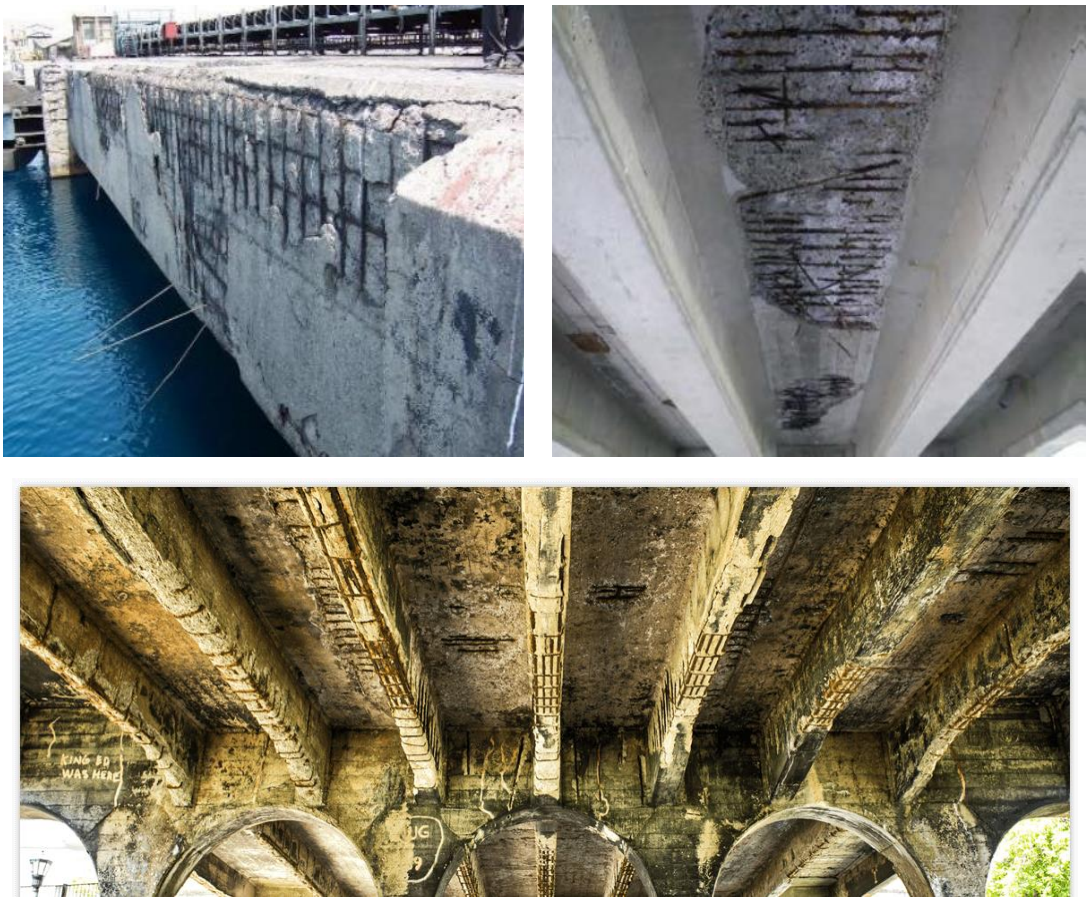

Figure (1-1): Corrosion in Steel Reinforcement [1]

FRP reinforcement for concrete structures has been under development since the 1960s in the United States and the 1970s in Europe and Japan. However, it was in the 1980s that the overall level of research, field demonstration, and commercialization became remarkable. Up to the mid-1990s, the Japanese have the most FRP reinforcement applications, with more than 100 demonstration or commercial projects. Fiber-reinforced polymer design provisions are included in the design and construction recommendations of the Japanese Society of Civil Engineering (1997b). In the 2000s, China became the largest user of composite reinforcement for new construction in applications that span from bridge decks to underground works.[2] The polymeric matrix with strong fibers embedded in it can be used to develop new material systems. The so-called FRP composite materials offered several advantages with respect to traditional metallic materials. Their innovative properties, such as high tensile strength and modulus, lightness, corrosion resistance, electromagnetic transparency, and the possibility to "engineer" their mechanical properties by changing constituent composition and fiber type and orientation, made FRP composites suitable for a number of applications in different industries [2]. The aerospace industry began to use FRP composites as lightweight material with superior strength and stiffness, which reduced the weight of aircraft structures. Later, other industries like naval, defense, and sporting goods started using FRP composites on an extensive basis.

FRP reinforcing bars (rebars) are anisotropic. Strength and stiffness of the FRP rebar in the direction of the fibers are significantly affected by the types of fibers and the ratio of the volume of fiber to the overall volume of the FRP. The type of resin affects the failure mechanism and the fracture toughness of the composite. Other factors influencing the properties of FRP rebars are fiber orientation, rate of resin curing, and manufacturing process and its quality control [3].

Until a few decades ago, steel bars are practically the only option for reinforcement of concrete structures. The combination of steel bars and concrete is mutually beneficial. Steel bars provide the capacity to resist tensile stresses. Concrete resists compression well and provides a high degree of protection to the reinforcing steel against corrosion as a result of its alkalinity.

Combinations of chlorides (depassivation of steel) and CO2 (carbonation of concrete) in presence of moisture produce corrosion of the steel reinforcement. This phenomenon causes the deterioration of the concrete and, ultimately, the loss of the usability of the structure [4]. Over the second half of the 1900s, the deterioration of several RC structures due to the chloride-ion induced corrosion of the internal steel reinforcement became a major concern. Various solutions are investigated for applications in aggressive corrosion environments. These included galvanized coatings, electrostatic spray fusion-bonded (powder resin) coatings, and polymer-impregnated concrete epoxy coatings. Eventually, fiber-reinforced polymer (FRP) reinforcing bars are considered as an alternative to steel bars. [3]

Composite materials made of fibers embedded in a polymeric resin, also known as fiber-reinforced polymer (FRP), are an alternative to steel reinforcement for concrete structures. Fiber-reinforced polymer reinforcing materials are made of continuous aramid fiber (AFRP), carbon fiber (CFRP), or glass fiber (GFRP) embedded in a resin matrix. Because FRP materials are nonmagnetic and noncorrosive, the problems of electromagnetic interference and steel corrosion can be avoided with FRP reinforcement. Additionally, FRP materials exhibit several properties, such as high tensile strength, that make them suitable for use as structural reinforcement. [2]

The FRP reinforcing bar became a commercially available viable solution as internal reinforcement for concrete structures in the late 1980s, when the

market demand for electromagnetic-transparent (therefore nonferrous) reinforcing bars increased. [3]

1.2 GFRP Reinforcement

Glass fiber is primarily made from silica sand and is commercially available in different grades. The most common types of glass are electrical (E-glass), high-strength (S-glass), and alkali-resistance (AR-glass). E-glass presents high electrical insulating properties, low susceptibility to moisture, and high mechanical properties. S-glass has higher tensile strength and modulus, but its higher cost makes it less preferable than E-glass. AR-glass is highly resistant to alkali attack in cement-based matrices, but, at the moment, sizing compatible with the thermoset resins that are commonly used to pultrude FRP bars are not available. Composites made from glass fiber exhibit good electrical and thermal insulation properties [3]. Figure (1-2) shows the type used in this study.

Figure (1-2): GFRP Bars

1.3 Considerations for the use of fibre reinforced polymer (FRP) reinforcing bars:

1.3.1 Benefits of Fiberglass Rebar

1. Tensile strengths greater than steel.
2. Electrically non-conductive.
3. Transparent to magnetic fields and radio frequencies.
4. Thermally non-conductive.
5. 1/4th the weight of steel rebar.
6. Resistant to chemical attacks from chloride ions and low PH.
7. Low cost

1.3.2 Differences between GFRP and steel

1. GFRP is anisotropic whereas steel is isotropic.
2. GFRP is linear elastic to failure whereas steel yields.
3. GFRP bars have a lower creep-rupture threshold than steel.
4. Due to lower modulus of GFRP bars, design for serviceability often controls.
5. Different longitudinal and radial coefficients of thermal expansion.
6. Unlike steel, which expands and leads to a collapse of the member, GFRP bars' degradation mechanisms are benign to the nearby concrete should they degrade.
7. Has a shorter durability time than steel in applications involving fire and high temperatures. [2]

1.3.3 Where should FRP bars be considered?

1. Any concrete structure that electromagnetic considerations require nonferrous reinforcing.

2. Any concrete structure subject to corrosion by chemicals or chloride ions.
3. A first cost-saving measure compared to steel bars
4. As a less expensive option to galvanized and epoxy-coated
5. Where machinery will “consume” the reinforced member, mainly in tunneling and mining
6. In hybrid applications with steel where mass concrete is exposed to marine chlorides close to chloride exposure.
7. Applications that need thermal nonconductivity. [2]

1.4 Aim of the study

There is a need for a more sustainable alternative to traditional steel bars. GFRP bars are a good option because they solve problems associated with steel bars. These materials are guaranteed to be corrosion-resistant, which reduces the lifecycle cost of concrete structures.

The main aim of this thesis is to compare the flexural behavior of steel and GFRP reinforced concrete element experimentally. The bond behavior will be investigated using pull-out test. The flexural test will be in two groups, first group is reinforced with GFRP bar and the other group is reinforced with steel bar. The beams will be subjected to flexural test until failure to determine the ultimate load capacity, failure mode, crack pattern and crack width attributed to each of the beam. The behavior of flat slabs reinforced with GFRP bars subjected to a concentric load for punching shear strength. To investigate the behavior and punching shear capacity of interior slab column.

the aim of the study is to investigate the main comparison between the GFRP and steel bars effects on the beams and slabs specimens through a detection

of flexural behavior of the beams and slabs reinforced with GFRP and steel bars, and the bond phenomena of GFRP and steel bars with concrete

1.5 Applications of GFRP bars:

GFRP rebars are suitable alternatives to steel, epoxy-coated steel, and stainless-steel bars in reinforced concrete applications if durability, electromagnetic transparency, or ease of demolition in temporary applications.

1.5.1 Marine Structures

The corrosion resistance of FRP reinforcement is a significant benefit for structures in highly corrosive environments such as seawalls as shown in Figure (1-3) and other marine structures, bridge decks and superstructures exposed to deicing salts, and pavements treated with deicing salts. Bridges at sea, retaining/sea walls, ports infrastructure, and dry docks. Bridge decks and railings where deicing salts are used. Seawalls are vertical structures erected to protect the environment against upland erosion and flooding as shown in Figure (1-4). Locks and dam weirs as shown in Figure (1-5). GFRP bar is corrosion free and exhibits higher strength making it an ideal material for marine application as shown in Figure (1-6).

Figure (1-3): Construction of Seawall with GFRP Bars.[1]

Figure (1-4): Honopapiilani Highway Retaining Sea Wall South (Lahaina, Maui Hawaii).[3]

Figure (1-5): GFRP Reinforced-Concrete for Ice Harbor lock and Dam Fish Weir (Walla Walla, Washington). [3]

Figure (1-6): GFRP Reinforcing in the Two Water Tanks.[1]

1.5.2 Parking Garages

Generally, parking garages are exposed to corrosion because vehicle carries salt and water from the environment on their body. GFRP is an ideal material for constructing parking garages as shown in Figure (1-7).

Figure (1-7): GFRP Rebar for Parking Garage.[5]

1.5.3 Bridges

Repair and maintenance of bridges is very expensive. When steel bars are exposed to deicing chlorides, the service of the structure is reduced. Bridges are open to environmental and stress factors. GFRP bars are designed in such a way there are able to sustain heavy traffic loads and also natural disasters like earthquakes. GFRP bars used in constructing bridges certainly reduces cost of maintenance as shown in Figure s (1-8) and (1-9).

Figure (1-8): Emma Park Bridge Deck Panel with GFRP Reinforcing Bars, Top and Bottom Mat. [2]

Figure (1-9): Bridge over State Ave. (Kansas City, KS).[2]

1.5.4 MRI Hospital Room

Medical and information technology facilities contain equipment that emits magnetic waves or require massive electric currents, this calls for non-magnetic, non-metallic and non-conductive materials to be used in constructing these facilities to avoid interference with delicate circuit or machines. Also, the GFRP bar has twice the tensile strength of the steel bars. In structures supporting Magnetic Resonance Imaging (MRI) as shown in Figure (1-10) units or other equipment sensitive to electromagnetic fields, the nonmagnetic properties of FRP reinforcement are of principal importance.

Figure (1-10): GFRP Reinforced-Concrete Slab for MRI Rooms in Hospital (York, Maine) [6]

1.5.5 Rail Plinths for Airport Link

GFRP bar are used in the rail plinths for airport link Glass FRP bars are selected, as they provided electrical insolation in the rail bed as shown in Figure (1-11).

Figure (1-11): GFRP bars used in rail plinths. [2]

1.5.6 Using GFRP in Airport Runways

With years airplanes are getting heavier and bigger. Achieving longer service life should be regarded when it comes to airport runways. GFRP bars used in reinforcing runways helps in withstanding the landing impact of airplanes which can be over 500,000 pounds. Flexibility and strength standards should be strictly adhered to when constructing concrete base of airport runways as shown in Figure (1-12).

Figure (1-12): Using GFRP in Airport.[7]

Reinforcing runways using GFRP bars makes it to be durable, flexible and strong. It is not advisable to use traditional steel for runways. GFRP bars can main the runway's integrity for over 100 years.

1.5.7 Using GFRP in Precast Concrete Constructions

Same way RC elements are susceptible to corrosion so is precast concrete. Using GFRP as reinforcement in precast concrete increases the service life to over 100 years. GFRP bars are non-metallic thereby making precast concrete elements to be non-corrodible and to avoid discoloration by rust stain. It also makes it lighter as shown in Figure (1-13).

Figure (1-13): Culvert bridge in City of Rolla, Phelps County, Missouri. [8]

1.5.8 Using GFRP in Special Structures

There are some special structures around the world which serve as a landmark mainly because of their special character and appearance. Some of the unique structures made using glass fibre reinforced polymer (GFRP) bar can be seen in Figure s (1-14) and (1-15).

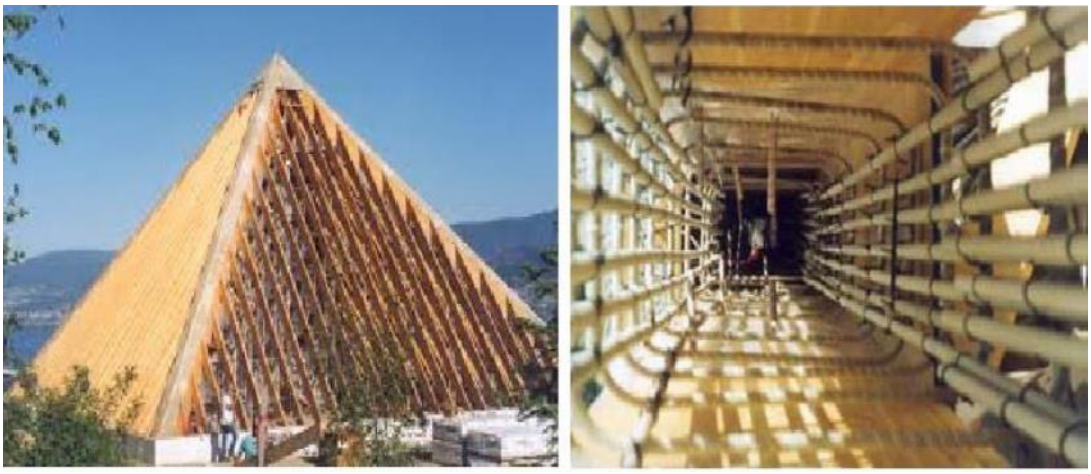

Figure (1-14): Pyramid shaped winery in British Columbia. [6]

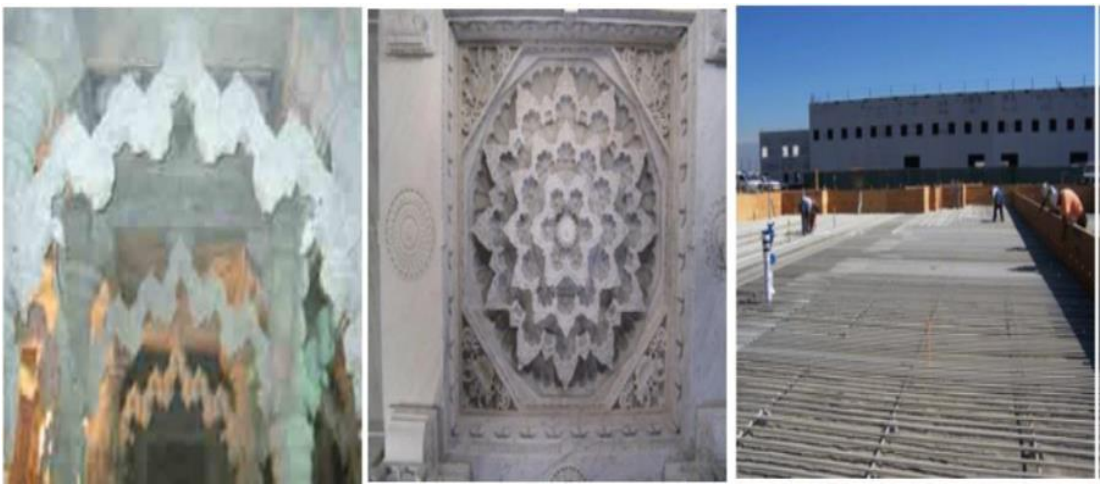

Figure (1-15): Hindu temple design with service life of 1000 years.[6]

1.5.9 Structures Temporarily

GFRP reinforcement is the ideal material to reinforce concrete structures temporarily, such as “soft-eyes” that have to be demolished partially by Tunnel Boring Machines (TBMs). The “soft-eye” consists of a reinforcing cage using GFRP bars, which can be easily cut by the TBM as shown in Figure (1-16). [3]

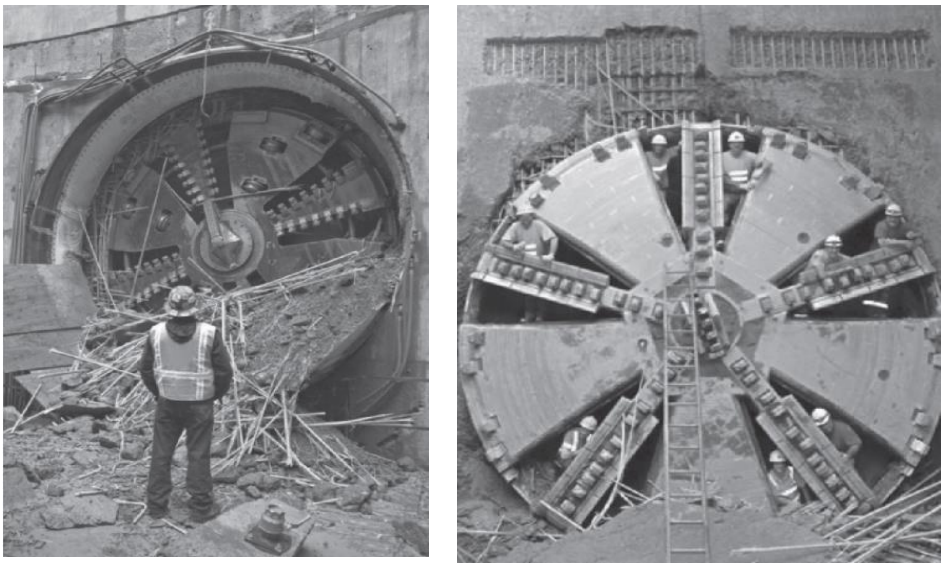

Figure (1-16): GFRP Reinforced-Concrete Soft-Eye for Tunnel Excavation TBM Emerges (London, UK). [3]

1.6 Thesis Layout

The thesis is made up of 5 chapters:

Chapter one: gives the general information regarding reinforced concrete and the problems associated. The aims, and thesis layout.

Chapter two: gives the in-depth information regarding fibre reinforced polymer (FRP) bars stating their physical and mechanical properties. Previous experimental studies done on GFRP bars will also be stated.

Chapter three: presents the experimental procedure that will be carried out on the reinforcement materials and the reinforced beams, slabs and bond slip.

Chapter four: presents the experimental results for comparison.

Chapter five: presents the conclusions and recommendations for future works.

Chapter Two

CHAPTER TWO

LITERATURE REVIEW

2.1 Introduction

The long-term durability of reinforced concrete structures has become a major concern over the past few decades, mainly due to the corrosion risk of steel reinforcements. Fiber-reinforced polymer (FRP) is being increasingly used in civil engineering as a reinforcement to replace steel bars because of its rather durable properties, especially in aggressive environments where steel reinforcements are easily corroded. Additionally, under some special circumstances, such as in the magnetic resonance imaging rooms of hospitals, there is a demand for electromagnetic permeability, and such needs can be met by FRP bars since they are non-metallic. Since FRP bars possess mechanical characteristics different from those of steel bars (e.g., lower elastic modulus, nonyielding properties), numerous experimental investigations have been carried out to study the behavior of concrete members reinforced by FRP bars.[9]

2.2 Properties Of FRP Composite Bars

2.2.1 Physical Properties of FRP Composites

The concept of polymeric resin controlling the physical nature of FRP composites was illustrated by [3]. The most significant factors are the fibre type and fibre-volume fraction, which is defined as the ratio of the volume of fibre to the overall volume of the bar. The density of the FRP material is one-sixth to

one-fourth of that of steel. The coefficients of thermal expansion of FRP bars are different in the longitudinal and transverse directions. The longitudinal coefficient of thermal expansion depends on the properties of the fibers, while the transverse coefficient depends on the properties of the resin [2]. Hollaway (2010) mentioned that the most dominant properties of polymers are physical and in-service characteristics. Conventional thermosetting matrices are considered to be brittle due to increase in cross-linking density observed during polymerization [10].

2.2.2 Mechanical Properties of FRP Composite Bar

2.2.2.1 Tensile Behavior

FRP composites are brittle in nature. Unlike steel reinforcement, they do not undergo a yielding plateau prior to rupture when they are loaded in tension. Instead, they exhibit a linear elastic stress-strain relationship up to failure as shown in figure (2-1).

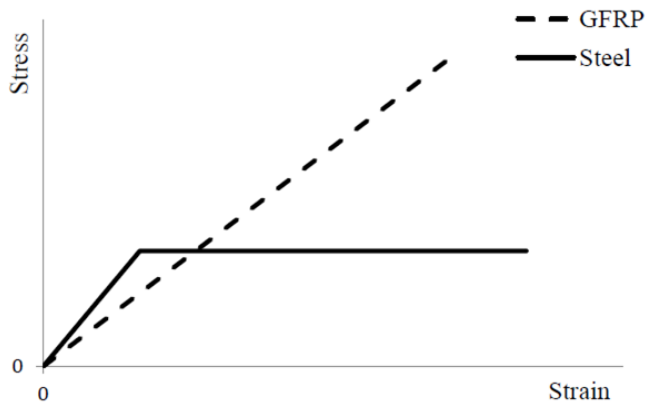

Figure (2-1): Typical stress-strain relationship

Many parameters affect the tensile strength and modulus of an FRP bar; some of them are the type of fibers and resin, the fibre-volume fraction and the diameter of the bar.

As shown in table (2-3), the tensile strength of the FRP composite bars is much higher than the yield strength of the steel bars. On the other hand, the stiffness of the FRP bars is lower than that of the steel bars.

Table (2-3): Typical tensile properties of reinforcing bars [2]

Reinforcement type	Steel	GFRP	CFRP	AFRP
Tensile strength (MPa)	276-517*	483-1600	600-3690	1720-2540
Tensile modulus (GPa)	200	35-51	120-580	41-125

*Yield strength

2.2.2.2 Compressive Behavior

failure for FRP bars under axial compression may be triggered by transverse tensile failure, internal buckling of the fibers, and/or shear failure depending on the type of fibers and resin and the fibre-volume fraction. The current design documents in North America (Canadian Standards Association 2012) and the American Concrete Institute guideline [2]. The FRP reinforcement in compression zones to have zero compressive strength. In general, is considered the compressive strength and compressive modulus of FRP bars is less than the tensile strength and modulus of the same product. The compressive strength reduction is between 22 % - 80 % compared to the tensile strength.

2.2.2.3 Transverse Shear Behavior of GFRP Bars

Properties of the matrix are the most dominant factors influencing the behavior of GFRP under transverse shear loading. GFRP bars are generally weak in transverse shear. However, shear strength can be increased by braiding or winding additional fibers in the direction transverse to the longitudinal one. In most cases, the shear strength of GFRP bars varies between 30 to 50 MPa [3].

2.2.2.4 Bond Behavior

Bond stresses between the FRP bars and the concrete is transferred by the adhesion between the concrete and the reinforcing bar (chemical bond), the frictional resistance due to roughness of the FRP bar's surface, the bearing of the bar deformations against the concrete (mechanical bond/interlock), the hydrostatic pressure exerted on the bars due to the shrinkage of the concrete and the expansion/swelling of the bars when subjected to high temperature [11].

When an FRP-RC element is tested, the chemical bond mechanism is the dominant mechanism transferring bond stresses between the concrete and the bars until initial pullout/slip of the bars; thereafter, frictional bond and mechanical interlock become the governing mechanisms depending on the surface texture.

The bond behavior of FRP bars is fairly different from that of steel bars because of the different surface preparations and the considerable differences in the material properties in both longitudinal and transverse directions. A reduction of 40% to 10% was found in the maximum bond strength of GFRP bars compared to steel bars with the same diameter. This was attributed to the fact that while the main contribution to the bond strength in case of steel

reinforcement comes from the bearing of the bar rips against the concrete; the rips of the GFRP bars do not provide enough lateral confinement since they have different geometry and lower shear strength and stiffness than those of steel bars [11].

2.3 Time-Dependent Behavior

These are time dependent characteristics of the FRP bars which regards to strength, it is an important factor when designing reinforced concrete structures. These properties are stated below.

2.3.1 Creep Rupture

Fiber-reinforced polymer reinforcing bars subjected to a constant tension over time can suddenly fail after a time period called the endurance time. This phenomenon is known as creep rupture or static fatigue. Creep rupture is not an issue with steel bars in reinforced concrete except in extremely high temperatures, such as those encountered in a fire. As the ratio of the sustained tensile stress to the short-term strength of the FRP bar increases, endurance time decreases. The creep rupture endurance time can also irreversibly decrease under sufficiently adverse environmental conditions such as high temperature, ultraviolet radiation exposure, high alkalinity, wet and dry cycles, or freezing-and-thawing cycles.

2.3.2 Fatigue

There is various amount of data for the past 30 years stored on the lifespan and fatigue of FRP but limited to aviation industries. No enough researches related to RC elements [2]. Reports explained that among all type of FRPs, GFRP is less prone to fatigue. At about a million cycle, there is a 30-50% decrease in fatigue strength when compared to initial static strength. AFRP bar

in concrete tends to lose 27-46% of its tensile strength at about 2 million cycles [2]. Fatigue behavior is strongly dependent on environmental conditions such as alkalinity, acidity and moisture in the concrete mass covering the bars. Fatigue limit cannot be clearly determined unlike steel [12]. It is important to keep in mind that degradation of resin or fibre interface under alkaline and moist environment can have a detrimental effect. Generally, behavior of fatigue in FRP largely depend on the bond between resin matrix and fibre.

2.3.3 Durability

Durability of FRP reinforced concrete element is dependent upon many factors such as water, acidic or alkaline solutions, elevated temperature, saline solutions and ultraviolet exposure. Stiffness and strength varies or remains constant which depend on the exposure condition or type of material. Bond and tensile properties are the most important parameters of FRP bars that needs to be regarded during construction of reinforced concrete structures [2].

2.4 RC Element Strengthened by GFRP Bars

2.4.1 Flexure Behavior of Beams

Ashour (2006) [13] This paper reports the test results of 12 concrete beams reinforced with glass fiber-reinforced polymer (GFRP) bars subjected to a four-point loading system. All test specimens have neither transverse shear nor compression reinforcement and are classified into two groups according to the concrete's compressive strength. The main parameters investigated in each group are the beam depth and the amount of GFRP reinforcement. Two modes of failure are observed, namely flexural and shear. The flexural failure is mainly occurred due to tensile rupture of GFRP bars either within the mid-span region

or under the applied point load. The shear failure is initiated by a major diagonal crack within the beam shear span. This diagonal crack extended horizontally at the level of the GFRP bars indicating bond failure. All the beams were reported to have failed in flexure due to rupture of FRP bars or crushing of concrete. The average and standard deviation of the ratio between predicted and experimental bending capacities are 0.99% and 14.6%, respectively. The predictions obtained from the analysis are in very good agreement with the experimental results.

Lau & Pam (2010) [14] Twelve specimens consisting of plain concrete beams, steel-reinforced concrete (SRC) beams, pure FRP beams and hybrid FRP beams are fabricated and tested. The test results show the hybrid FRP beams behave in a more ductile manner when compared with the pure FRP beams. Also, it is observed that a higher degree of over reinforcement in the beam specimen resulted in a more ductile FRP beams. Hence, the addition of steel reinforcement can improve the flexural ductility of FRP members, and over-reinforcement is a preferred approach in the design of FRP members. Flexural ductility of FRP members can be improved by two methods, i.e. by increasing the degree of over-reinforcement and by adding conventional steel rebars. The ductility improvement by adding steel rebars is higher in over-reinforced FRP members than in the under-reinforced counterparts, and the increase is considerably larger in the over-reinforced member than the balanced-reinforced counterpart.

Kalpana & Subramanian (2011) [15] The present study focuses on gaining an insight into the behavior of concrete beams reinforced with GFRP bars subjected to two-point loading system by varying the grade of the concrete and diameter of the bar. The modes of failure and the crack width at each stage of loading are observed. The results of load-deflection and load-crack width

characteristics are discussed. The crack pattern of the GFRP beams under loading is also reported. The comparisons between the flexural capacity of GFRP beams and steel beams from theoretical analysis and GFRP beams with that of the experimental are done. The reduction in stiffness of the GFRP bars results in an increased crack width. As the concrete strength increases, the changes in ultimate crack widths are relatively small. The increase in the width of cracks significantly decreases with the increase in the size of the reinforcing bar. The reduction in stiffness of the GFRP bars results in an increased crack width.

Barris et. al, (2012) [16] experimente on GFRP reinforced concrete beams to determine their short-term behavior in flexure using distinct ratio of reinforcement and varying the effective depth to height ratio. They examine some prediction models and try to compare them with experimental results. They conclude that the beam behaved linearly until cracking as a result of absence of plasticity of GFRP bar, but the failure is experienced at larger displacements. The prediction by ACI 440.1R regarding flexural load at service load level closely agree to the experimental result but that is not the case in higher load levels. The crack width from experimental result closely fits the minimum value proposed by ACI 440.1R which signified good bonding between GFRP bars and concrete. All beam failed as 30 a result of concrete crushing and the experimental ultimate capacity of the beam is more than the expected as per the ACI standard.

Shanour et al., (2014) [17] performs experiment on beams having dimensions of 120x300x2800mm reinforced using locally made GFRP bars and steel reinforced beams. The main parameters of concern they regard are the impacts of compressive strength, the ratio of reinforcement and the type of

material used (Steel or GFRP). The beams are subjected to four-point bend tests and concluded that mid span deflection and crack width is reduced by increasing the ratio of reinforcement. Also, the ultimate capacity of the beam significantly increases as the reinforcement ration increases. The test results revealed that the crack widths and mid-span deflection were significantly decreased by increasing the reinforcement ratio. The failure in GFRP RC beams reinforced with more than the balanced reinforcement was compression failure due to concrete crushing. While, Beams reinforced with GFRP ratio in order of lower than or almost equal the balanced reinforcement ratio exhibited rupture of GFRP reinforcement. Increasing the concrete compressive strength in the order of 25Mpa to 45Mpa exhibit reducing in the crack width by 52%. The loads deflection curves were bilinear for all GFRP reinforced beams. The first part of the curve up to cracking represents the behavior of the un-cracked beams. The second part represents the behavior of the cracked beams with reduced stiffness.

Kheni et. al, (2016) [18] performs an experimental and analytical study to study the how GFRP RC element behave in comparison to steel RC element. Concrete beams are made with 20MPa and 25MPa concrete and also different reinforcement size combination. The analytical study is performed using finite element modelling software (ATENA 3D) to simulate each of the beams. Comparing the two results shows the ultimate capacity of GFRP reinforced beam is higher than steel reinforced beam. They also suggested that combining steel and GFRP bars together will result much higher ultimate capacity.

Chidananda & Khadiranaikar, (2017) [19] performs experiments on 12 beams having dimensions of 150x180x1200mm reinforced with glass fiber-reinforced polymer (GFRP) bars subjected to a four-point loading system. which is subjected to four-point test. The beams where in 4 groups each with

different ratio of reinforcement. They also conclude that increasing the ratio of reinforcement elevates the ultimate capacity of the beams and also show how applicable the ACI standard is in beam design.

Saleh et. al, (2019) [20] two design codes for the flexural design of Fibre Reinforced Polymer (FRP) bar reinforced concrete beams have been reviewed and compared with the results of the experimental investigations of eight GFRP (Glass Fibre-Reinforced Polymer) bar reinforced concrete (GFRP) beams. It has been demonstrated that experimentally determined load carrying capacities, maximum deflections and energy absorbing capacities have been over predicted by the relevant code recommendations for the under-reinforced and balanced GFRP beams while being under-predicted for the over-reinforced GFRP beams.

Moolaei et. al, (2021) [21] seven beams are reinforced with the steel and Glass Fiber Reinforced Polymer (GFRP) bars in a hybrid system and the experimental behavior of beams is investigated. Three groups of beams are reinforced, including only-GFRP, only-steel, and hybrid steel-GFRP rebar subjected to four-point bending tests, respectively. To enhance the ductility of beams, conventional concrete is substituted with the High-Performance Fiber Reinforced Cementitious Composites (HPFRCC). The beams of the first and second group are separately constructed by conventional concrete and HPFRCC; however, the third group is only consisted of HPFRCC. The results indicated that HPFRCC concrete positively influenced on the strength, ductility, and energy absorption of reinforced beams using composite and hybrid bars.

In (2021) Putri,[22], This paper proposes an analytical study to predict the flexural capacity of structure elements reinforced with glass fibre reinforced polymer (GFRP) bars. To consider the contribution of concrete under compression, a nonlinear stress-strain curve of concrete is used. The results are

also compared to the ACI 440.1R-15 code and validated against a published experiment. The rupture modes predicted in the analytical investigation are comparable to those observed in the experiment, with an average flexural capacity ratio estimated using Todeschini's nonlinear curve ranging from 0.78 to 0.86. Furthermore, the flexural capacity calculated using Todeschini's nonlinear stress-strain curve for specimens with reinforcement ratios greater than the balanced reinforcement ratio outperformed the ACI code.

2.4.2 Bond Slip Behavior

Aiello & Ombres, (2000) [23] The use of a general method in the analysis of FRP reinforced concrete beams is needed in order to take into account all parameters influencing the structural behavior of such elements. The method is found based on the use of moment-curvature diagrams of a concrete block between two contiguous cracks. The local bond-slip and the tension stiffening effects are considered. The wide variability of geometrical and mechanical properties of FRP rebars available on the market does not allow to define a unique model able to predict the serviceability behavior of FRP reinforced concrete beams for any load and support condition. The use of empirical models, such as Codes models, in some cases is not able for a reliable structural analysis. essential for the structural analysis. Consequently, bond tests should be considered as fundamental for the mechanical characterization of FRP rebars. The general method predicts very well deflections of CFRP reinforced concrete beams for low values of the reinforcement ratio, while for high values of the reinforcement ratio it underestimates experimental values.

Achillides & Pilakoutas, (2004) [24] This paper examines the behavior of Eurocrete fiber-reinforced polymer (FRP)bars (glass, carbon, aramid, and hybrid) in concrete under direct pullout conditions. More than 130 cube specimens are tested in direct pullout where no splitting is allowed to develop. In normal concrete, the mode of bond failure of FRP bars is found to differ substantially from that of deformed steel bars because of damage to the resin rich surface of the bar when pullout takes place. This paper reports in detail on the influence of various parameters that affect bond strength and development such as the embedment length, type, shape, surface characteristics, and diameter of the bar as well as concrete strength.

Carvalho, (2017) [25] The steel-concrete bond is a fundamental property in reinforced concrete structures. Although there are several studies on the steel concrete bond, few of them have evaluated the performance of reinforcing bars with diameters less than 10.0 mm, which includes 5.0, 6.3, and 8.0 mm diameters, which are normally used in reinforced- concrete elements. This study experimentally evaluates the bond between thin steel bars and concrete of 25MPa compression strength. Three types of methods of testing the bond-strength were performed: confined bar test, pull-out test and beam test. The pull-out test resulted in better results in terms of evaluating the bond behavior. Regarding the specimens for the pull-out tests, a modified model with an anchorage length equal to 10 times the bar diameter is suggested.

Cruz et.al, (2018) [26] Structures when exposed to marine environments (e.g. ports, offshore structures, buildings located by the sea) are subjected to the simultaneous action of several physical and chemical deterioration processes that accelerate their degradation and greatly reduce their service life. The program is composed of 24 direct pullout tests divided into 8 series. Studied

parameters are (i) type of water used in the concrete composition (SW- seawater or TP- tap water), (ii) GFRP rods diameter (Ø8 or Ø12) and (iii) anchorage length (5Ø or 10Ø). Influence of the GFRP diameter it can be concluded that the bond strength tends to increase with the increase of the rod diameter. Influence of the anchorage length the results demonstrated that by increasing anchorage length the bond strength has increased.

Gao et.al, (2019) **[27]** This paper presents the results of a series of pullout tests that are performed on Glass-fiber-reinforced polymer (GFRP) bars embedded in concrete, while providing a detailed report on the influence of various variables that impinge upon bond behavior, such as the surface characteristics and diameter of the bars, concrete strength, as well as the confined effect of stirrups. The Bertero-Popov-Eligehausen (BPE) and Cosenza-Manfredi-Realfonzo (CMR) models analyzed the bond stress (t)–slip (s) relationship between GFRP bar and stirrups-confined concrete. The tests results indicate that when the bond failure interface only occurs on the surface of a GFRP bar, the bond strength is not dependent upon the concrete strength. The improvement of concrete strength does not necessarily render an increase in the bond strength of the GFRP bars. Moreover, the results indicate that in comparison to specimens without stirrups, their stirrup-containing counterparts are more prone to pullout failure with greater ductility and higher bond strength and corresponding slip.

Solyom & Balázs, (2020) [28] This paper presents an extensive experimental study of the effect of surface characteristics on the bond behavior of Fibre Reinforced Polymer (FRP) bars in concrete. A wide range of commercially available FRP bars with different surface profiles (total of 13 different surface configurations) are involved. For comparison, ribbed steel bars

were used. To investigate whether the effect of surface characteristics is in interaction with other factors, further parameters are included in the study such as concrete compressive strength (35 and 66 MPa), bar diameter (6 to 12 mm) and test type (pull-out [P-O] and direct tension [DT] pull-out). This resulted a total of 200 P-O and 38 DT tests. The bond behavior of the bars is evaluated by bond strength, bond stress-slip relationship, representative bond stresses and failure mode. It is found that the bond strength as well as bond stress-slip behavior and failure mode vary considerably depending on surface characteristics. Furthermore, even within the same surface category the bond strength difference can be significant (e.g., SC surface with different sand fineness). The concrete strength influences the bond strength even if it is higher than the limit stated in literature (approximately 30 MPa). Furthermore, the bond strength results of all FRP bars are consistently higher than those of steel bars. Some results reported in this paper considerably differ from those previously reported in other papers based on testing similar bars. The difference, in terms of bond strength, can be explained by the alteration of surface configuration, the improvements in material properties and fabrication processes.

2.4.3 Flexural Behavior of Two-Way Slab

In (2013) Hassan et. al, [29] The punching-shear behavior of two-way concrete slabs reinforced with glass fiber–reinforced polymer (GFRP) bars of various grades are examined in this work. A total of 10 full-scale interior slab-column specimens measuring 2,500 × 2,500 mm with thicknesses of either 200 or 350 mm and 300 × 300 mm square column stubs are fabricated with normal and high-strength concretes. The specimens are tested under monotonic

concentric loading until failure. The effects of concrete strength, as well as the type and ratio of reinforcing are studied. Increased reinforcement ratio resulted in higher punching-shear capacity, lower reinforcement and concrete strains, and reduced deflections, according to the test results. Furthermore, because to its high tensile strength and modulus of elasticity, the high-strength concrete increased punching-shear capacity, significantly reduced concrete strains, increased strains in the GFRP reinforcing bars, and reduced deflection.

In (2013) Dulude et. al, [30] An experimental study's results 10 internal slab-column samples with dimensions of 2.5 x 2.5 m were built and tested to failure. The followings are the test parameters:

1) reinforcement type (GFRP and steel)
2) slab thickness (200 and 350 mm)
3) column dimensions (300 x 300 mm and 450 x 450 mm)

All test samples showed punching shear failure, and the crack patterns at failure are same regardless of reinforcing type or ratio. Furthermore, when the same reinforcement ratio is used, the GFRP-reinforced samples have lower punching capacity than the steel-reinforced samples due to the lower modulus of GFRP bars compared to steel. The comparisons show that the ACI 440.1R equation yield very conservative.

Kara & Sinani (2016) [31] an innovative solution to the corrosion problem is the use of fiber-reinforced polymer (FRP) as an alternative reinforcing material in concrete structures. In addition to the noncorrodible nature of FRP materials, they also have a high strength-to-weight ratio that makes them attractive as reinforcement for concrete structures. Extensive research programs have been carried out to investigate the flexural behavior of concrete members

reinforced with FRP reinforcement. On the other hand, the shear behavior of concrete members, especially punching shear of two-way slabs, reinforced with FRP bars has not yet been fully explored. The existing provisions for punching of slabs in most international design standards for reinforced concrete are based on tests of steel reinforced slabs. The elastic stiffness and bonding characteristics of FRP reinforcement are sufficiently different from those of steel to affect punching strength. In the present study, the equations of existing design standards for shear capacity of FRP reinforced concrete beams have been evaluated using the large database collected. The experimental punching shear strengths were compared with the available theoretical predictions, including the CSA S806 (CSA 2012), ACI-440.1R-15 (ACI 2015), BS 8110 (BSI 1997), JSCE (1997) a number of models proposed by some researchers in the literature. The existing design methods for FRP reinforced concrete slabs give conservative predictions for the specimens in the database. This paper also presents a simple yet improved model to calculate the punching shear capacity of FRP reinforced concrete slabs. The proposed model provides the accurate results in calculating the punching shear strengths of FRP-reinforced concrete slender slabs. The proposed model provided the most accurate results s in calculating the punching shear strength FRP-RC slabs among existing shear equations considered. The theoretical results indicated that the direct implementation of the FRP axial stiffness into the punching-shear equations provided good predictions.

Ahmed et. al, (2017) [32] Parking garages are among the concrete structures that suffer from corrosion and deterioration due to exposure to deicing salts. This study provides details on the design, construction, and performance of GFRP-reinforced-concrete (GFRP-RC) flat slabs under real

service loads and conditions over 3.5 years. In addition, it provides a comparative cost analysis of the steel-RC and GFRP-RC designs. The cost comparison confirms that the initial higher cost of GFRP compared to steel does not necessarily lead to a higher total cost and that a cost-effective design could be achieved. No obstacles to construction are encountered as the result of using the GFRP bars in the flat slabs. The GFRP bars withstood normal on-site handling and concrete placement with no problems. The GFRP-RC flat slabs showed normal structural performance in terms of strain and cracking throughout 3.5 years of real service conditions. The maximum measured strains in the GFRP bars did not exceed 20% of their strain capacity, but were lower than the expected strains. The midspan sections in flat slabs should be designed so as to resist the bending moments resulting from the redistributed negative moment due to cracking and change in the flexural stiffness.

In (2017). Mohamed & Khattab,[33] Reinforcing two-way concrete slabs with Fibre Reinforced Polymer (FRP) bars can increase service life, decrease maintenance costs, and improve life cycle cost efficiency. Traditional reinforcing steel is replaced by FRP reinforcing bars, which are more environmentally friendly. Shear behavior of reinforced concrete structural members is a complicated phenomenon that is dependent on the development of internal load-carrying mechanisms, the magnitude and combination of which are still being studied. Many building codes and design standards provide design formulas for estimation of punching shear capacity of FRP reinforced flat slabs. Building code formulas take into account the effects of the axial stiffness of main reinforcement bars, the ratio of the perimeter of the critical section to the slab effective depth, and the slab thickness on the punching shear capacity of two-way slabs reinforced with FRP bars or grids. The purpose of

this research is to compare actual data from the literature with building code formulae for estimating punching shear capacity of concrete flat slabs reinforced with FRP bars. Emphasis in this paper is on two North American codes, namely, ACI 440.1R15 and CSA S806-12. In terms of forecasting punching shear capacity, both ACI 440.1R-15 and CSA S806-12 are shown to be in good agreement with test results.

Ju et. al, (2018) [34] This study investigated the punching strength behavior of two-way concrete slabs reinforced with non-corrosive GFRP bars. The punching shear strength, deflection and crack width are examined in terms of strength and serviceability performance. All test specimens displayed punching shear failure. The STS specimen exhibited stiffer behavior until failure than the GFS specimens that are reinforced using an equivalent reinforcement ratio. For the tested service load of the GFS specimens, the load carrying capacity was 1.4–1.6 times higher than the designed service load. Additionally, the experimental results demonstrated that the structural capacity is sufficient to resist the concentrated design load the amount of GFRP bars is designed using the minimum reinforcement ratio. The test results demonstrated that the two-way concrete slabs with GFRP bars satisfied the allowable deflection and crack width under the service load specified by the design specification even in the state of the minimum reinforcement ratio.

Chapter Three

CHAPTER THREE

EXPERIMENTAL WORK

3.1 Introduction

This chapter provides the detailed explanation of the experimental work that was done in the Laboratories of the Civil Engineering Department at the University of Kerbala for this thesis. The details of test specimens which includes the geometry, reinforcement details and how the specimens are prepared is clearly stated. Compression, pull-out, punching, and flexural tests will be performed on the specimens, and the procedure will be clearly specified. The material properties of concrete, GFRP and steel bars are also evaluated and reported.

3.2 Description of Specimens

The focus of this study is to investigate both the flexural of simply supported RC beams, the punching shear of flat slab and the bond of reinforcement of bar, therefore; three groups of specimens. The first group was designed to ensure flexural failure in beam with GFRP bars and steel bars also rupture in concrete in beam with GFRP bar, while the second group was designed to punching shear failure in slab with GFRP bars and steel bars and the third group was to test the bond between concrete and steel bar, concrete and GFRP bar.

The element types were identified by using three terms. The first term, alphabetic term, of the identification corresponded to a beam(B) or slab (S) or bond test pullout (P). The second term, alphabetic term, of the identification corresponded to GFRP bar (G) or Steel bar (S). The third term, numerical term,

represent of the identification corresponded to number of longitudinal bar or distance of bar in concrete in pullout test.

3.2.1 Dimensions of Specimens

3.2.1.1 Group One Beam specimens

This group consists of three beams, The first beam consists of two bars from GFRP (BG2), The second beam consists of four bars from Steel (BS4), The third beam consists of four bars from GFRP (BG4). the bar diameter is the same Ø6 for all specimens

All beams have a rectangular cross-section of 150×200 mm, with a total length of 1300 mm The span between the supports was 1200 mm. The specimens were tested under two-point loads, the distance between loads being 400 mm. To avoid shear failure, steel stirrups were used with an adequate amount Ø6 @100mm, two nominal 6mm steel rebar were used as top reinforcement. All beams had a similar clear cover of 15 mm from each face to the secondary reinforcement as shown in Figure (3-1).

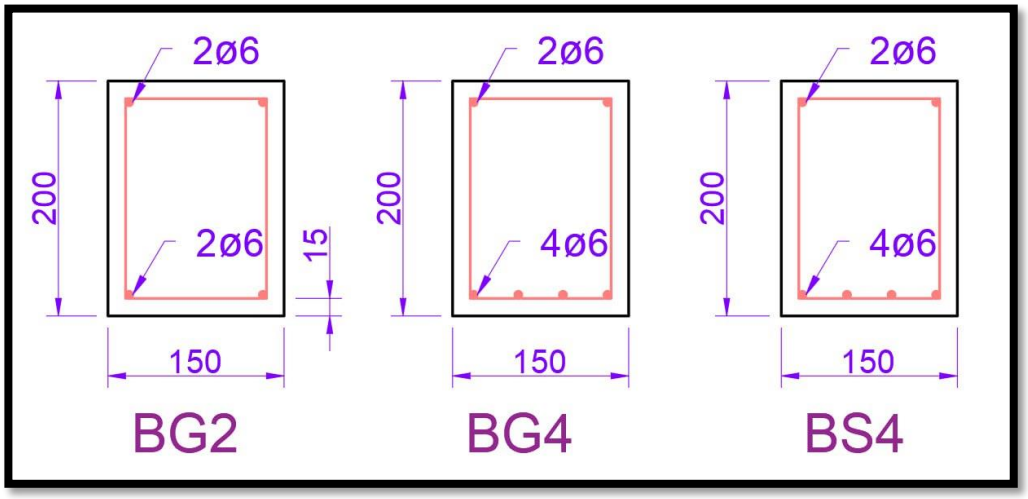

a) Cross-Section of Beams

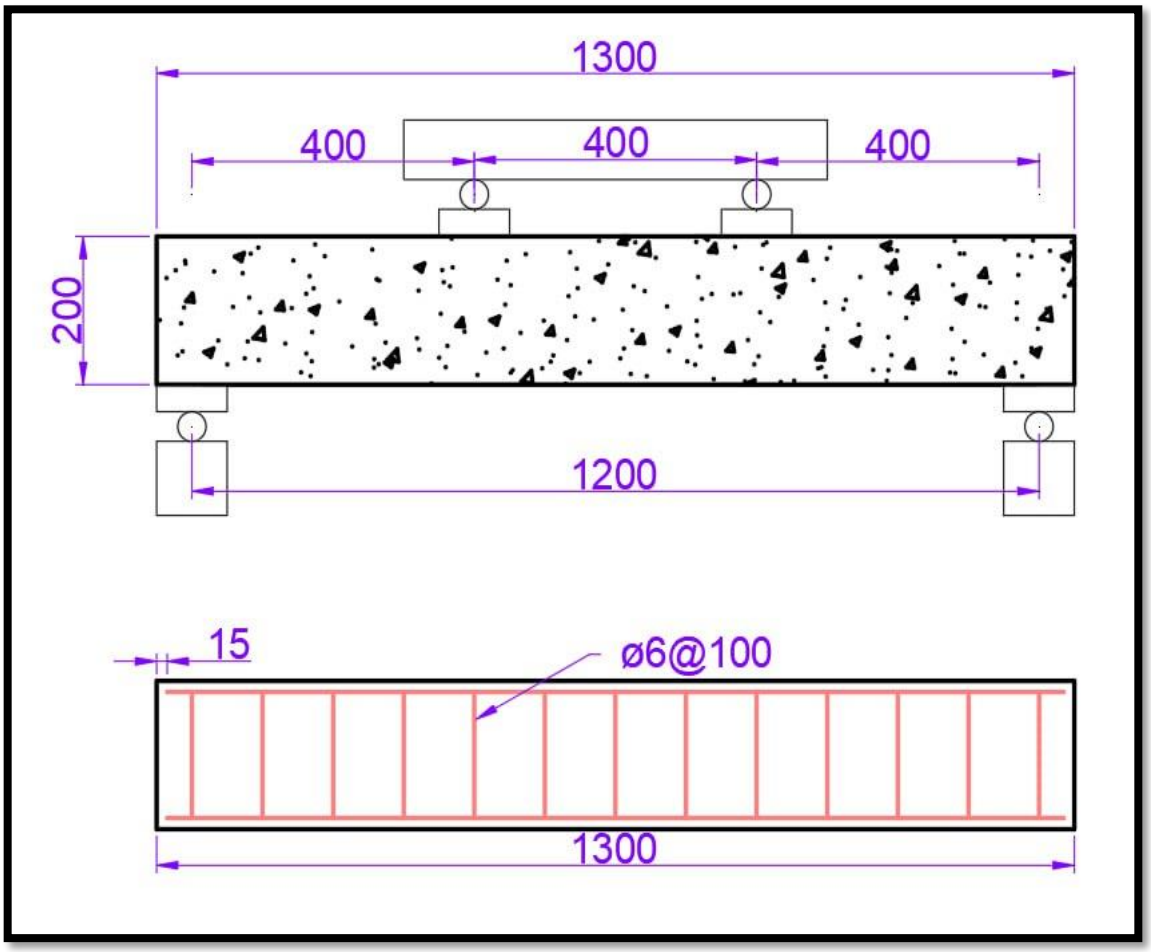

b) Stirrups and Reinforcement

Figure (3-1): Reinforcement and Test of Beam

3.2.1.2 Group Two Slab Specimens

Four two-way slab specimens were constructed and tested under central patch of (100x100) mm square plate load up to failure. The first and second slab consists of 7Ø6 bar in two-way these specimens are SG7 and SS7 for GFRP and steel rebars, respectively, with a reinforcement ratio of 4.5% and 3.8% respectively GFRP and Steel. The third and fourth slab consists of 14Ø6 bar in two-way these specimens are SG14 and SS14 for GFRP and steel rebars, respectively, with a reinforcement ratio of9 % and 7.5% respectively for GFRP and Steel as shown in Figure (3-2).

The main parameters studied were the effect of flexural reinforcement spacing on the punching shear strength. The concrete strength was kept constant at around 30 MPa. The concluded specimens were a square of 1100 mm long in both directions with a thickness of 70 mm. Simple support was used for all specimens acting on all four edges with a clear span of 1000 mm. A patch load was then applied to the slab by loading a square steel plate of cross-section (100*100) mm and with 20mm thickness.

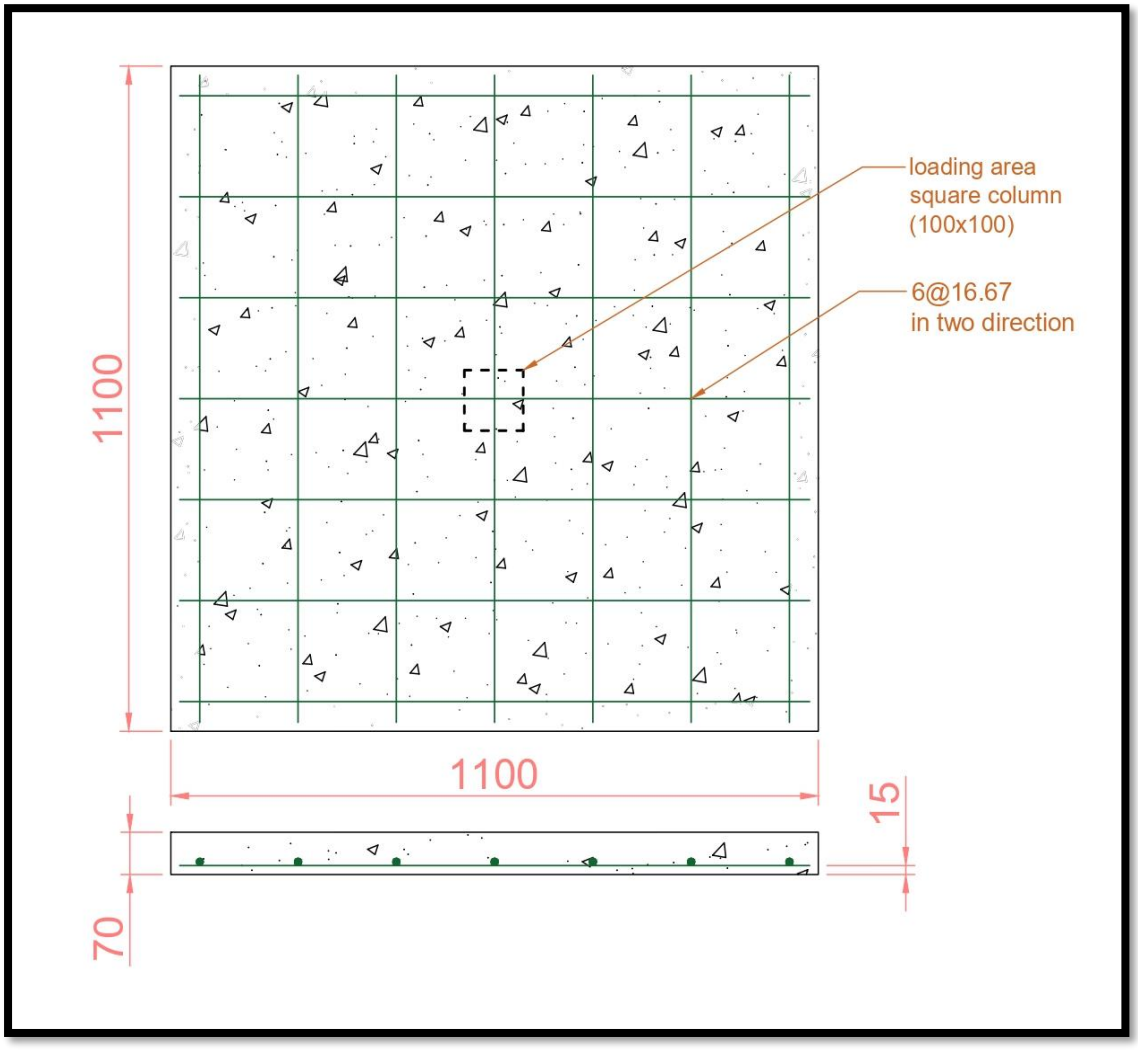

a) Specimens SG7 and SS7

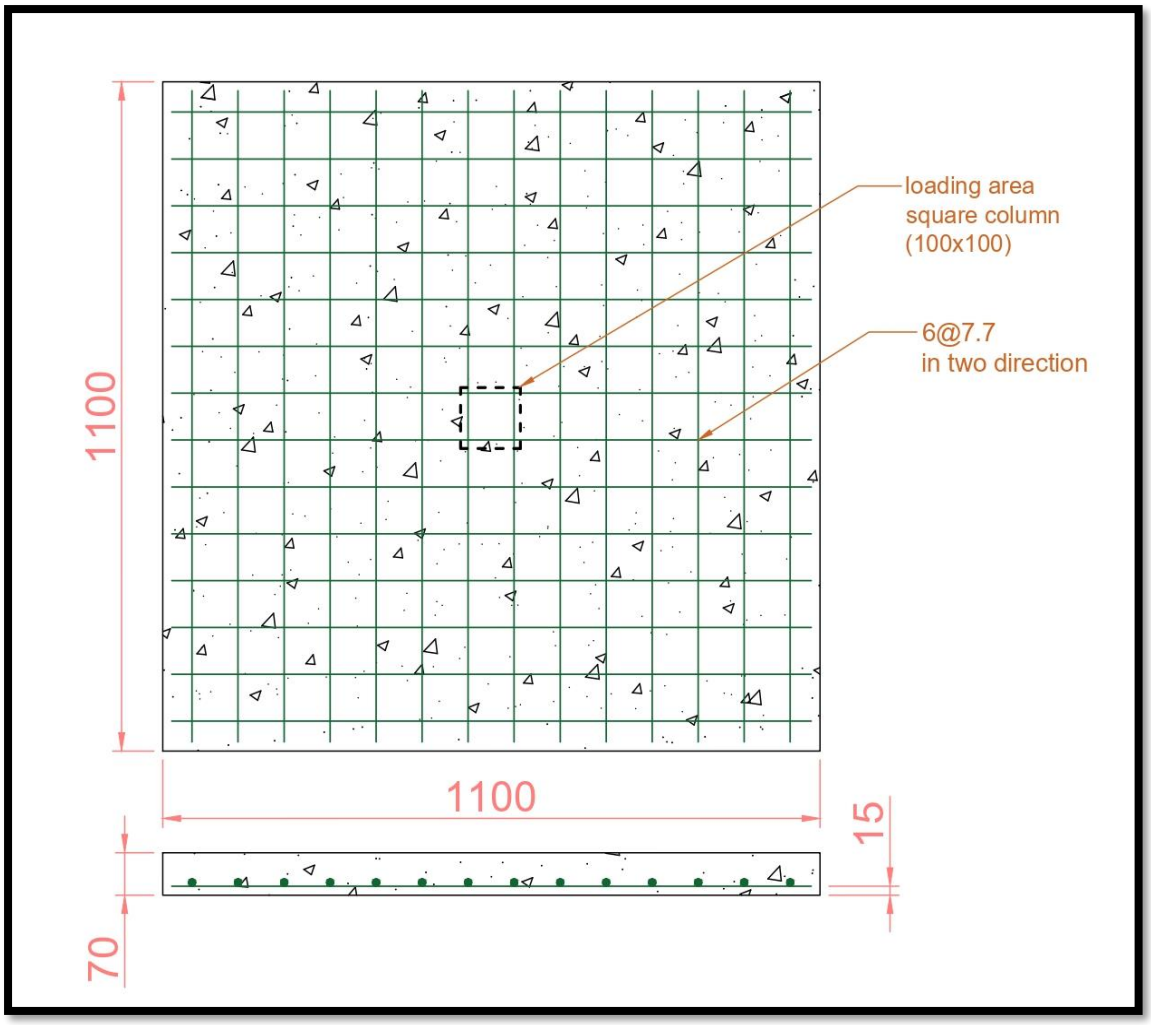

b) Specimens SG14 and SS14

Figure (3- 2) Geometry Reinforcement of Slabs' Specimens

3.2.1.3 Group Three Bond Slip Specimens

The test specimens consisted of six cubes. Pull-out specimens were reinforced with three GFRP and three steel re-bars. The geometrical dimensions of the pull-out cube of 200 mm side to this is according to ACI-440 [2] as shown in Figure (3-3) The main parameters investigated in pull-out cubes were bar diameter (6 mm for GFRP bar and steel bar) and embedment length (5, 7.5, and 10, times bar diameter). Surface texture for GFRP bar was helical wrapping

testing pull-out. The bar location in the concrete cube was centric. The influence of these factors on bond strength were analyzed and discussed to deeply understand the bond behavior between GFRP re-bars and concrete.

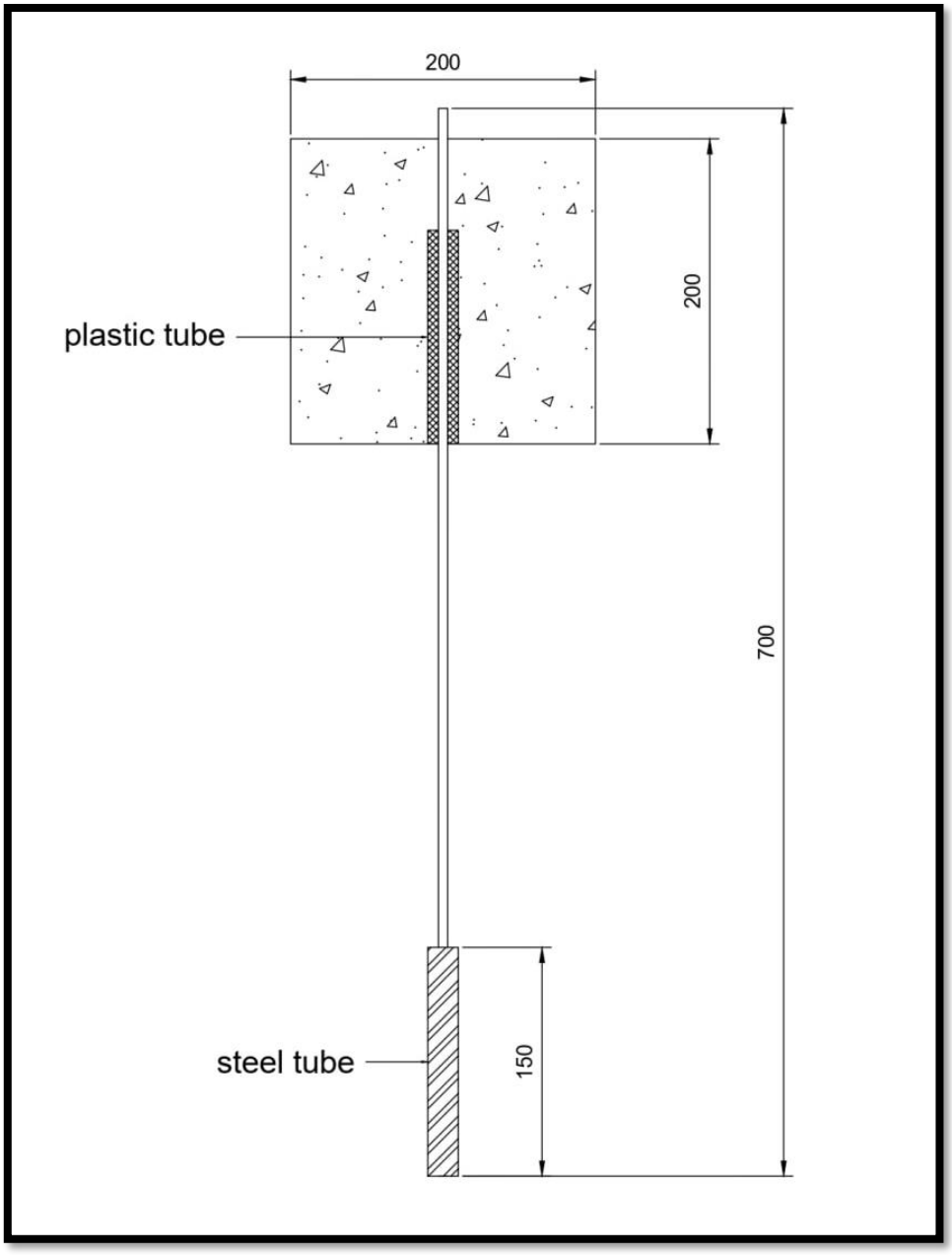

Figure (3-3) Pull-Out Cube Bond

3.3 Material of The Experimental Work

3.3.1 Concrete

The materials used in producing concrete are locally available materials, which includes cement, natural gravel, natural sand, and water. A C30 grade concrete was used for the whole experimental works.

3.3.1.1 Cement

Ordinary Portland cement (Iraqi manufactured by Karasta) is used in this study for casting all specimens and concrete testes. Its chemical composition and physical properties supplied by the manufacturer as given in Table (3-1) and Table (3-2), respectively, and it conforms to the Iraqi specification (IQS No. 5/2019) [35].

Table (3-1): Chemical analysis and main compounds of cement.

Chemical composition	Item	Test Result (%)	Limits of Iraqi specification No.5/2019
Silicon oxide	SiO_2	20.58	-
Aluminum oxide	Al_2O_3	5.6	-
Ferric oxide	Fe_2O_3	3.28	-
Calcium oxide	CaO	62.79	-
Magnesium oxide	MgO	2.79	≤ 5.0%
Sulphur trioxide	SO_3	2.35	≤ 2.8%
Loss of ignition	L.O.I	1.94	≤ 4.0%
Insoluble residue	I.R	1	≤ 1.5%
Lime saturation factor	L.S.F	0.9	0.66-1.02

Main compound composition			
Tri-calcium silicate	C3S	50.12	-
Di-calcium silicate	C2S	21.26	-
Tri-calcium aluminate	C3A	9.29	-
Tetra-calcium aluminate ferrite	C4AF	9.98	-

Table (3-2): Physical properties of cement.

Item	Test Result	Iraqi specification No. 5/1984
Blaine fineness (m2/kg)	314	≥ 230
Compressive Strength (MPa) 3 days 7 days	 20.8 28.0	 ≥ 20 ≥ 23
Time of setting (Vicat) Initial (hours: minutes) Final (hours: minutes)	 2:05 4:20	 ≥ 00:45 ≤ 10:00 hrs

3.3.1.2 Fine Aggregate (Sand)

Natural sand of 4.75 mm maximum size was used in this investigation. Before being ready to use, the sand was washed and cleaned by water several times, later it was spread out and left to dry in air to avoid the humidity saturation which may affect the water content extensively. Table 3-3 shows grading and properties of fine aggregate, which conforms to the Iraqi standard specification (IQS No.45/1984) [36]

Table (3-3): Fine aggregate grading and properties

Sieve's opening size	passing %	
	Fine aggregate	Iraqi specification No.45/1984
10 mm	100	100
4.75 mm	92	90-100
2.36 mm	81	75-100
1.18 mm	73	55-90
600 μm	55	35-59
300 μm	24	8-30
150 μm	7	0-10
SO3 content=0.35% (specification requirements up to 0.5%) Fineness modulus = 2.68		

3.3.1.3 Coarse Aggregate (Gravel)

A maximum size of 14 mm of local gravel was used in the current study. The gravel waswashed and cleaned by water several times and left to dry in air. Table 3-4 shows grading and properties of the coarse aggregate, which conforms to the Iraqi standard specification (IQ. S No.45/1984) [36].

Table (3-4): Coarse aggregate grading and properties

Sieve size (mm)	Passing %	
	Coarse aggregate	Iraqi specification No.45/1984
19	100	100
14	96	95-100
10	46.6	8-50
5	5.1	0-10
2.36	0.2	-------
SO3 content=0.07% (specification requirements up to 0.1%)		

3.3.1.4 Mixing Water

Tap water has been used for casting and curing all the beam specimens as well as forwashing the fine and coarse aggregates.

3.3.2 Reinforcing Bars

Tensile test was carried out on Ø6 mm mild deformed steel bars. Three samples for each size were tested، at the material laboratory of Kerbala University. The main properties of the reinforcing bars are presented in Table (3-5) and it is in agree with the standard specification ASTM A615 [37]. The digital machine used for testing steel bars is shown in Figure (3-4). GFRP bars with a diameter of 6 mm were used. The surface texture is helical wrapped Ultimate Strength (896 MPa), as shown in [Appendix B].

Table (3-5): Test results of reinforcing bars.

Bar Material	Diameter (mm)	Area (mm^2)	Tensile modulus (GPa)	Yield stress (MPa)	Ultimate Strength (MPa)
GFRP	6.35 (6)	31.67	46	———	896
Steel	5.8 (6)	26.42	200	514	535
Values between brackets based on nominal diameter					

Figure (3-4): Testing Machine of Steel Reinforcement.

3.4 Preparation of Specimens

3.4.1 Mix Design

3.4.1.1 Concrete Mix Design

To select the mixture proportion for normal weight concrete with target compressive strength of 30 MPa at 28 days. The selected mixture for casting all beam specimens was (1 cement: 1.73 sand: 2.2 gravel, by weight). The average compressive strength f_{cu} at 28 days was 37.5 MPa. Table (3-6) shows the mixture proportions (by weight) of the selected concrete mix.

Table (3-6): Mixture proportions for the selected concrete mix.

Materials	The selected concrete mix
Water/cement ratio	0.47
Water (kg/m3)	207
Cement (kg/m3)	423
Fine aggregate (kg/m3)	732
Coarse aggregate (kg/m3)	934

3.4.2 Mix Procedure

3.4.2.1 Mix The Normal Concrete Procedure

The mixing procedure was as follows:

1. All quantities of construction materials were weighed and packed in clean containers prior to mixing.
2. Before placing the materials, the mixer's interior surface was cleaned and moistened and making sure that do not contain any amount of water.
3. The coarse and fine aggregate is stocked in a horizontal rotary mixer with a capacity of (0.04 m^3) and mixed in (2/3) of the required water for (1) minute and then the cement and rest water added and mixed for (3) minutes.
4. Finally, the concrete was slightly poured into oiled wood molds.

3.4.3 Placement of Reinforcement, Casting and Curing Process

The specimens were reinforced with steel bars and GFRP bars. Wooden mold was used for casting the specimens as shown in Figure (3-5). Oil was rubbed on the inner surface of the moulds to enable easy exit of the specimen after setting. The reinforcement was detailed and bonded together by wires to form the designed reinforcement. The reinforcement was inserted into the moulds with spacer attached to achieve the concrete cover of 15mm. Each specimen beam and slab were cast in one layer, and then vibrated by a steel vibration rod to make sure that the concrete was adequately condensed and no segregation would occur, as shown in Figure (3-6). The specimens were removed from the moulds after 48 hours and inserted into curing tank containing water at a temperature of 20±2°C. After 28days curing the specimens were ready for testing.

a) Wooden Mode and Reinforcement of Slabs

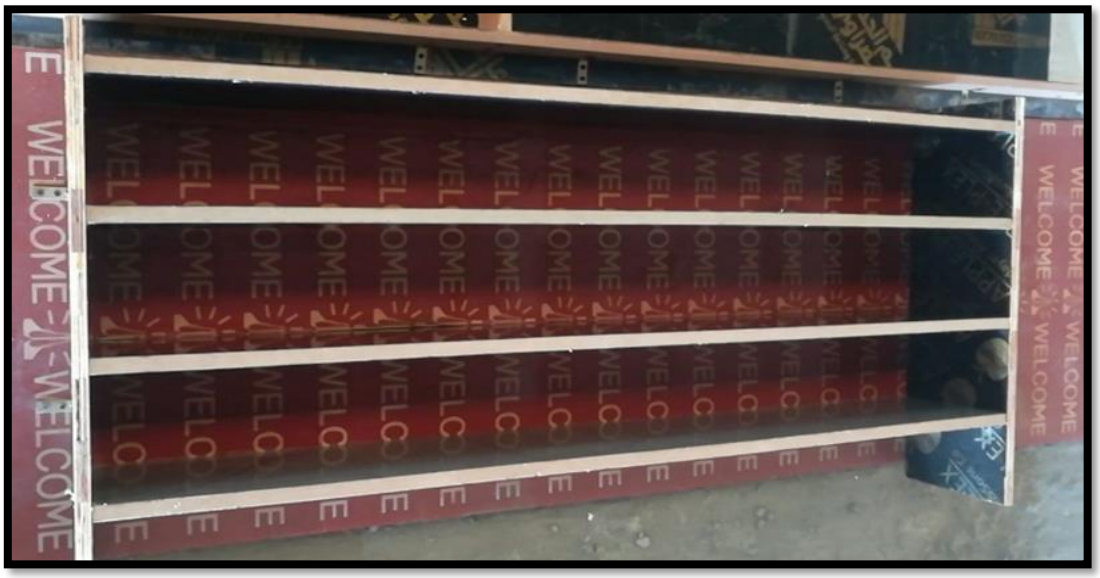

b) Wooden Mode of Beams

Continued

Continues

c) Rebars Cage

Continued

Continues

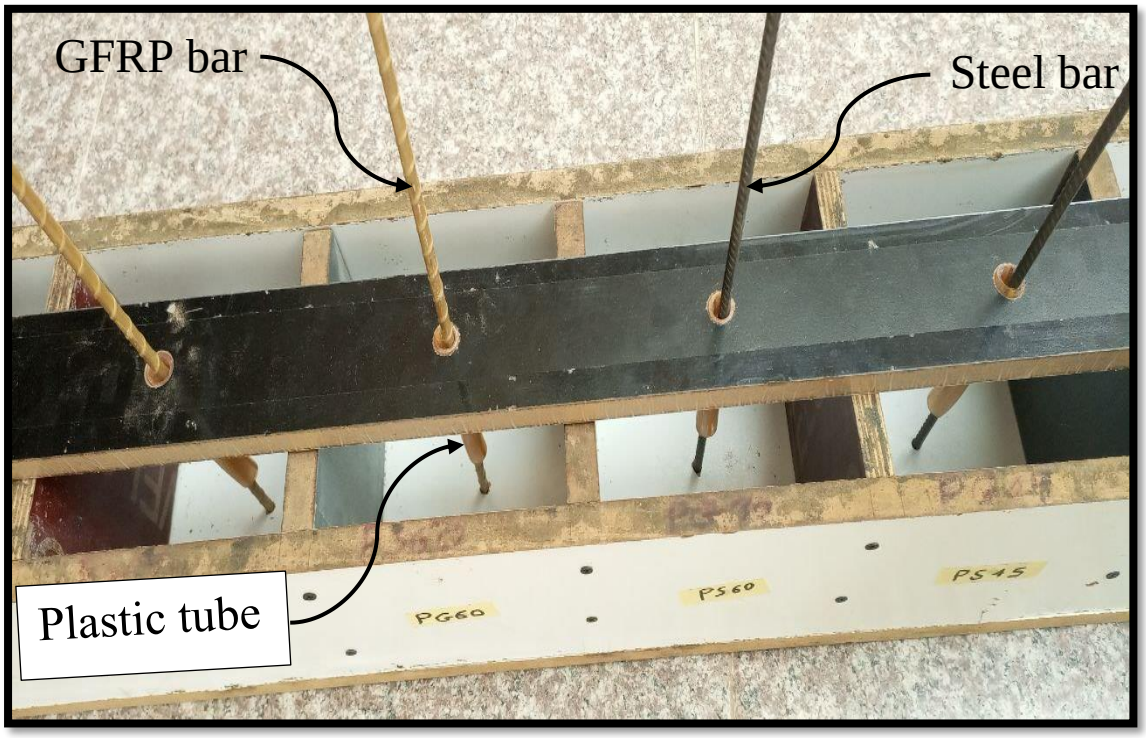

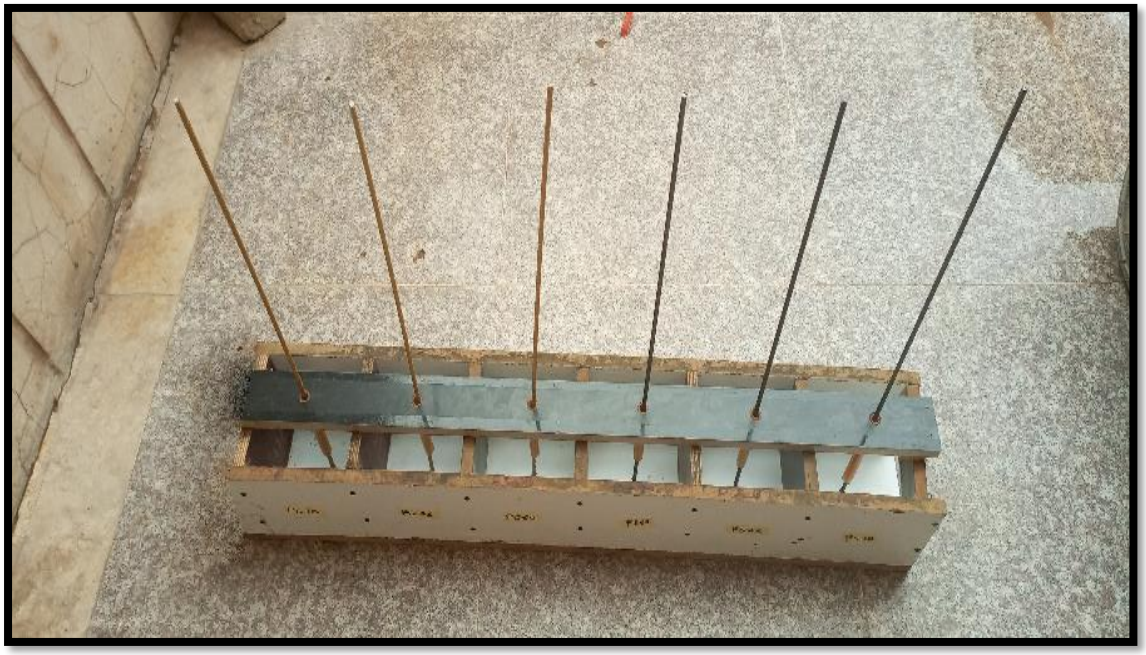

d) Pull-out setup

Figure (3-5) Wooden Mold and Reinforcement

Continued

Continues

Figure (3- 6) Casting and Compacting of Concrete by External Vibrator.

3.5 Mechanical Properties of Hardened Concrete

3.5.1 Compressive Strength (f_{cu})

The concrete cube compressive strength of control samples (f_{cu}) was obtained according to the British Standard BS1881-part 116:1989 [38]. The tests were carried out at the structural laboratories of Kerbala University. Six cubes of (150×150×150) mm were tested at 28 days by using hydraulic compression testers for cubes with a capacity of 2000 kN, capacity ELE digital machine, as shown in Figure (3-7). The load was applying perpendicular to the direction of casting at rate of 0.3 MPa per second.

Figure (3-7) Compressive Strength Machine.

3.5.2 Modulus of Rupture (Flexural Strength Test)

Concrete prism specimens of dimensions (100×100×400) mm were tested with third-point loading according to ASTM C78-2010 [39]. All prisms were tested at 28 days using a universal flexural testing machine with a capacity of 150 kN, the rate of load was 1 MPa per minute. Figure (3-8) shows the modulus of rupture test setup. An average of three samples was adopted in the calculations. The following formula was applied to determine the modulus of rupture:

$$fr = PL/bh^2 \quad \ldots\ldots (3\text{-}1)$$

Where:

f_r = modulus of rupture (MPa)

P = maximum applied load (N)

L= span length (mm)

b= width of specimen (mm)

h= depth of specimen (mm)

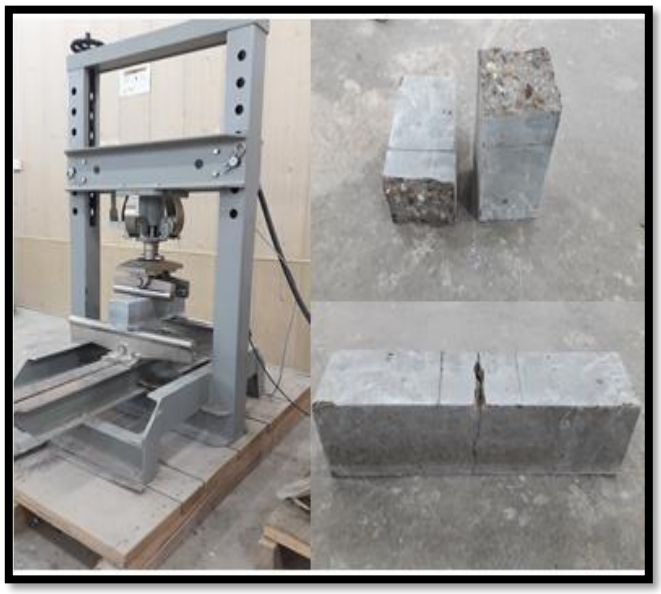

Figure (3-8) Flexural Tensile Test Setup

3.5.3 Splitting Tensile Strength (f_{sp})

The splitting tensile strength was carried out on cylindrical concrete specimens of 150 mm diameter and 300 mm height in accordance with ASTM C496-2011 [40], and an average of three samples was adopted in the calculations. The specimens were tested at 28 days by using hydraulic compression testers for cubes and cylinders with a capacity of 2000 kN, the rate of load was 0.018 MPa per second. Figure (3-9) shows the splitting tensile test setup. The splitting tensile strength was calculated from the following:

$$f_{sp} = \frac{2P}{\pi dL} \quad \ldots\ldots (3\text{-}2)$$

Where:

f_{sp} = splitting tensile strength (MPa)

P = maximum applied load (N)

d = diameter of cylinder (mm).

L = length of cylinder (mm)

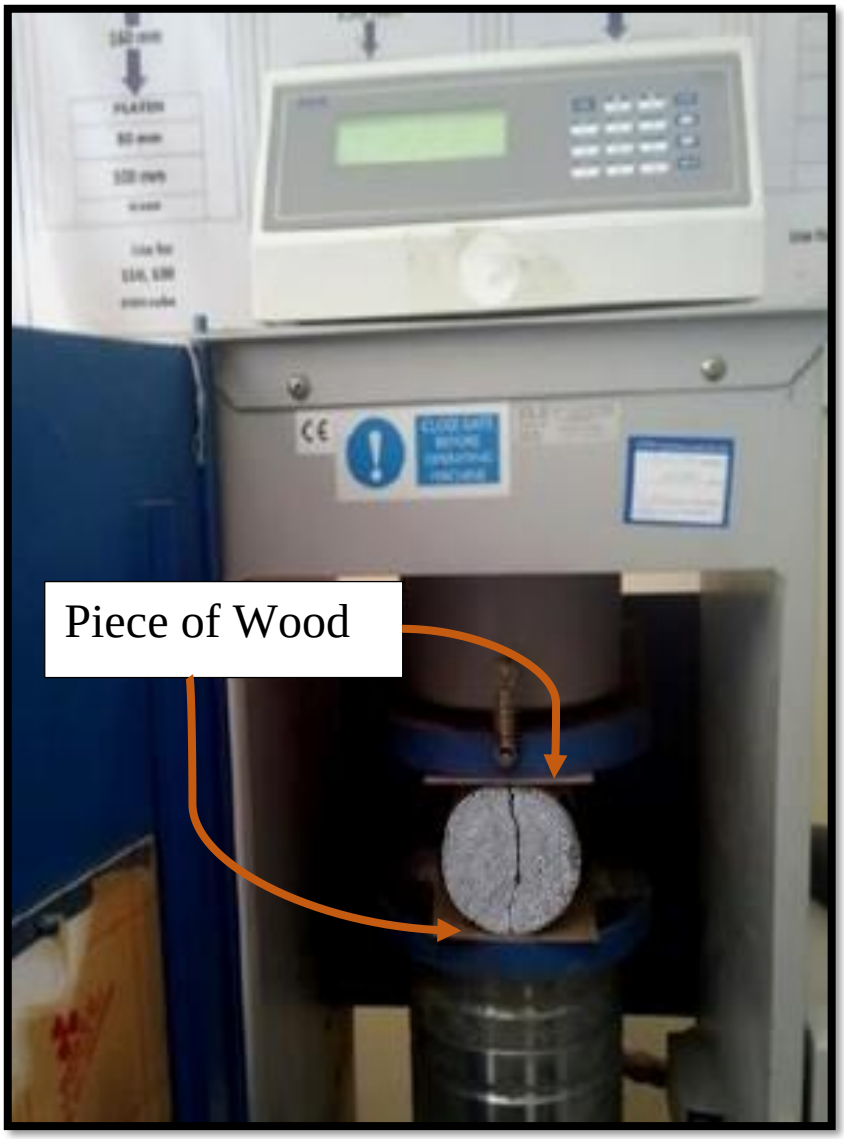

Continued

Continues

Figure (3-9): Splitting Tensile Test Setup

3.6 Test Procedure

3.6.1 Beams Testing

All beams were taken out from the curing water tank after 28 days, left to dry, and then painted with white color, so that cracks can be easily detected. The composite concrete beams were tested up to failure by using the testing machine under monotonic loads, and repeated loads as shown in Figure (3-10). The beams were loaded with four-point loads. The applied loads were distributed on beam by using steel plates under hydraulic jack. The loads were applied in successive increments up to failure. In every 5 kN step, the mid span deflection was recorded.

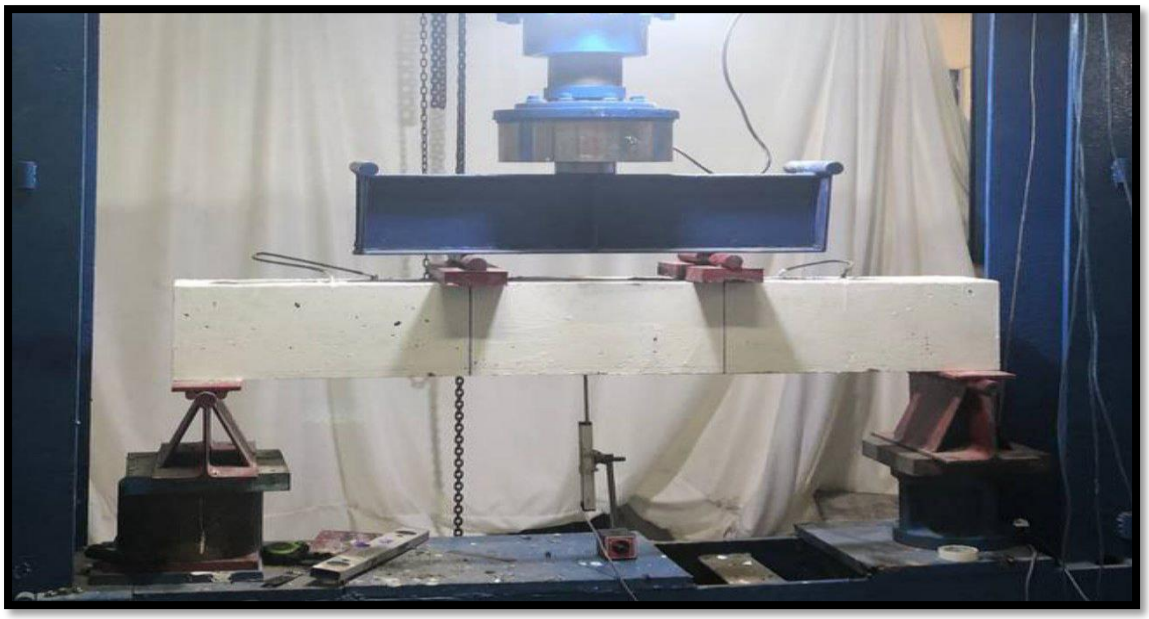

Figure (3-10) Test of Beam

All the test was conducted in the concrete laboratory of the civil engineering department – University of Kerbala. A universal testing machine with (2000 kN) loading capacity designed and manufactured for the structural loading test was used for the experimental testing program. The machine is equipped with electronically controlled gages (linear variable differential transformer -LVDT) and loading cells, which collects load, deflection data using a computerized system programmed by (LABVIEW) software.

All other sensors and load cells were linked to Lab VIEW 2018software. This program was used to translate the electric signals to mathematic value conversely. Also, data could be saved in the excel sheet directly. The coordinate system, which was used here, was a data acquisition (DAQ) type NI6052E. This device can read the signal from the sensors and translate it into the program. This program was able to read all sensors devices, namely; load cell, and LVDT's at the same time. Also, this program could display the data in the

mounter; when the values were being measured during the testing process, as shown in Figure (3-11).

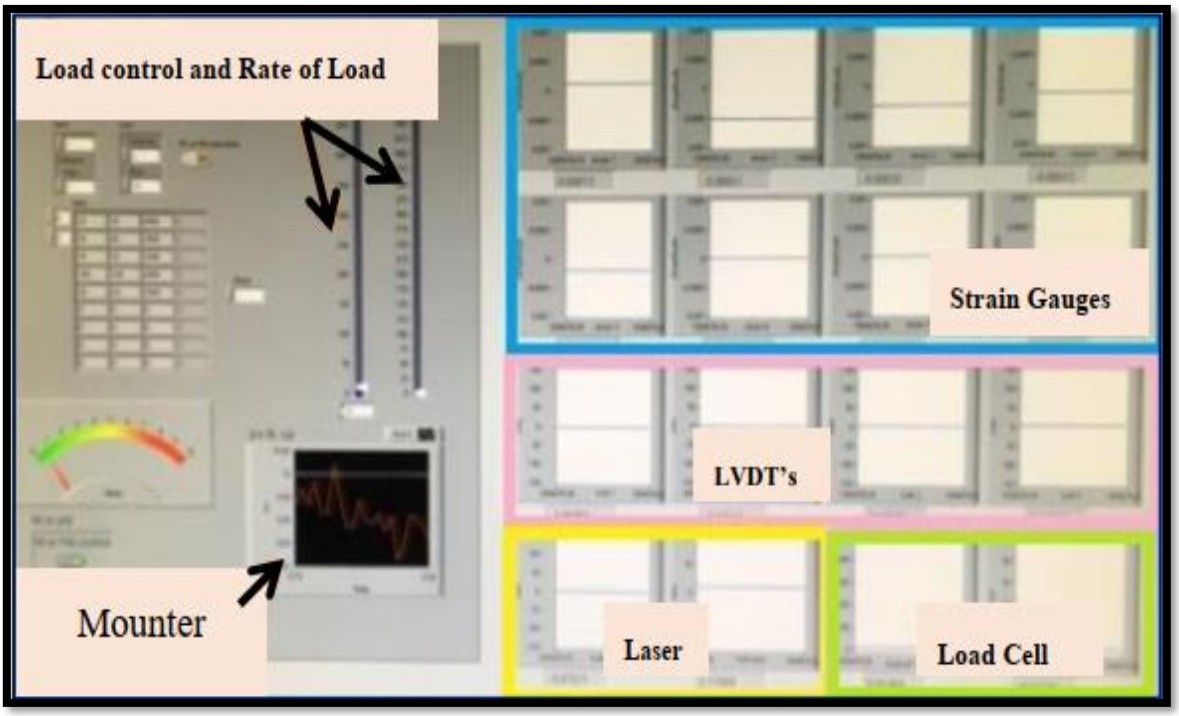

Figure (3-11) View of the Controlling Program

3.6.1.1 Design of flexural

Whether the FRP-reinforced flexural member is limited by FRP rupture or concrete crushing determines its flexural capacity. One may determine the governing limit state by comparing the FRP reinforcement ratio to the balanced reinforcement ratio (ρ_{fb}), a ratio where concrete crushing and FRP rupture occur concurrently. FRP does not yield, hence its design tensile strength is used to calculate the balanced ratio of FRP reinforcement. Equation (3-3) may be used to get the FRP reinforcement ratio, and Equation (3-4) can be used to determine

the balanced FRP reinforcement ratio. The FRP rupture limit state takes control if the reinforcement ratio is less than the balanced ratio ($\rho_f < \rho_{fb}$), if not, the limit state for concrete crushing takes control ($\rho_f > \rho_{fb}$).

Flexural strength nominal Concrete crushing is the governing limit state when ($\rho_f > \rho_{fb}$), and the ACI-440 [2] rectangular stress block may be used to approximate the stress distribution in concrete. The following can be deduced from the equilibrium of forces and strain compatibility shown in Figure (3-12). The nominal flexural strength may be calculated using Equations (3-5), (3-6) and (3-7). Since the FRP reinforcement is linearly elastic at the concrete crushing limit state, Equation (3-7) may be used to calculate the stress level in the FRP since it is smaller than f_{fu}.

When ($\rho_f < \rho_{fb}$), it is possible to compute the nominal flexural strength at a section using the formula in Equation (3-8), with the rupture of the FRP reinforcement serving as the regulatory limit state. The analysis has two unknowns despite the fact that the stress in the reinforcement is known: the distance from the neutral axis c and the concrete compressive strain at ultimate when the FRP ruptures in tension (εc). The analysis gets complex and challenging to solve using a closed-form solution when these unknowns are present.

The maximum concrete strain ($\varepsilon c < \varepsilon cu$) may not be obtained, hence the ACI [2] equivalent rectangular stress block criteria are also not applicable. Based on the material properties and the FRP reinforcement ratio, the product of $\beta 1c$ in Equation (3-8) varies for a specific section. When the maximum concrete strain (0.003) is reached for a segment controlled by the limit state of FRP rupture, the maximum value for this product, which is equivalent to $\beta 1c_b$, is reached.

Therefore, a more precise and conservative lower bound for the member's nominal flexural strength may be determined using Equations (3-9) and (3-10).

The fiber percentage ratio is:

$$\rho_f = \frac{A_f}{bd} \tag{3-3}$$

While the balance ratio is:

$$\rho_{fb} = 0.85\beta_1 \frac{f_c'}{f_{fu}} \frac{E_f \varepsilon_{cu}}{E_f \varepsilon_{cu} + f_{fu}} \tag{3-4}$$

According to that the nominal bending strength can be written:

$$M_n = A_f f_f (d - \frac{a}{2}) \tag{3-5}$$

From which

$$a = \frac{A_f f_f}{0.85 f_c' b} \tag{3-6}$$

Also, the strength in the fiber

$$f_f = \left(\sqrt{\frac{(E_f \varepsilon_{cu})^2}{4} + \frac{0.85\beta_1 f_c'}{\rho_f} E_f \varepsilon_{cu}} - 0.5 E_f \varepsilon_{cu} \right) \leq f_{fu} \tag{3-7}$$

$$M_n = A_f f_{fu} \left(d - \frac{\beta_1 c}{2} \right) \tag{3-8}$$

$$M_n = A_f f_{fu} \left(d - \frac{\beta_1 c_b}{2} \right) \tag{3-9}$$

$$c_b = \left(\frac{\varepsilon_{cu}}{\varepsilon_{cu} + \varepsilon_{fu}} \right) d \tag{3-10}$$

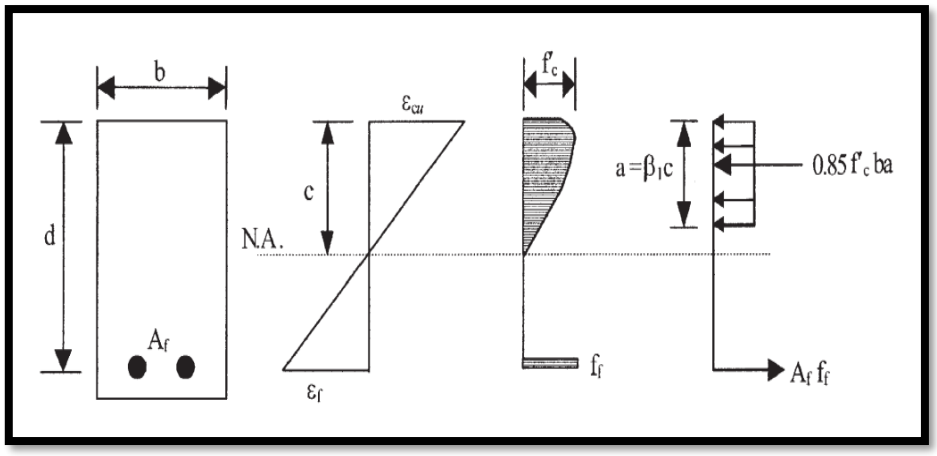

(a) Failure Governed by Concrete Crushing

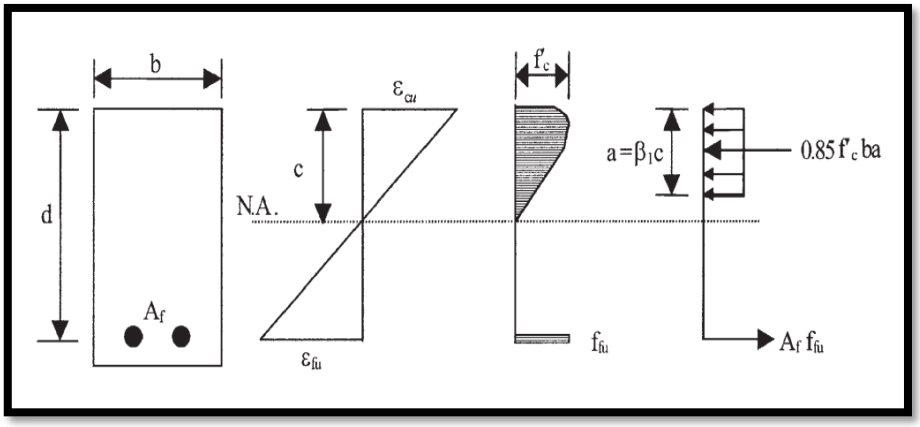

(b) Balanced Failure Condition

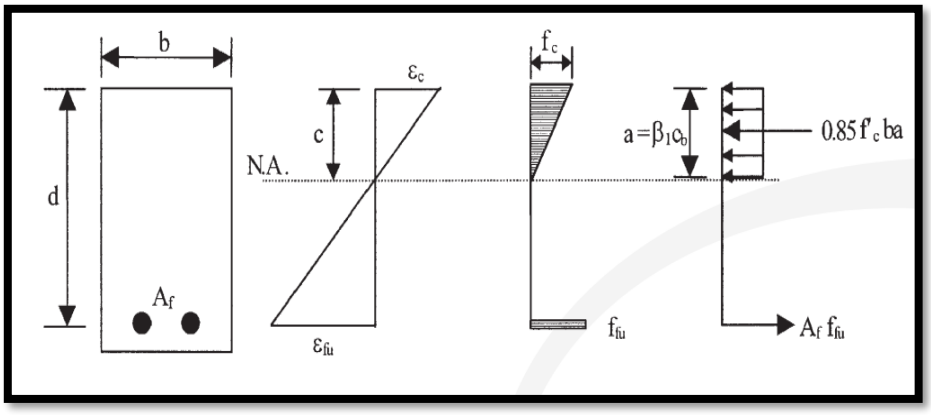

(c) Failure Governed by FRP Rupture (Concrete Stress May Be Nonlinear)

Figure (3-12) Strain and Stress Distribution at Ultimate Conditions.[2]

3.6.2 Slab Testing

Each slab was tested by applying load up to failure. The tested specimens were tested by applying a load at the center of slab by a solid segment of steel with dimensions (100 * 100 * 20 mm) as shown in Figure (3-13). All specimens were examined by simple support for all support. The simple support of the tested concrete slab was applied by solid rod and rigid steel bases as shown in Figure (3-14).

Figure (3-13) slab specimen and Steel Plate

Figure (3-14) Simple Support frame for the specimens

The compatibility of the concrete and the reinforcement causes them to deflect together under load. The load-deflection curves were obtained using LVDT measures to the limit (100 mm) with (0.01 mm) accuracy. For all the tested specimens, LVDT was used to measure the displacement at center of the specimens as shown in Figure (3-15).

Figure (3-15) LVDT in Mid Span of the specimens

The applied loads cause the plate to fail in punching shear, flexural tension, or concrete crushing. four plates (1100*1100*70 mm) were tested by a bounded load test; each plate was loaded to fail and the deflection was recorded as shown in Figure (3-16).

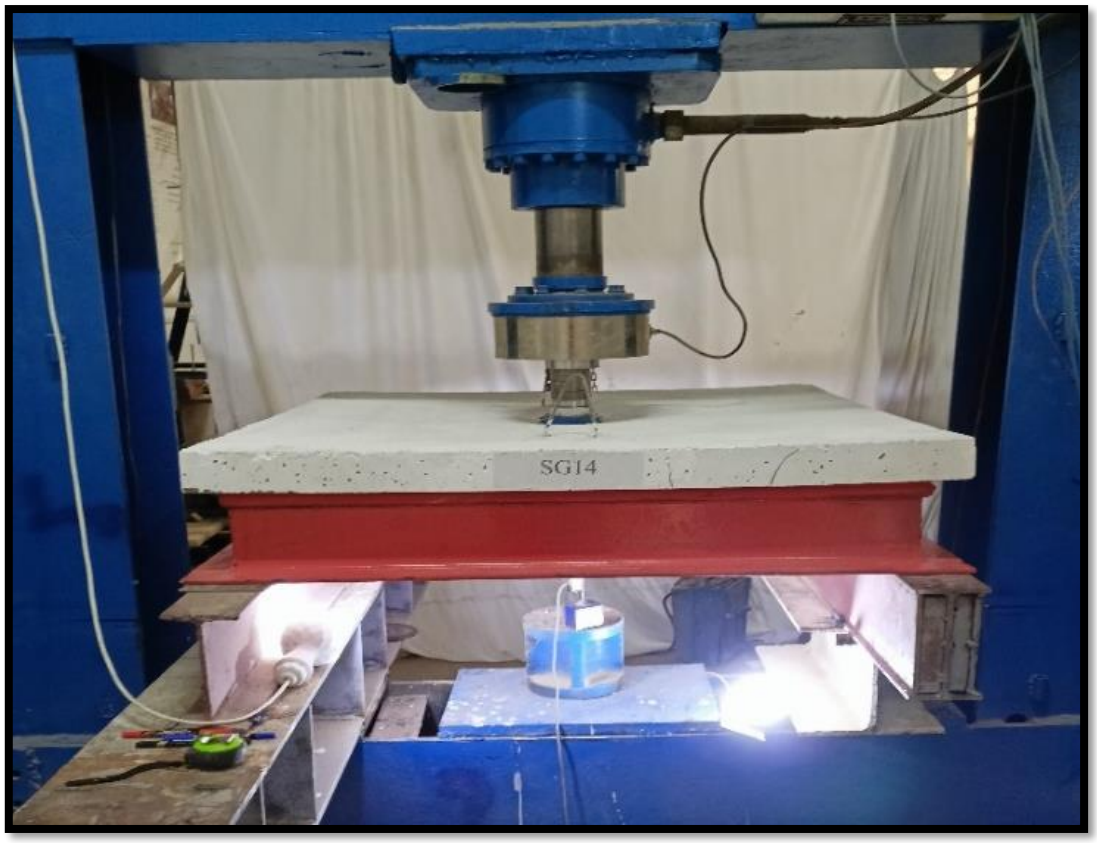

Figure (3-16) Test of Slab

Immediately prior to testing, zero readings of all the measuring devices were taken and recorded. The axial load was increased in small increments till failure. The locations of the crack were marked. The extension of a crack at any particular load was indicated by the axial load at which the extension of the crack was occurred.

3.6.3 Bond Testing

The wooden molds with sizes of (200x200x200mm) was made to cast concrete cubes. The FRP bars were positioned vertically and centrally in the molds and passed through a circle hole at the bottom and top of the molds to

hold the bars as shown in Figure (3-17). The concrete has been placed in four layers of approximately equal thickness, and rode each layer 25 times with a 16 mm-diameter tamping bar. The casting direction was parallel to the bar in cubes. Before casting, the inner sides of molds were covered by a thin film of oil to ease demolding of the specimens.

The pullout test is shown in Figure (3-18) The concrete cube with the embedded bar was placed in a specially made steel frame that was positioned in the testing machine. The device consisted of two steel plates 25 mm thick, which were connected at the four edges with four rods 20 mm in diameter. The bottom plate had a hole 30 mm in diameter in its center allowing the GFRP bar to run through. On this plate were three additional holes in a triangular arrangement around the main hole, which allowed three linear voltage displacement transducers (LVDT), located at the loaded end of the specimen, to touch the top surface of the concrete cube as shown in Figure (3-19a). A fourth LVDT was attached on a small aluminum frame that was glued to the bottom surface of the concrete cube to measure the slip at the free unloaded end of the bar as shown in Figure (3.19b). In Figure (3-20), the LVDT holder is shown. The top end of the device was secured in the jaws of the testing machine, which provided the reaction to the pullout load resisted by the specimen.

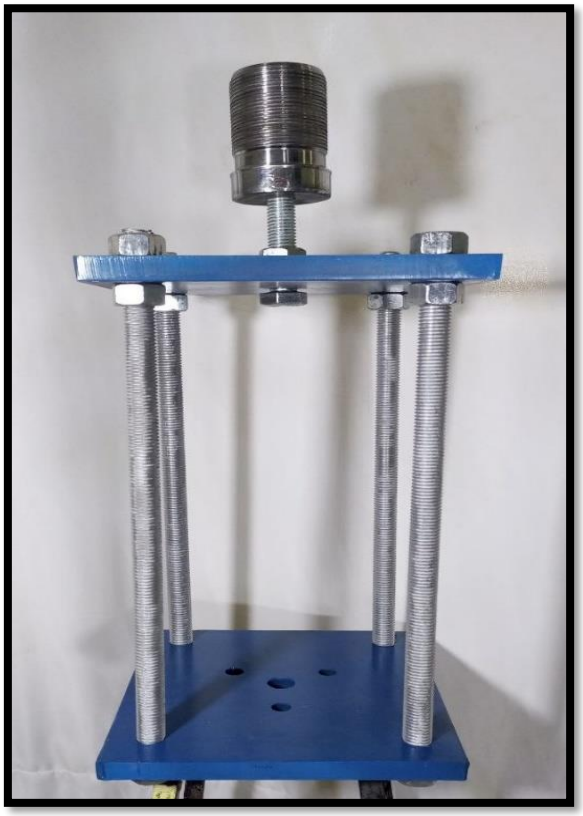

Figure (3-17) Frame of Pullout Testing

Figure (3-18) Testing of Pullout

a) LVDTs in the Loaded End

b) LVDT in the Free End

Figure (3- 19) Location of LVDTs

Figure (3-20) LVDT Holder

Figure (3-21) Wooden Board

Between the concrete block and the bearing steel plate, a 5-mm-thick wooden plate was introduced to secure the contact between the top surface of the concrete block and the steel bearing plate as shown in Figure (3-21). This was necessary because small irregularities at the top surface of the cube might introduce accidental bending on the bar during loading or movements caused by local crushing. The test specimen was positioned in a testing machine, [The load should be applied to the reinforcement bar at a rate not greater than 20 kN/min or at the no-load speed of the testing machine head of not greater than 1.3 mm/min, depending on the type of testing machine used and the means provided for ascertaining or controlling testing speed] ACI 3R 04 [41].

As shown in Figure (3-22), the ends of GFRP bar specimens were embedded into steel tubes filled with epoxy sikadur-330 at a 4:1 ratio of component A to component B as shown in Figure (3-23). This facilitated gripping of the bar specimens. The anchor tube is then threaded or gripped by the base of the testing machine as shown in Figure (3-24). Steel tubes are 20mm diameter and 150 mm length, and the inside gradation for hollow tubes is 8, 10, 12, 14, and 16 mm. Each gradient is 30 mm long.to prevent slippage between the epoxy and the tube.

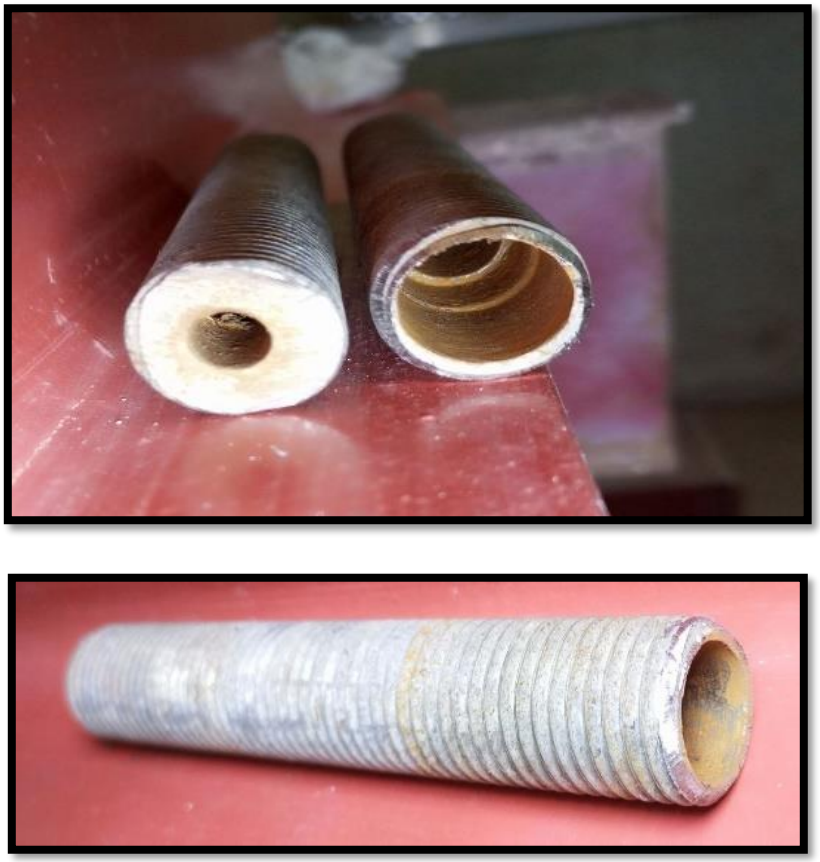

Figure (3-22) the Inside Gradation for Hollow Tube

a) The Epoxy used Inside the Hollow Tube

Continued

Continues

b) Tube to Fill by Epoxy

Figure (3-23) Tube and Epoxy

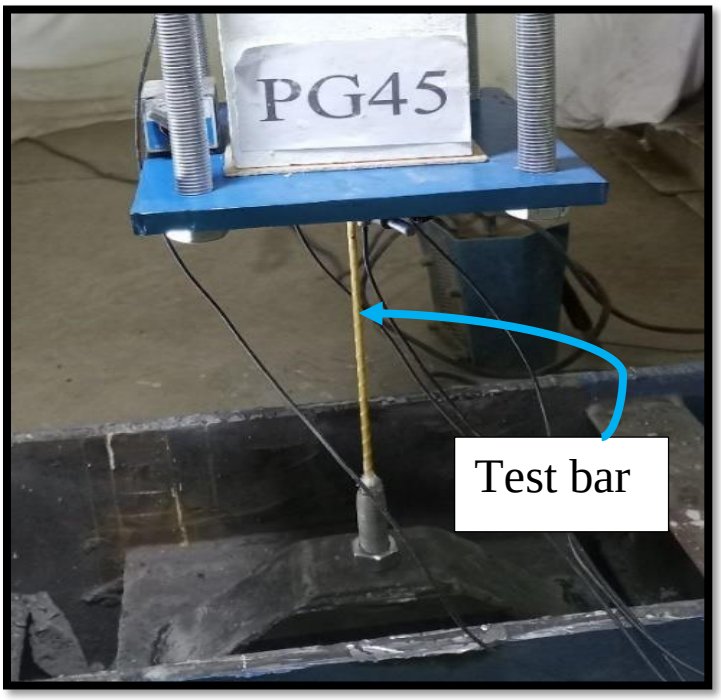

Figure (3-24) Connect the Tube to the Base of the Test Machine.

Chapter Four

CHAPTER FOUR

RESULTS AND DISCUSSION

4.1 Introduction

This chapter contains the detailed observations experienced during the beam test, pull-out test, and slab test. The main objectives of the study were to determine flexural behavior of beams and punching behavior of slabs reinforced with steel and GFRP as well, the bond behavior of steel and GFRP bars with concrete. Concrete of the same strength was used for the whole work.

First, the properties of hardened concrete obtained from tests of the control samples (cubes, cylinders, and prisms). Then, test results obtained from specimens are represented and discussed including, ultimate load, modes of failure, load-deflection response, and results of cracking behavior, and ductility are also attained.

4.2 Mechanical Properties of Concrete

After duration of curing, several tests are carried out on the control samples (cubes, cylinders, and prisms) to find the mechanical properties of the hardened concrete, which used to cast all the beam specimens. The average of three samples has been taken to calculate each value. Results show that, the

experimental values are always higher than the theoretical one, which provided by ACI-318 [43] code as shown in Table (4-1).

Table (4-1): Mechanical Properties of the Hardened Concrete.

Cube Compressive Strength f_{cu} (MPa)	Cylinder Compressive Strength f_c' (MPa)*	Splitting Tensile Strength (MPa)	flexural tensile Strength f_r (MPa)	Theoretical flexural tensile Strength fr (MPa)**	Theoretical Modulus of Elasticity Ec (MPa)***
37.57	30.05	3.01	4.72	3.39	25764

* $f_c' = 0.8 f_{cu}$ *(MPa)* according to (BS8110-1-97) [42] equation (4-1)

** $f_r = 0.62\sqrt{f_{c'}}$ *(MPa)* according to (ACI 318-19) [43] equation (4-2)

*** $E_c = 4700\sqrt{f_{c'}}$ *(MPa)* according to (ACI 318-19) [43] equation (4-3)

4.3 Test Result of Specimens

4.3.1 Beam Specimens

4.3.1.1 Ultimate Load Capacity

ACI-440[2], and ACI-318[43] predicted responses of the steel and GFRP beams that were more in line with the experimental results for maximum loads and midspan deflections at maximum loads code as shown in Table (4-2). the experimental maximum load for a beam with a 0.4 % reinforcement ratio, BS4, was 55 kN ACI318 [43] predicted a force of 45.5 kN [Appendix A] The maximum load was 17.27% over-predicted by the ACI318[43]. The experimental maximum load for beam BG4 with a reinforcement ratio of 0.48 percent was 111.42 kN The nominal loads estimated by ACI-440 [2] were 75.15 kN [Appendix A] The maximum load was 32.55% over-predicted by the

ACI-440 [2]. The experimental maximum load for beams BG2 with reinforcement ratio 0.25% was 52.47 kN the nominal loads estimated by ACI-440 [2] was 47.1 kN [Appendix A], the maximum load was 10.23% over-predicted by the ACI-440 [2]. Hence, the predictions of the GFRP were twice to the steel RC for a reinforcement ratio of 0.4% for both ACI [2,43]and experimental results, on the other hand, the predictions of the GFRP RC were equivalent to the steel RC for a reinforcement ratio of 0.24% and 0.48% respectively for both ACI-440[2], and ACI-318[43].

Table (4-2): Experimental Flexural Test Results

Spacemen	ρ%	Pu (kN)	Δu (mm)	Pcr (kN)	Δcr (mm)	Mode of failure
BS4	0.4	55.00	7.36	20	1.48	Flexure failure
BG4	0.48	111.42	14.90	20	2.03	Flexure failure
BG2	0.24	52.47	25.78	20	6.1	Flexure failure (Rupture failure)

4.3.1.2 Load Deflection at Mid-Span

Figure (4-1) shows the load-midspan deflection behavior for all tested beams of this group. Generally, the typical load-deflection curve can be divided into three stages: pre-cracking, post-cracking, and ultimate stage. In pre-cracking stage, vertical deflection increases linearly with loading for all specimens. After reaching cracking load, i.e., stage of post-cracking, there is also a linear relation between the load and vertical displacement but with different slopes up to yielding of longitudinal reinforcement. After this stage, there is a curvature in load deflection curve

up to failure, i.e., the slope of load deflection curve reduced largely with rapid increments in deflection, and slightly increases in loading until failure.

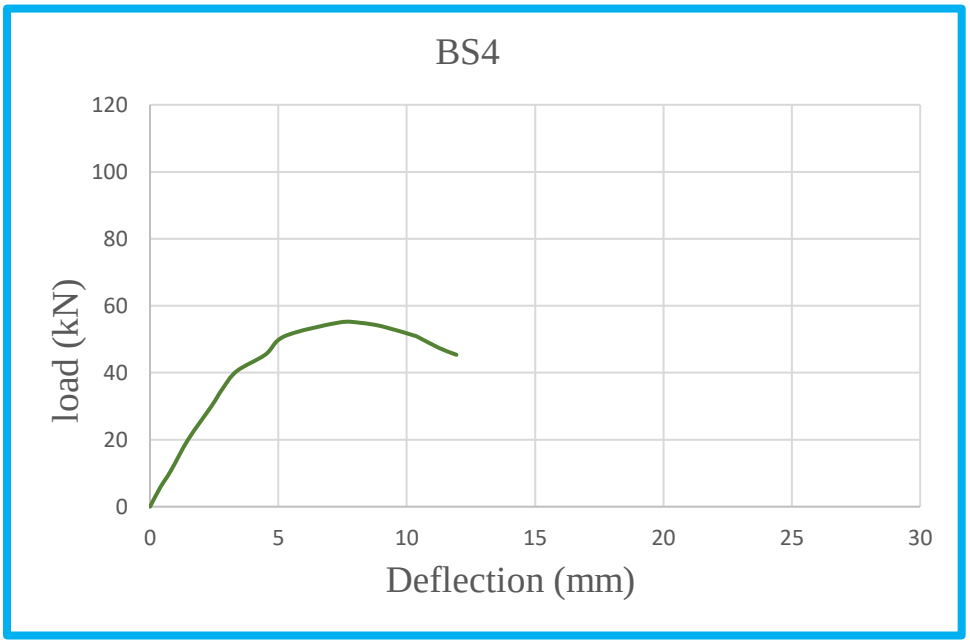

(a) BS4

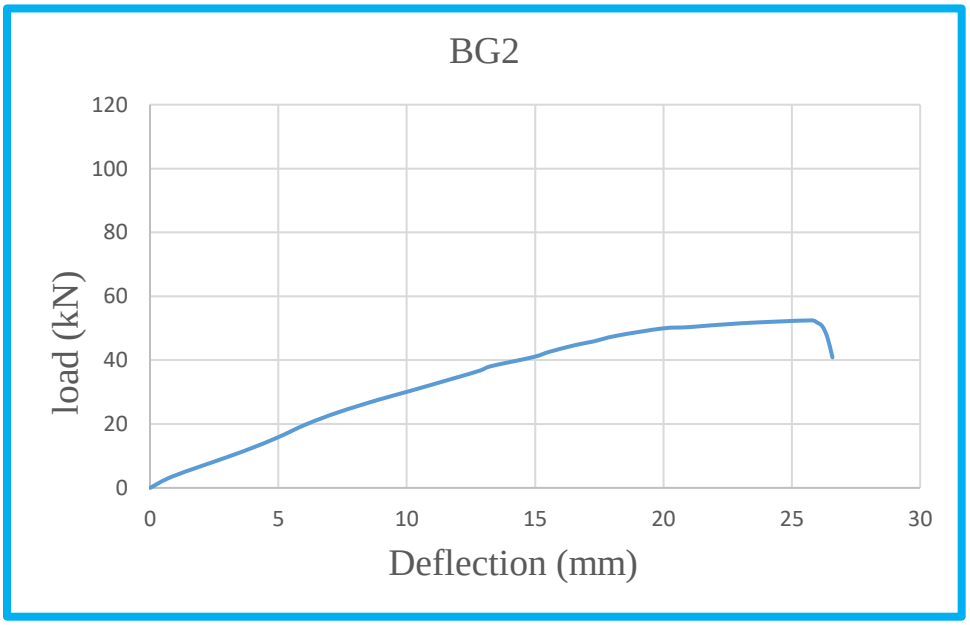

(b) BG2

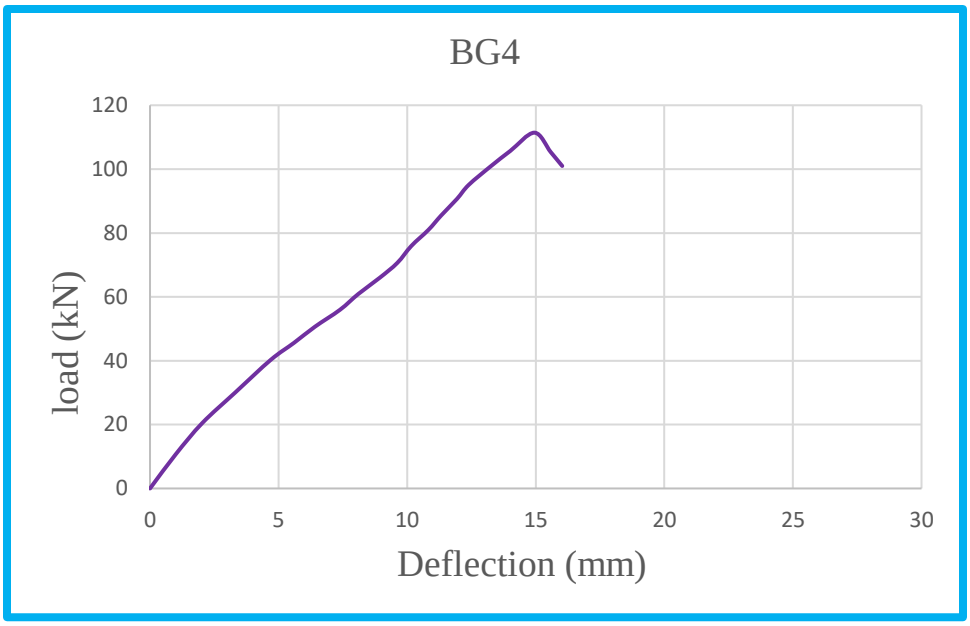

(c) BG4

Figure (4-1): Load Deflection Curve

4.3.1.3 Failure Modes

The ACI-440[2], and ACI-318[43] predicted the failure modes of GFRP and Steel beams. Beam BS4 with a reinforcement ratio (ρ_f/ρ_{fb}) of 0.1837 (less than 1) failed due to Steel bar break off, (calculated as per ACI-318 [43]). Beam BG2 with a reinforcement ratio (ρ_f/ρ_{fb}) of 0.7813 (less than 1) failed due to GFRP bar rupture, (calculated as per ACI-440 [2]). Beam BG4 with an over reinforced beams with reinforcement ratios (ρ_f/ρ_{fb}) of 1.5625 (higher than 1.4) failed due to concrete crushing on the compression side, the crushing failure for this specimen is not recognized clearly as it must be behaver according to ACI-440 [2]. The code predicted that beams with an over reinforcement ratio failure by crashing the concrete in the compression zone, while the actual failure occurred when cracks appeared in the tension zone, grew toward the load points, and finally flexural failure.

4.3.1.4 Cracking Behavior

Due to the lower modulus of the GFRP bars compared to steel, the flexural behavior of GFRP-reinforced concrete components displays less stiffness and wider cracks than that of concrete elements reinforced with steel at the same reinforcement ratio. Figure (4-2) shows load -crack width curve. The deflection and cracking under the service load therefore dictate the design of GFRP-reinforced concrete beams. Figure (4-3) shown the Crack width becomes unaesthetic when it is excessive and also results to problems that leads to degradation or damage of concrete. GFRP bars are resistant to corrosion unlike steel bars, this makes the extensive cracks attributed to GFRP reinforced beams to be tolerated when compared to steel reinforced beams when the basis for crack control is corrosion. Crack width consideration is important when creep rupture, shear effects and aesthetics are regarded.

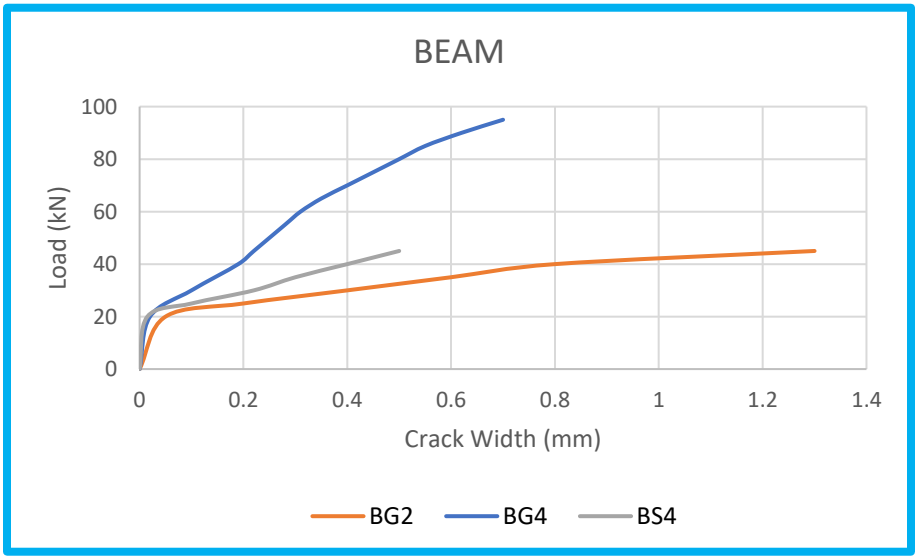

Figure (4-2) Load Crack Width Curve

From Figure (4-3) it can be conducted that the number of cracks for specimen with the same area of steel BS4 and BG4 are the same, but the crack width for

specimen BS4 is wider than for BG4. While the number of cracks is less for specimen BG2 this due to that the percentage of reinforcement is less. According to ACI 440 [2], if crack width is based on aesthetic conditions, an acceptable range from 0.4 to 0.7mm is adopted.

(a) BS4

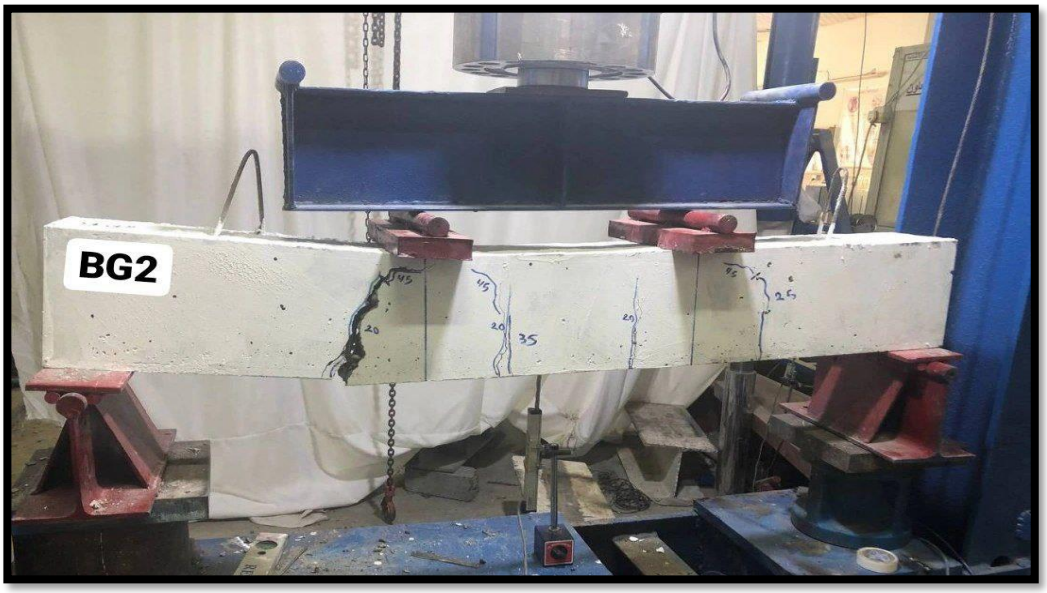

(b) BG2

Figure (4-3): cracking patterns beams (continues)

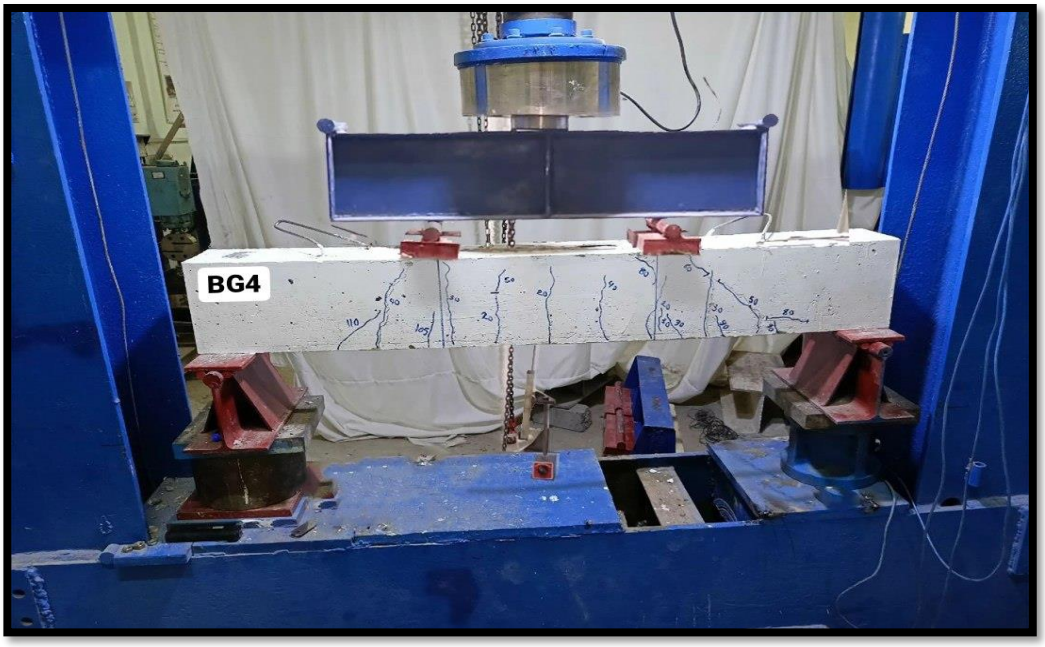

(c) BG4

Figure (4-3) Cracking Patterns Beams (continued)

4.3.1.5 Ductility Index

The ductility of a structure is defined as the capacity of the material to sustain plastic deformation under tensile strain while still carrying a load. As stated in [44] the ductility factor was defined as D.I = ($\Delta \boldsymbol{u}$/ Δy). The vertical displacement at maximum load divided by vertical displacement at yield load s is utilized to determine ductility index in the current reserch.

Δy= displacement at yield load (Py =0.75 Pu). [45]

The ductility index values for all beams are provided in Table (4-3), a comparison of the ductility index for the tested beam shown in Figure (4-4).

Table (4-3): Ductility Index of Tested Beams

Specimen	Pu (kN)	Δu (mm)	Py (kN)	Δy (mm)	D.I
BS4	55.00	7.36	41.25	3.41	2.15
BG4	111.42	14.90	83.57	11.07	1.34
BG2	52.47	25.78	39.35	14.27	1.8

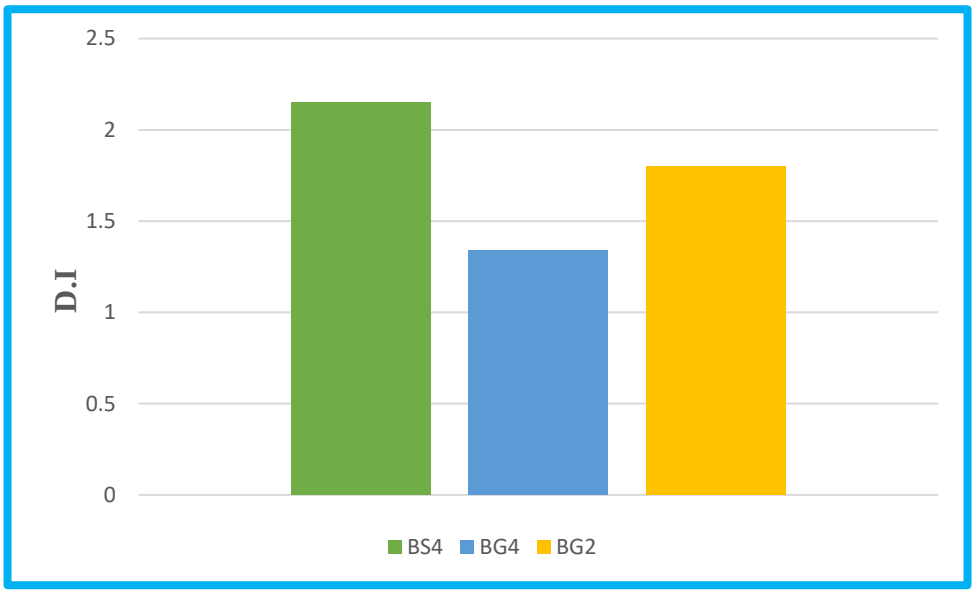

Figure (4-4):A Comparison in Ductility Index for Tested Beam

4.3.1.6 Flexural Stiffness

Stiffness is defined as the load required for producing unit deformation in the member. The slope of the secant drawn to the load-deflection curve at a load of) 0.75 (times the ultimate load can be utilized as stiffness criteria [46]. The stiffness was calculated as shown in Tables (4-4), a comparison in stiffness criteria for tested beam shown in Figure (4-5).

Table (4-4) Stiffness Criteria of Tested Subjected

Specimen	Pu (kN)	75% Pu (kN)	$\Delta_{75\%Pu}$ (mm)	Stiffness K (kN/mm)
BS4	55	41.25	3.42	12.06
BG4	111.42	83.57	11.14	7.5
BG2	52.47	39.35	13.51	2.91

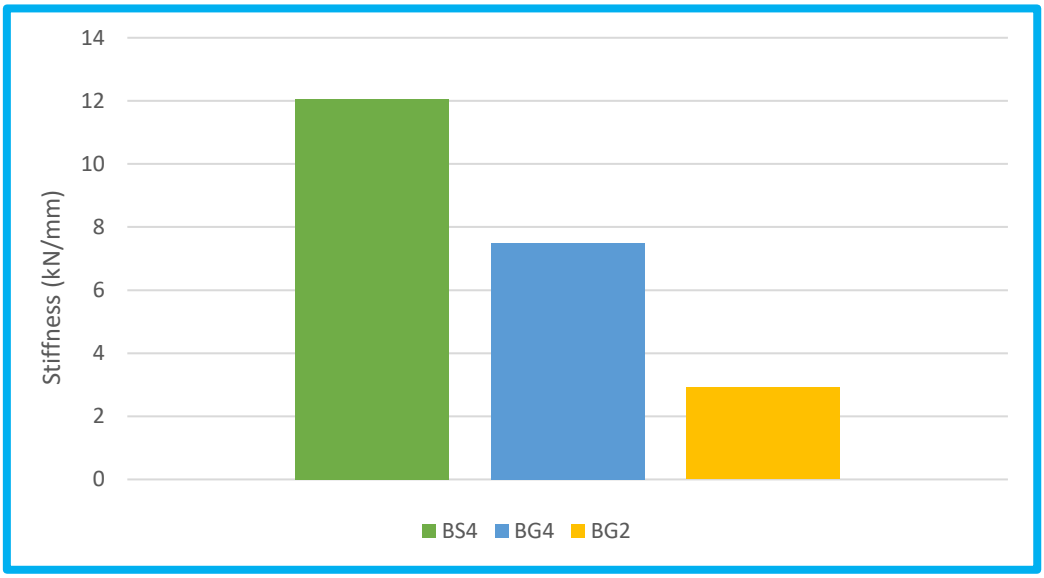

Figure(4-5):A Comparison in Stiffness Criteria for Tested Beam

4.3.2 Slab Specimens

The results of the experimental work are presented in terms of failure modes, punching shear capacity, and load-deflection response in this chapter.

4.3.2.1 Study the Influence of The Major Parameters

In the following, the major parameters effects on the behavior and the strength and other characteristics during the progress of the testing of the slabs were observed, reported and later discussed, cracks were marked and

recorded; slab deflection were recorded deflection of the slabs and the failure mechanisms of the connections were all reported and discussed. The effect of variables on the above characteristics and mechanism of failure is discussed under consideration of experimental evidences as follows. Experimental test results for slabs shown in Table (4-5).

Table (4-5): Experimental Test Results for Slabs

Specimen	ρ%	Pcr (kN)	Δcr (mm)	Pu (kN)	Δu (mm)
SS14	0.75	13.1	2.1	69.78	23.8
SS7	0.38	10.3	2.8	46.27	21.2
SG14	0.9	13.0	5.0	46.1	30
SG7	0.45	19.2	4.4	32.5	16.7

- **Slab specimen SS14**

The specimen was progressively loaded until the initial crack appeared. At 13 kN as shown in Figure (4-6) on the tension face of the slab, the cracks were first noticed; cracks (punching shear) appeared under the load point. As the load was raised further, many shear cracks appeared in the tension zones. The loading was increased gradually until the maximum load was reached. When the load reached 69.78 kN, the final failure (loss of strength) happened through a punching cone. In Figures (4-6), SS14 is shown under loading, and in Figures (4-7) are shown cracks in the compression face of the slab.

Figure (4-6) First Crack of SS14

Figure (4-7) Specimen SS14 at Failure Stage

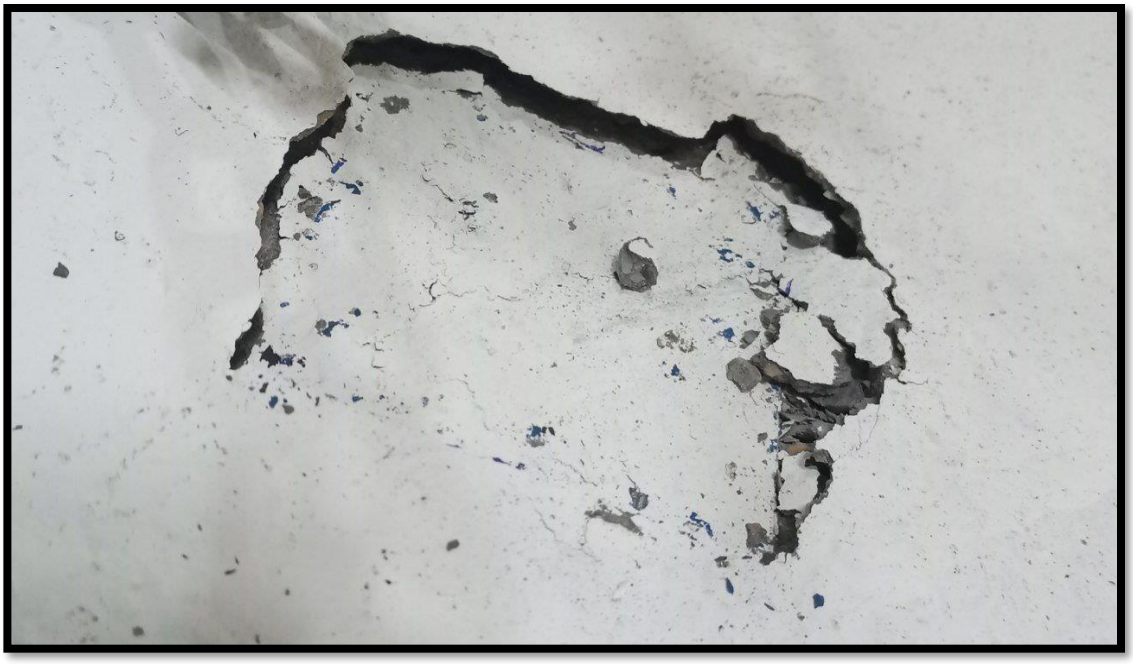

Figure (4-8) Punching under Load Cell

Figure (4-9) shows the load deflection curve for slab SS14.

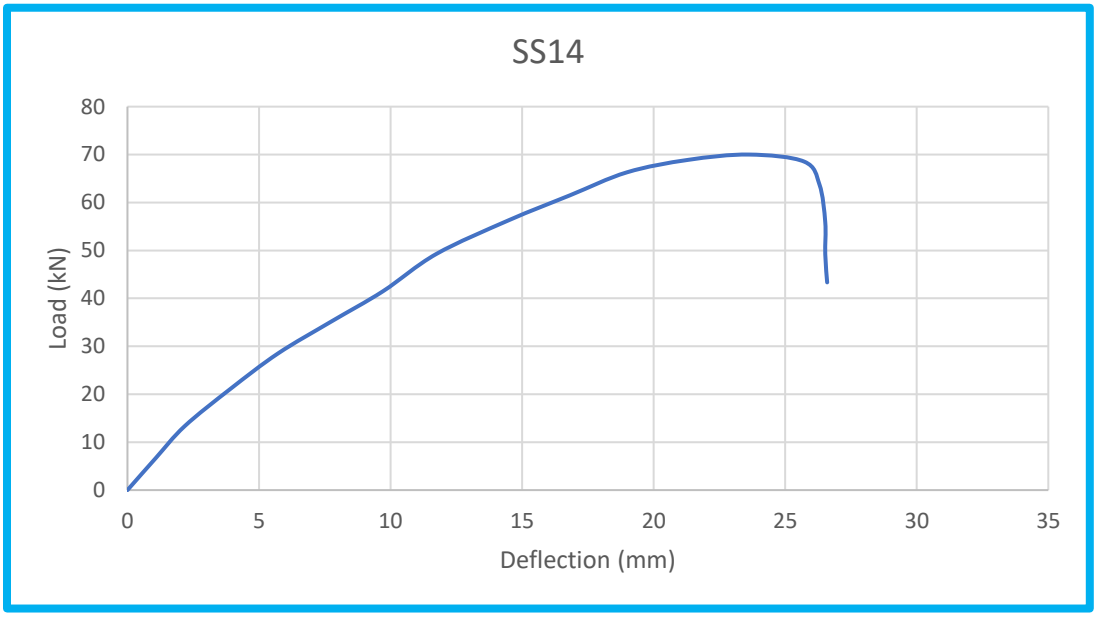

Figure (4-9) Load Deflection Curve for specimen SS14.

- **Slab specimen SS7**

The specimen was progressively loaded until the initial crack appeared. At 10 kN on the tension face of the slab, the cracks were first noticed; cracks (flexural crack) appeared under the load point. As the load was raised further, many flexural cracks appeared in the tension zones as shown in Figure (4-10). The loading was increased gradually until the maximum load was reached. When the load reached 46.27 kN, the final failure (loss of strength) happened through a flexural failure. Figure (4-11) shows the failure pattern for slab SS7.

Figure (4-10) Specimen SS7 at Failure Stage

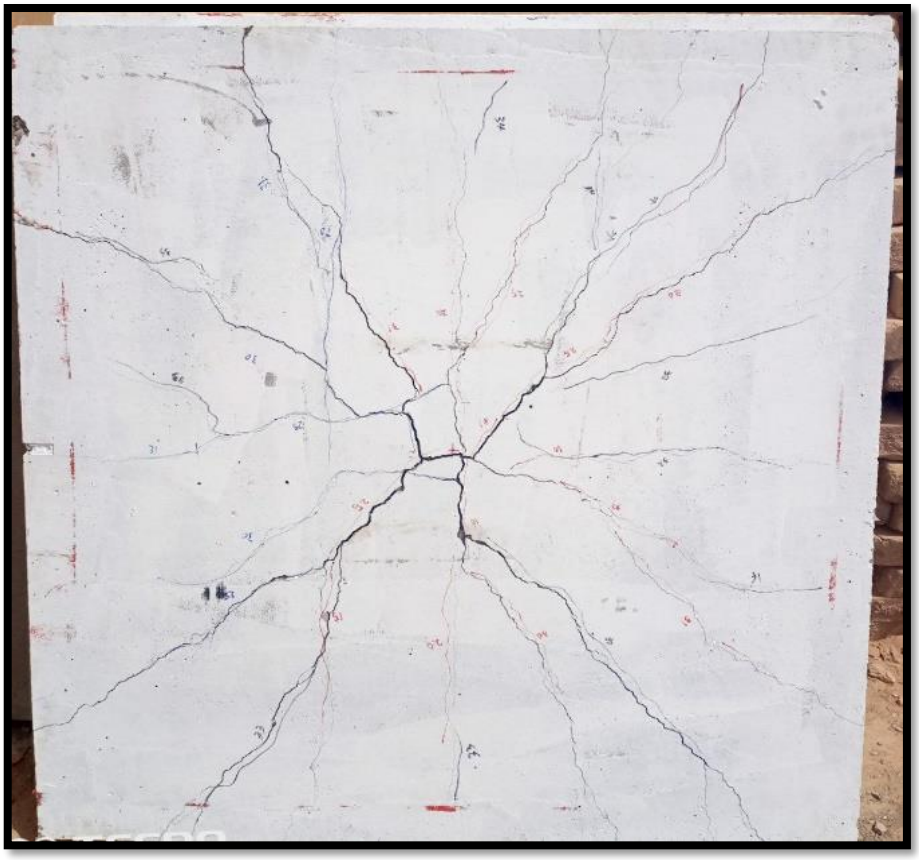

Figure (4-11) Failure Crack Patterns

Figure (4-12) shows the load deflection curve for slab SS7.

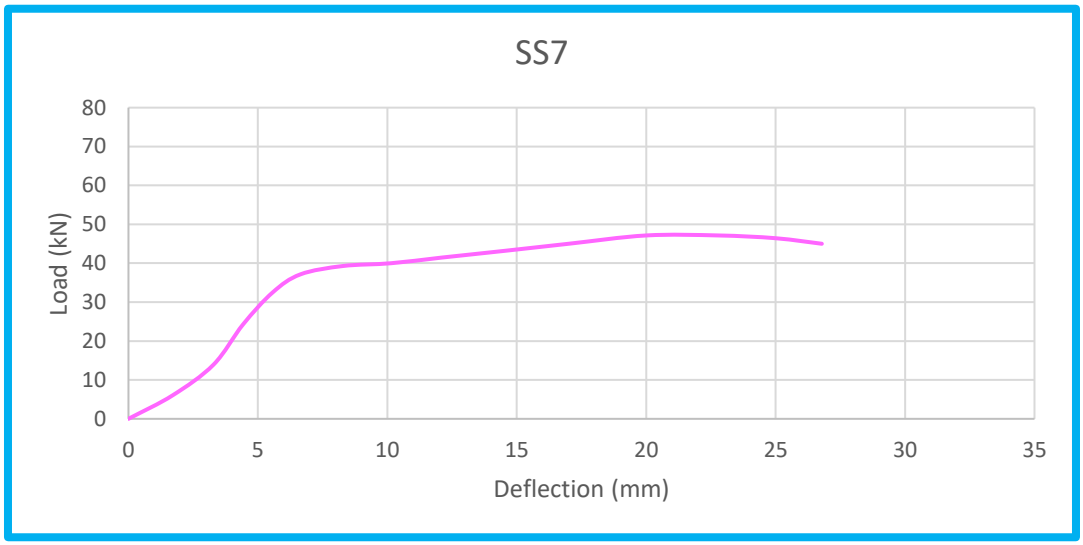

Figure (4-12) Load Deflection Curve specimen **SS7**.

- **Slab specimen SG14**

The specimen was progressively loaded until the initial crack appeared. At 13 kN as shown in Figure (4-13) on the tension face of the slab. As the load was raised further, many shear cracks appeared in the tension zones. The loading was increased gradually until the maximum load was reached. When the load reached 46.1 kN, the final failure (loss of strength) happened through a punching cone. In Figures (4-14), SG14 is shown under loading.

Figure (4-13) First Crack for SG14

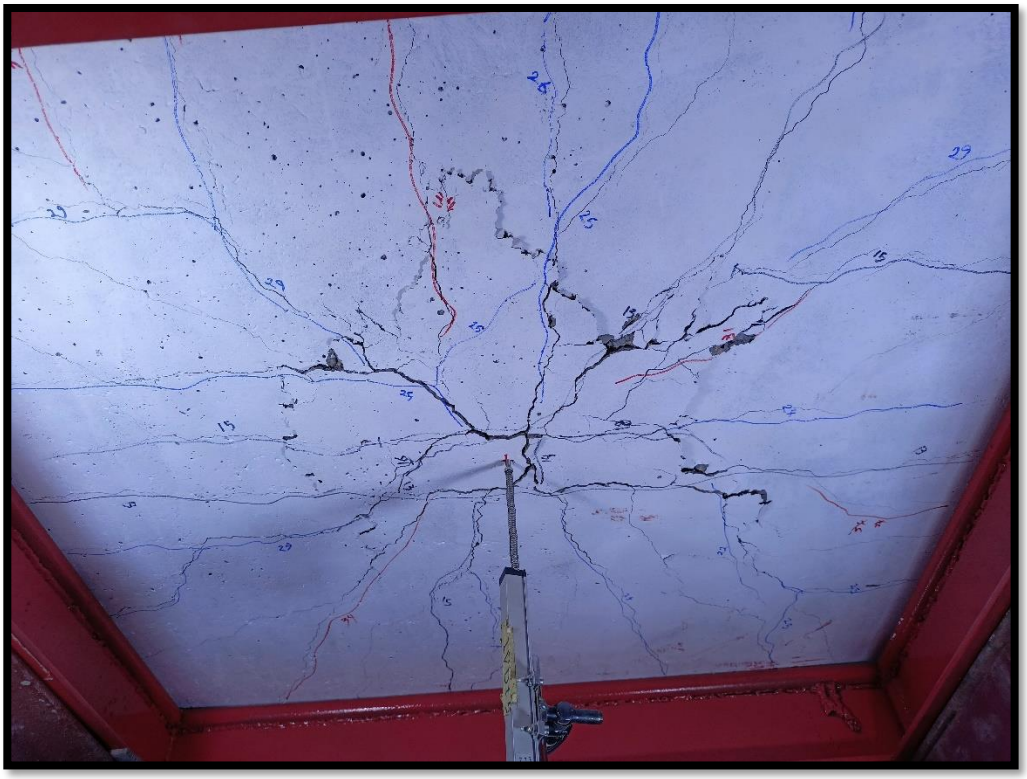

Figure (4-14) Specimen SG14 at Failure Stage

Figure (4-15) shows the load deflection curve for slab SG14.

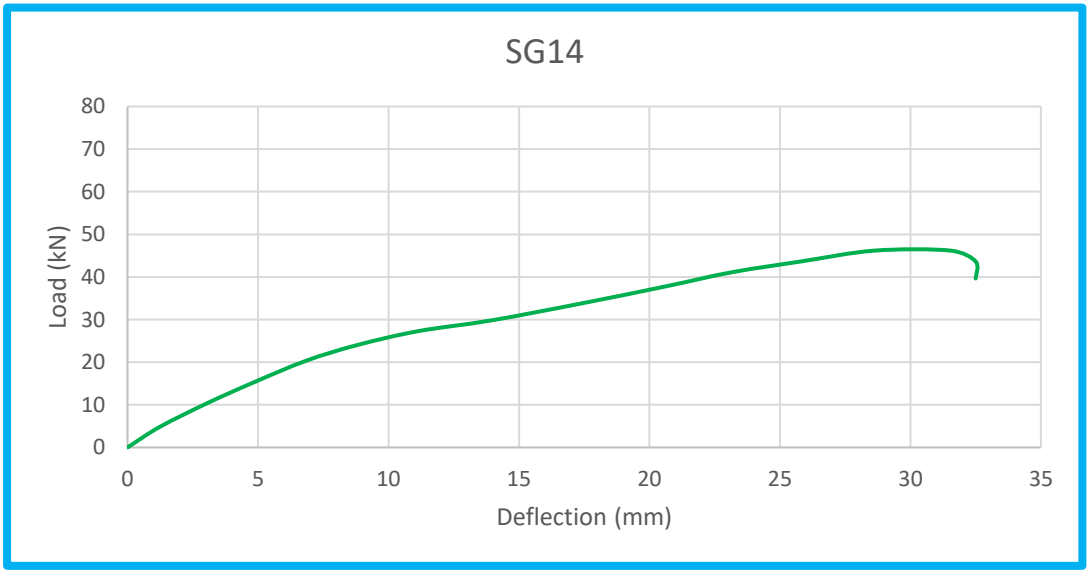

Figure (4-15) Load Deflection Curve of Specimen SG14

- **Slab specimen SG7**

Slab SG7 failed in a more brittle mode at a load of about 32 kN evidenced by the gradual loss of stiffness after the ultimate load. At 19 kN on the tension face of the slab the cracks were first noticed, and it was sudden and branching from the center to the midpoints of the edges, as in the Figure (4-16). This is followed by the appearance of cracks at 32 kN and the sudden flexural failure. as in the Figure (4-17).

Figure (4-16) First Crack for SG7

Figure (4-17) Specimen SG7 at Failure Stage

Figure (4-18) shows the load deflection curve for slab SG7.

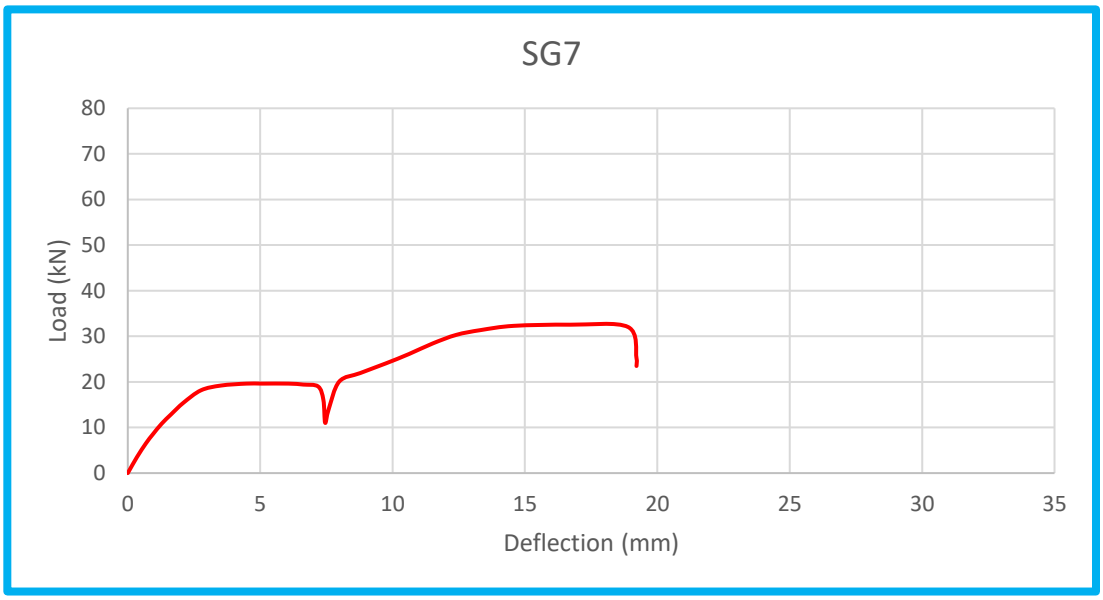

Figure (4-18) Load Deflection Curve of Specimen SG7

In Figure (4-19) load deflection curve for all slabs

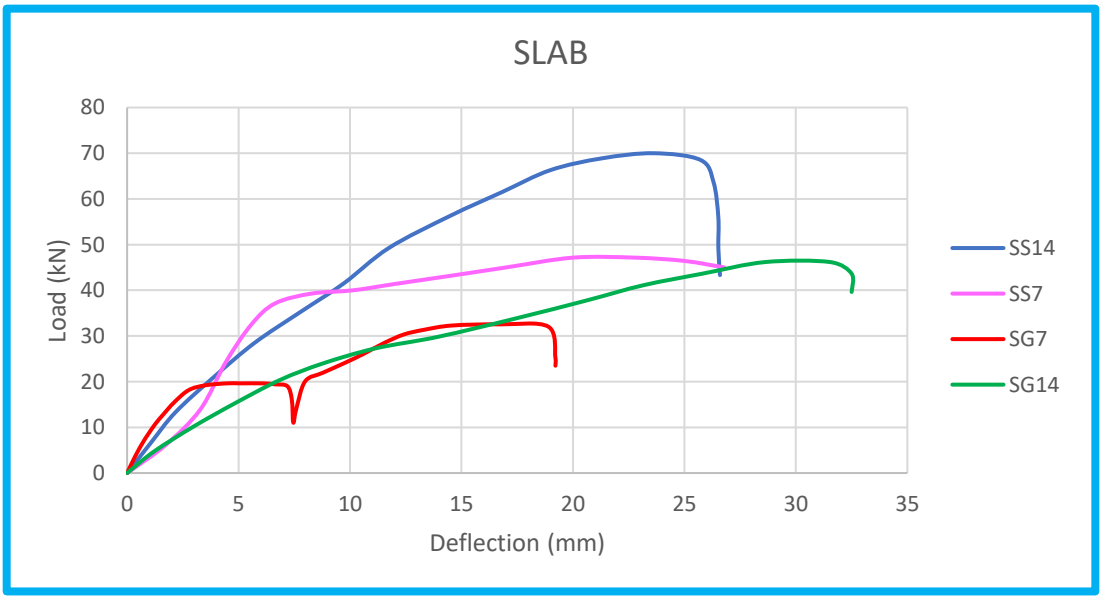

Figure (4-19) Load Deflection for All Slabs

4.3.2.2 Reinforcement Ratio

traditional steel reinforcement ratio, ρ_S, and GFRP reinforcement ratio ρ_G.

Slab reinforcement type, Specimens (SS14), (SS7), (SG14) and (SG7):

The variables studied in this group were the slab reinforcement type, GFRP or traditional steel and the steel reinforcement ratio. Specimen SS14 was reinforced with steel bars with reinforcement ratio, ρ_S = 0.75%, Specimens SS7 was reinforced with steel bars with reinforcement ratio, ρ_S = 0.38%, The reinforcement ratio of the GFRP bars used to strengthen the SG14 specimens was, ρ_G = 0.9%, and the reinforcement ratio of the GFRP bars used to strengthen the SG7 specimens was, ρ_G = 0.45%. The Load Deflection Curve Following application of loads, the following behaviors were observed in models of reinforced concrete slabs:

The First Step: Initially, the load-deflection curve included a straight portion (the elastic stage). At this point, the relationship between load and deflection was practically linear. There were no cracks in the portion, and the concrete and reinforcing were acting elastically.

The Second Stage: was a region of nonlinearity characterized by a gradual but noticeable change in slope as deflections increased (elastic-plastic stage)

The Third Stage: nonlinear part where slight increases in load resulted in excessively huge changes in deflection (represent the plastic stage).

4.3.2.3 Molds of Failure

According to the failure modes, high reinforcement ratio slabs fail by punching shear, whereas low reinforcement ratio slabs fail by flexural failure, without regard to whether the reinforcement is steel or GFRP, as shown in Table (4-6). When compared between the slabs reinforced with steel and

GFRP bars that failed due to punching shearing and flexural failure, the resistance of a slabs with steel rebar increased by 34% and 30%, respectively.

Table (4-6): Mold of Failure

Specimen	Pcr (kN)	Pu (kN)	Molde of failure
SS14	13.1	69.78	Punching shear
SS7	10.3	46.27	flexural failure
SG14	13.0	46.1	Punching shear
SG7	19.2	32.5	flexural failure

4.3.2.4 Crack Pattern

The crack patterns of specimens SS14 and SG14 were found to be similar in shape, but they were different in strength. The crack patterns of specimens SS7 and SG7 were found to be similar in shape, but they were different in strength. Low percentages of reinforcement cause slabs to fail suddenly and quickly. High-reinforcement slabs have a lot of cracks that are multiple, wide-spread, and branching. In addition, the GFRP reinforced specimens have fewer cracks, see Table (4-7) and Figure (4-20).

Table (4-7): First Crack and Ultimate Load

Specimen	ρ%	Pcr (kN)	Δcr (mm)	Pu (kN)	Δu (mm)
SS14	0.75	13	2.1	69.78	23.81
SS7	0.38	10	2.8	46.27	21.17
SG14	0.9	13	5.0	46.1	30.03
SG7	0.45	19	4.4	32.5	16.72

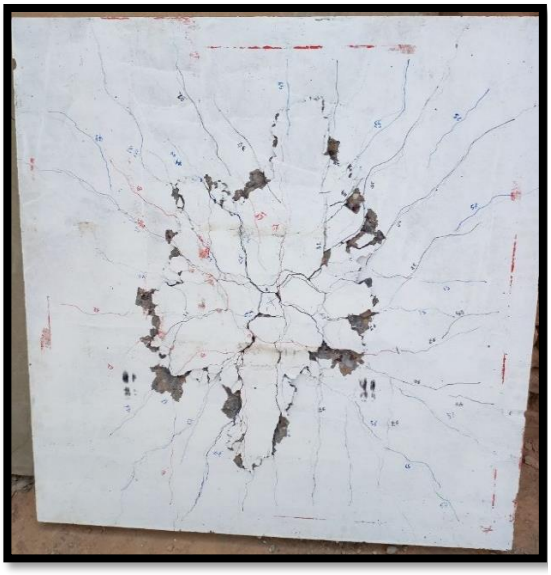

SS14

SS7

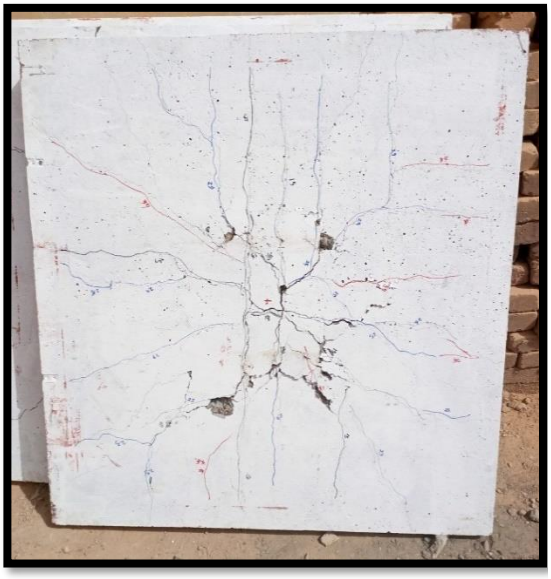

SG14

SG7

Figure (4-20) Post Failure Crack Patterns

4.3.2.5 Ductility Index

The ductility of a structure is defined as the capacity of the material to sustain plastic deformation under tensile strain while still carrying a load. As

stated in [44], the ductility factor was defined as D.I = ($\Delta \boldsymbol{u}$/ Δy). The vertical displacement at maximum load divided by vertical displacement at yield load s is utilized to determine ductility index in the current reserch.

Δy= displacement at yield load (P**y**=0.75 Vu) [45]. The ductility index values for all slabs are provided in Table (4-8), a comparison of the ductility index for the tested slab shown in Figure (4-21).

Table (4-8): Ductility Index of Tested Slabs

Specimen	**Vu (kN)**	**Δu (mm)**	**Vy (kN)**	**Δs (mm)**	**D.I**
SS14	69.78	23.81	52.34	13.1	1.82
SS7	46.27	21.17	34.70	5.87	3.61
SG14	46.1	30.03	34.58	19.22	1.56
SG7	32.5	16.72	24.38	10.26	1.63

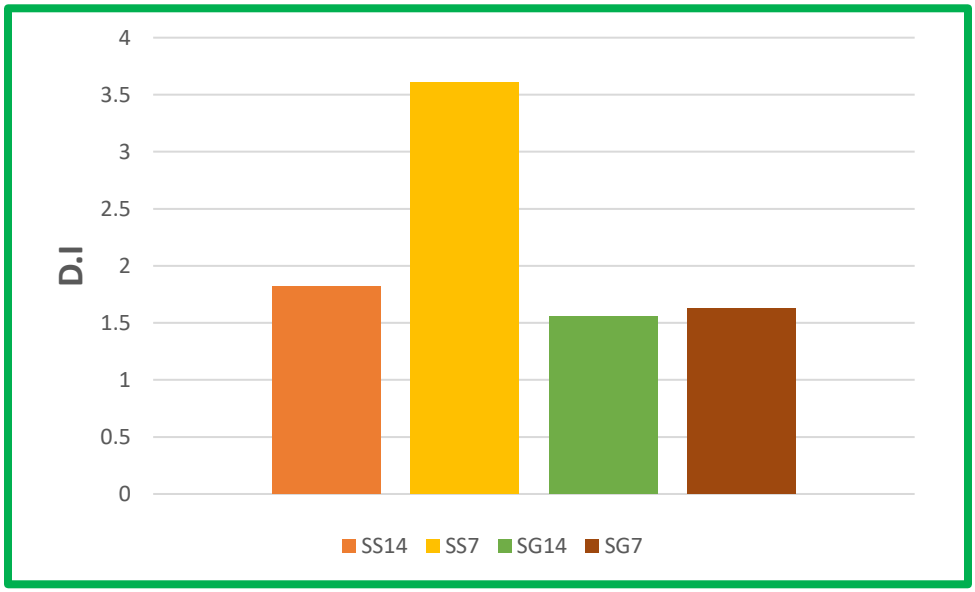

Figure (4-21): A Comparison in Ductility Index for Tested Slab

4.3.2.6 Stiffness Criteria

Stiffness is defined as the load required for producing unit deformation in the member. The slope of the secant drawn to the load-deflection curve at a load of (0.75) times the ultimate load can be utilized as stiffness criteria [46]. The stiffness was calculated as shown in Tables (4-9), a comparison in stiffness criteria for tested slab shown in Figure (4-22).

Table (4-9) Stiffness Criteria of Tested Subjected

Specimen	Vu (kN)	75%Vu (kN)	$\Delta_{75\%Vu}$ (mm)	Stiffness K (kN/mm)
SS14	69.78	52.34	12.85	4.07
SS7	46.27	34.7	5.8	5.98
SG14	46.1	34.58	19.22	1.8
SG7	32.5	24.38	10.32	2.36

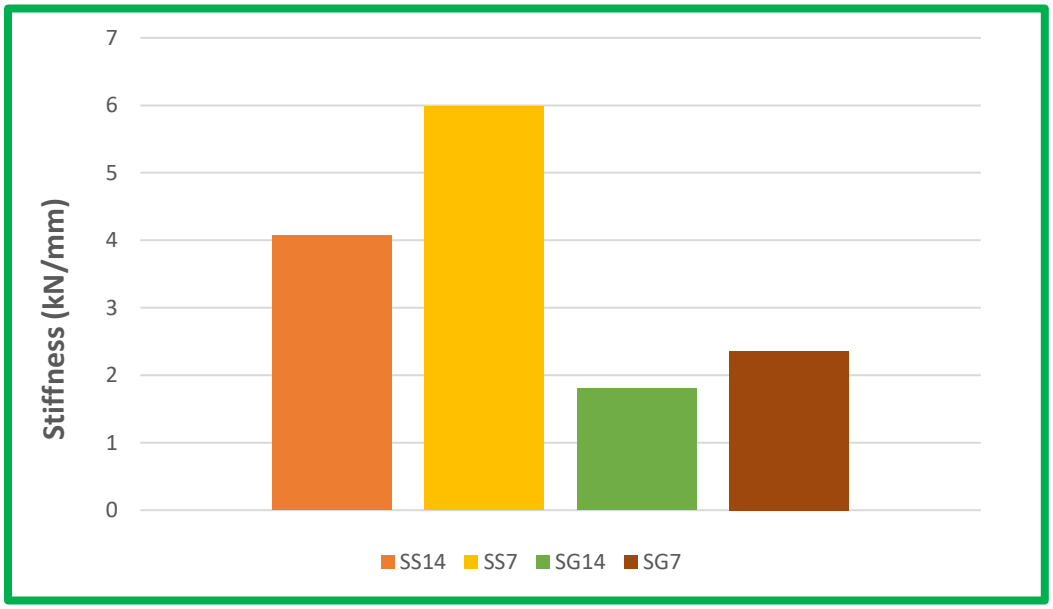

Figure (4-22): A Comparison in Stiffness Criteria for Tested Slab

4.3.3 Bond-slip

Pull out failure occurs when heavy confinement is present or a minimum concrete cover (5-10 times bar diameter) is provided. In this case, the bond strength is a function of mechanical interlock between bar deformations and the surrounding concrete.

Forces are transferred from the reinforcing bar to the concrete through three bond mechanisms: chemical adhesion, friction and mechanical interlock, Figure (4-23). Chemical adhesion, which is the chemical interaction between the concrete interface and the bar, is considered to contribute marginally to bond strength for steel as well as GFRP bars. This is why smooth bars are avoided in practice [48].

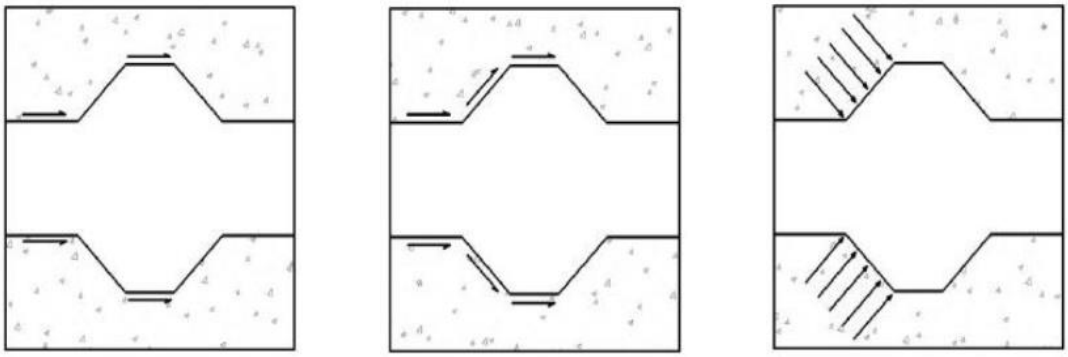

(a) (b) (c)

Figure (4-23): Bond Mechanisms (A) Chemical Adhesion, (B) Friction, and (C) Mechanical Interlock [48]

However, unlike steel bars, GFRP bars are less sensitive to chemical attacks, hence; chemical treatments of GFRP bars may improve their chemical adhesion. Friction is developed between surfaces by deformations or sand coating. Mechanical interlock is caused by bearing of the bar ribs on the concrete. Bond failure of conventional steel bars is a result of bearing which cause side splitting or shearing of concrete. In contrast, bearing stresses in

GFRP bars can exceed the shear strength between the bar core and the surface deformation resulting in a bond failure at this interface [48].

Where bond stress is the shear stress at the bar-concrete interface and bar slip is the relative displacement of the bar to the undisturbed concrete, an average bond stress - bar slip curve is used to characterize bond behavior [47]. Before the peak, mechanical interlock between bar deformations and concrete starts to generate splitting cracks because chemical adhesion is lost and internal transverse cracks occur. If the cracks in the concrete spread to the surface, the concrete splits, or the bars deform, the bond will fail.

After then, the bar starts to pull and big slips start to show up on the bar. As shown in Figure (4-24) [48], the smooth falling curve in the post-peak region is caused by residual bond stresses due to the presence of interface friction.

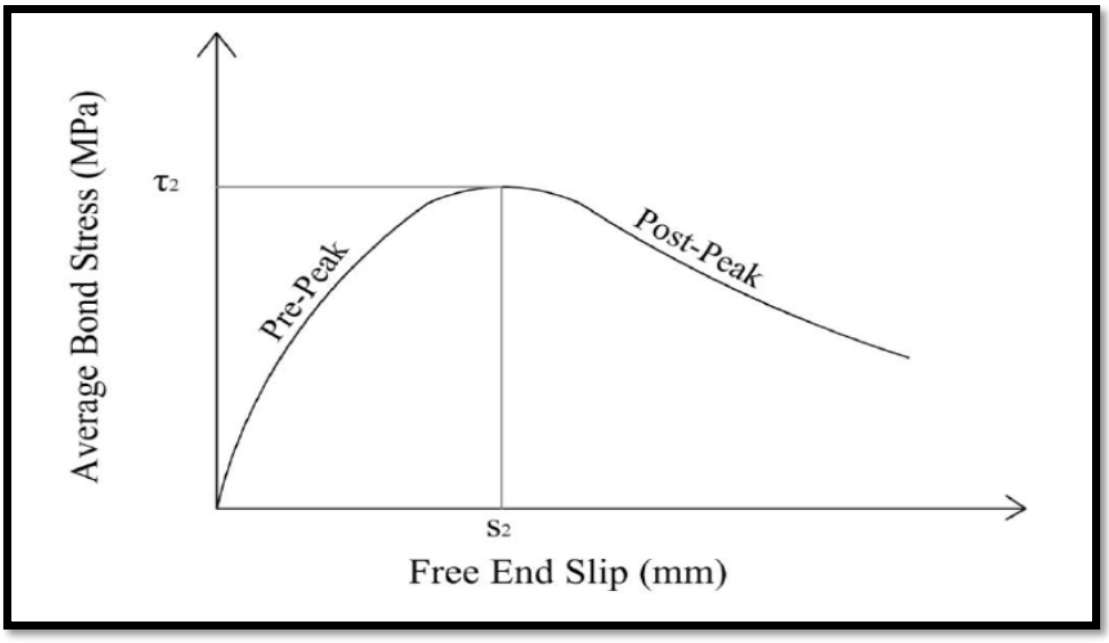

Figure (4-24): Typical Bond Stress Versus Bar Slip Relationship for Steel and GFRP Bars [48]

4.3.3.1 Bond Failure Modes

Pull out failure occurs when heavy confinement is present or a minimum concrete cover (five times bar diameter) is provided. In this case, the bond strength is a function of mechanical interlock between bar deformations and the surrounding concrete [49]

4.3.3.2 Bond stress-slip relationships

When analyzing the bond behavior between reinforcement and concrete, bond stress-slip relationships provide valuable information. The curves were prepared by using the data registered during the pull-out tests. Bond stress is calculated by equation (4-4) the ultimate load is replaced by the continuously changing load. Loaded end slip is calculated by subtracting the elastic elongation of the relevant portion of the bar (the length of the bar between gripping of the LVDTs and beginning of bonded zone) from the average of the measurements of the three LVDTs placed at the loaded end of the GFRP bar. Free end slip is defined as the registered LVDT measurement connected to the free end of the bar [41].

$$\boldsymbol{\tau = \frac{F}{C_b \cdot l}} \qquad (4\text{-}4)$$

Where:

τ = average bond stress, MPa;

F = tensile load, N;

C_b = equivalent circumference of FRP bar, mm; and

l = bonded length, mm.

At each load level, the slip at the loaded end should be calculated as the average of the readings of the LVDTs, minus the elongation Sc of the FRP bar in the length Lc between the top surface of bonded length and the point of attachment of the measuring device on the FRP bar, the latter being calculated as follows [41].

$$S_C = \frac{FL_C}{E_L .A} \quad (4\text{-}4)$$

where

Sc= elastic elongation, mm;

F = tensile load, N;

L_C = length from the top of the embedded bar to the point of the attachment of the measuring device mm;

E_L = longitudinal modulus of elasticity of GFRP bar, MPa; and

A = cross-sectional area, mm2

A total of six specimens were used to test the bond behavior of steel and GFRP. All specimens were tested after 28 days of curing. Both the steel and GFRP are ribbed and wrapped bars. Specimens PG30, PG45, and PG60 contained GFRP bars. The specimens failed due to bar pull-out from the concrete cube because of slippage between the GFRP bar and concrete. as seen in Table (4-10) this is a result of weak bonding between GFRP bar and concrete. Specimens PS30, PS45, and PS60 contained steel bars; the specimens failed due to bar cutting. In different places, PS30 was cut at the contact area between the concrete and the reinforcing steel, PS45 was cut at the end of the concrete cube, and PS60 was cut at the contact area between the holding arm and the rod. as shown in Table (4-10) this is a result of the excellent bond between the steel bar and concrete.

Table (4-10): Experimental Pullout Test Results

Specimen	Embedded length (mm)	Max Shear Stress (MPa)	Slip load end (mm)	Slip free end (mm)	Average slip (mm)	Mode failure
PG30	30	20.15	4.84	5.25	5.05	Bar pull-out
PG45	45	17.58	5.53	5.42	5.48	Bar pull-out
PG60	60	15.75	6.46	6.41	6.44	Bar pull-out
PS30	30	25.7	4.1	3.9	4	Bar cutting
PS45	45	16.73	4.12	4.2	4.16	Bar cutting
PS60	60	12.6	2.62	2.96	2.79	Bar cutting

- **Bond-slip specimen PG30**

The Figures (4-25) and (4-26) with respect to the pullout failure of the free end and loaded end, respectively. The shear slip curve for PG30 is shown in Figure (4-27).

Figure (4-25): PG30 Free End

Figure (4-26): PG30 Loaded End

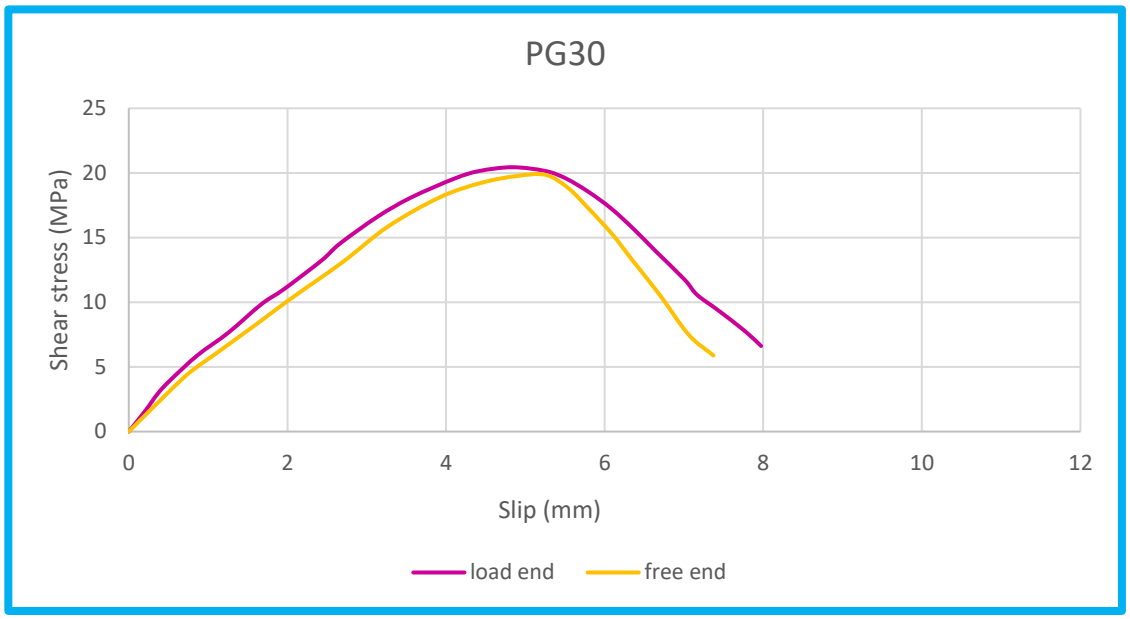

Figure (4-27) PG30 Shear Slip Curve

- **Bond-slip specimen PG45**

in Figure (4-28) show PG45 before testing, Figures (4-29) and (4-30) Regarding the loaded end and free end respectively for PG45 before Testing, Figure (4-31) shows PG45 free end after pullout failure and Figure (4-32) shows shear slip curve for PG45.

Figure (4-28): PG45 before Testing

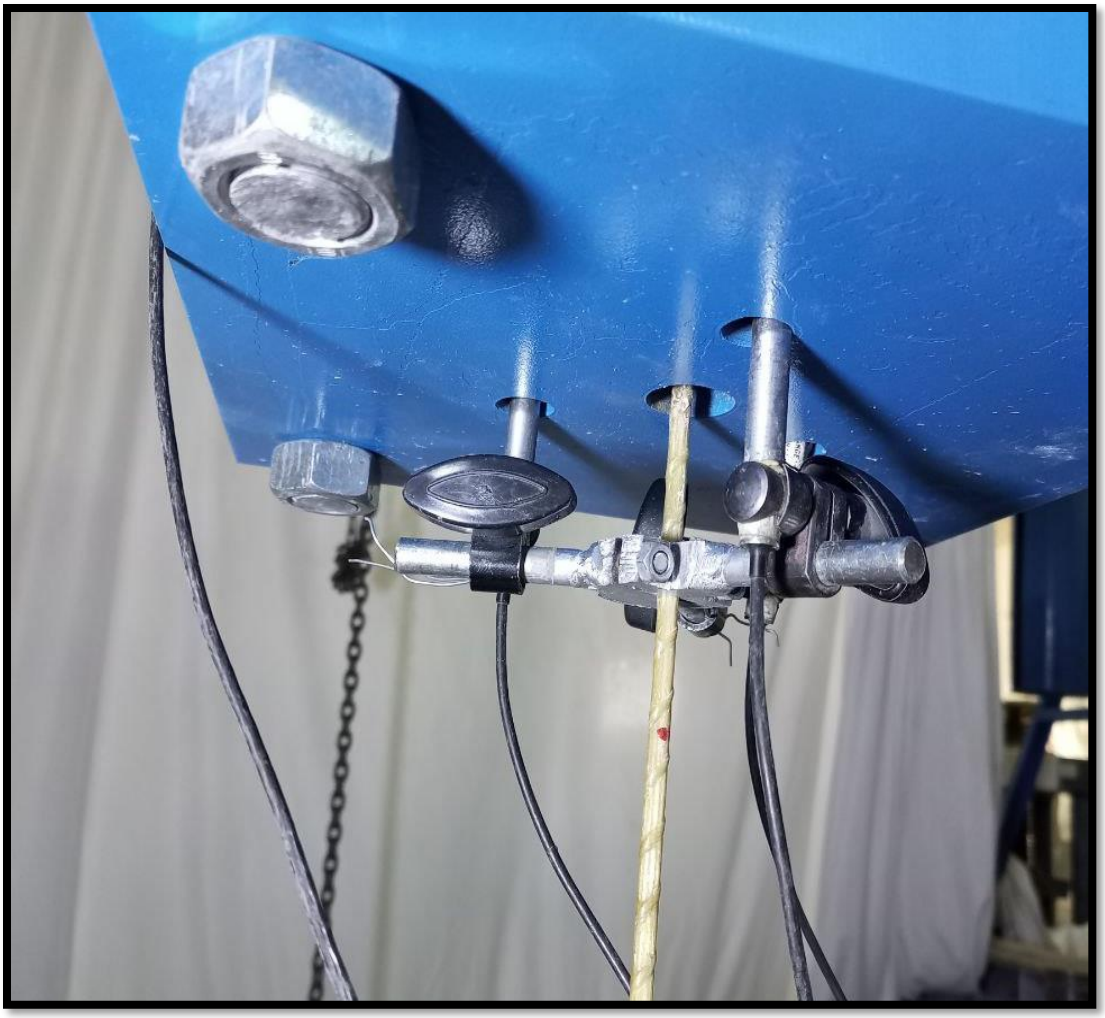

Figure (4-29): PG45 Loaded End before Testing

Figure (4-30): PG45 Free End before Testing

Figure (4-31): PG45 Free End after Slip

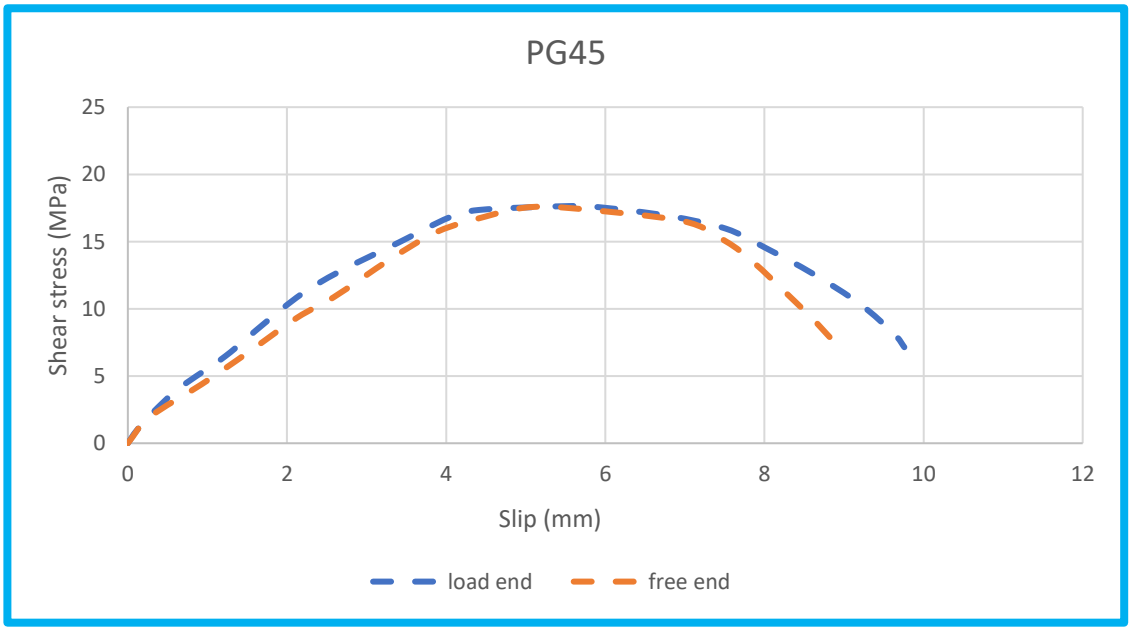

Figure (4-32): PG45 Shear Slip Curve

- **Bond-slip specimen PG60**

The failure of the free end to pull out is shown in Figure (4-33). The shear slip curve for PG60 is shown in Figure (4-34). And Figure (4-35) shear slip curve for GFRP bars.

Figure (4-33): PG60 Free End after Slip

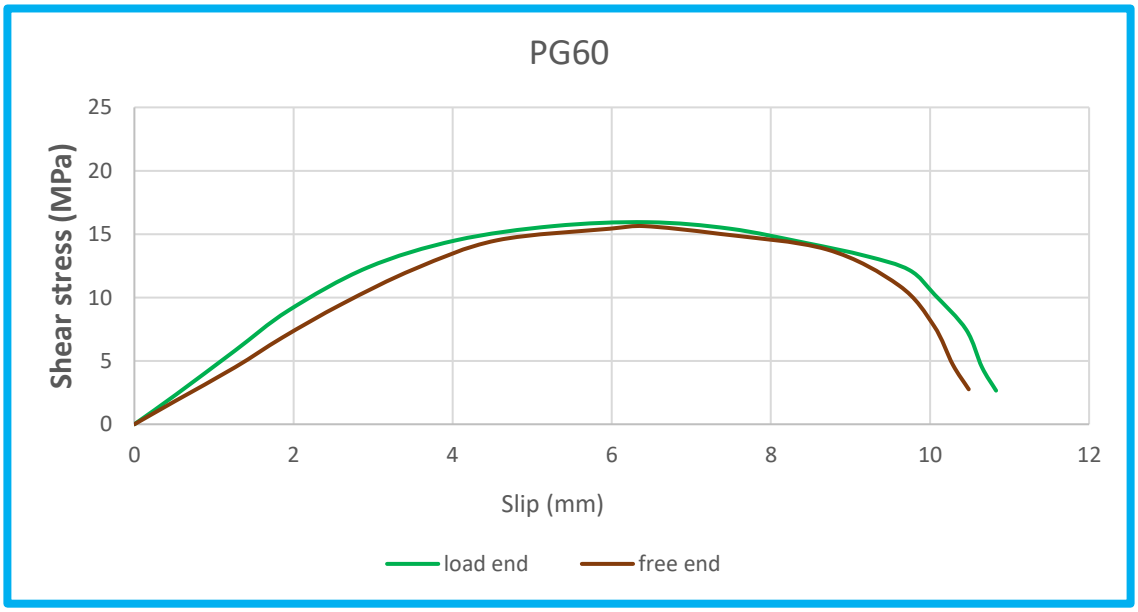

Figure (4-34): PG60 Shear Slip Curve

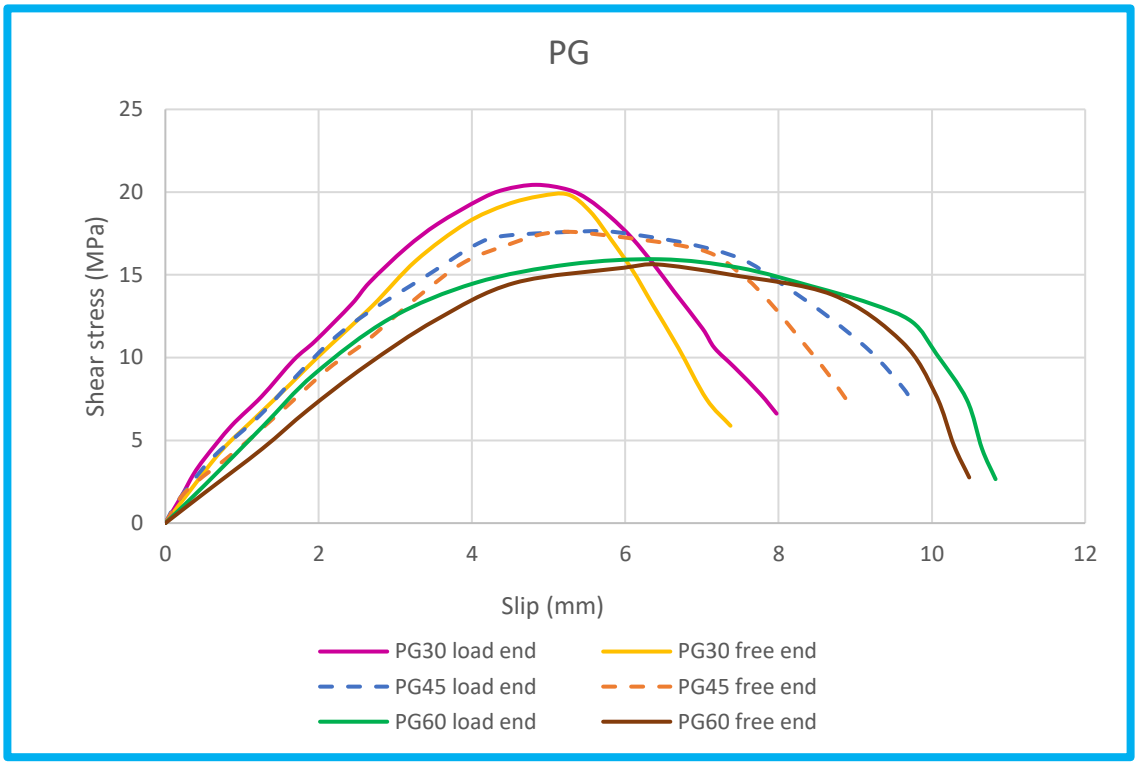

Figure (4-35): Shear Slip Curve for GFRP Bars

- **Bond-slip specimen PS30**

The Figure (4-36) the bar cutting failure of PS30 was cut at the contact area between the concrete and the reinforcing steel. The shear slip curve for PS30 is shown in Figure (4-37).

Figure (4-36): PS30 after Bar Cutting

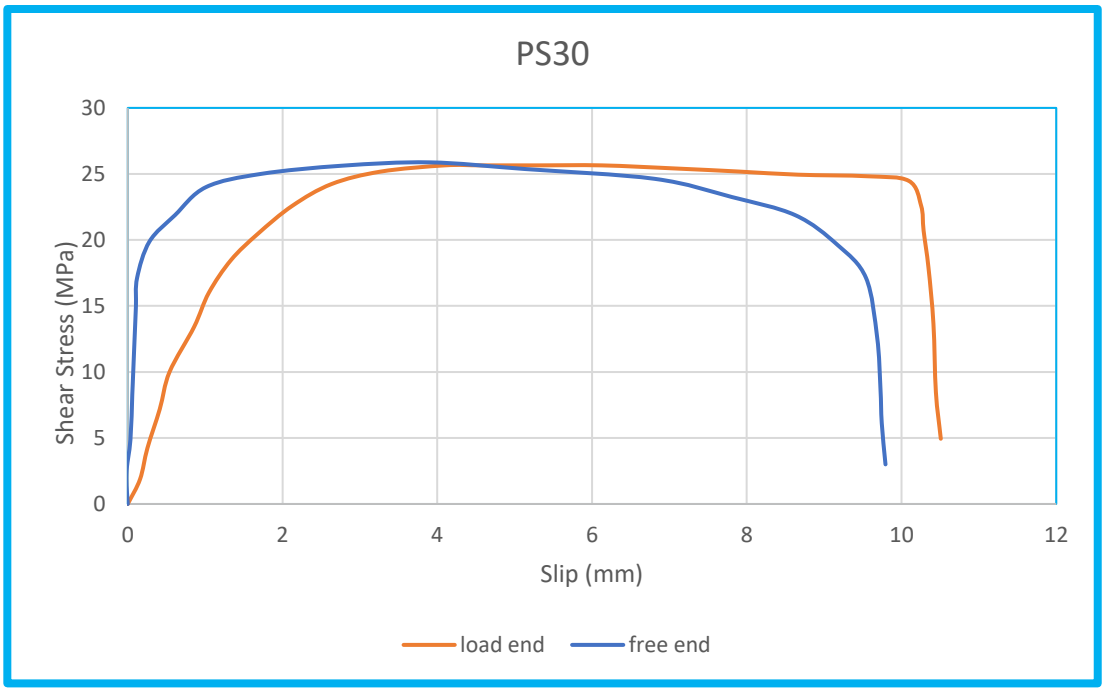

Figure (4-37): PS30 Shear Slip Curve

- **Bond-slip specimen PS45**

In Figure (4-38) show PS45 before testing, Figure (4-39) PS45 free end before testing and Figure (4-40) the loaded end for PS45 after testing, Figure (4-41) shows PS45 after upload loadcell, Figure (4-42) shows PS45 cut at the end of the concrete cube, Figure (4-43) shows PS45 free end after bar cutting failure and Figure (4-44) shows shear slip curve for PS45.

Figure (4-38): PS45 Before Testing

Figure (4-39): PS45 Free End before Testing

Figure (4-40): PS45 Loaded End after Testing

Continued

Continues

Figure (4-41): PS45 After Upload Loadcell

Figure (4-42): PS45 Cut at The End of The Concrete Cube

Figure (4-43): PS45 Free End After testing

Figure (4-44): PS45 Shear Slip Curve

- **Bond-slip specimen PS60**

Figure (4-45) shows PS60 before testing, Figure (4-46) shows PS60 cut at the contact area between the holding arm and the rod. The shear slip curve for PG60 is shown in Figure (4-47).

Figure (4-45): PS60 Before Testing

Figure (4-46): PS60 Cut at the Contact Area Between the Holding Arm and the Rod

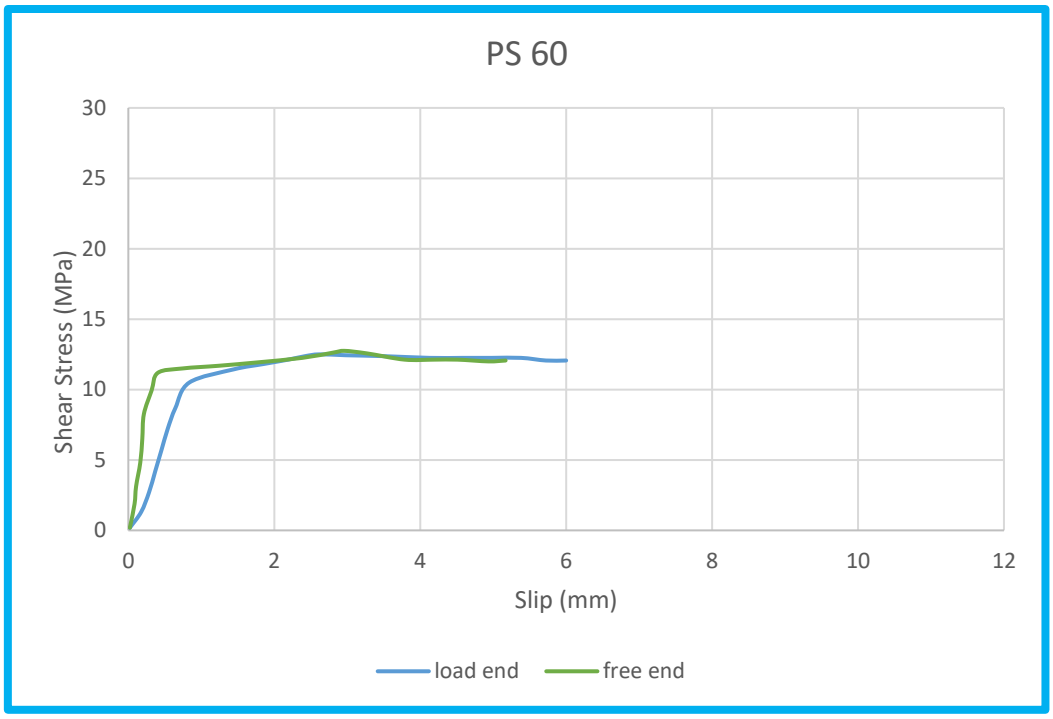

Figure (4-47): PS60 Shear Slip Curve

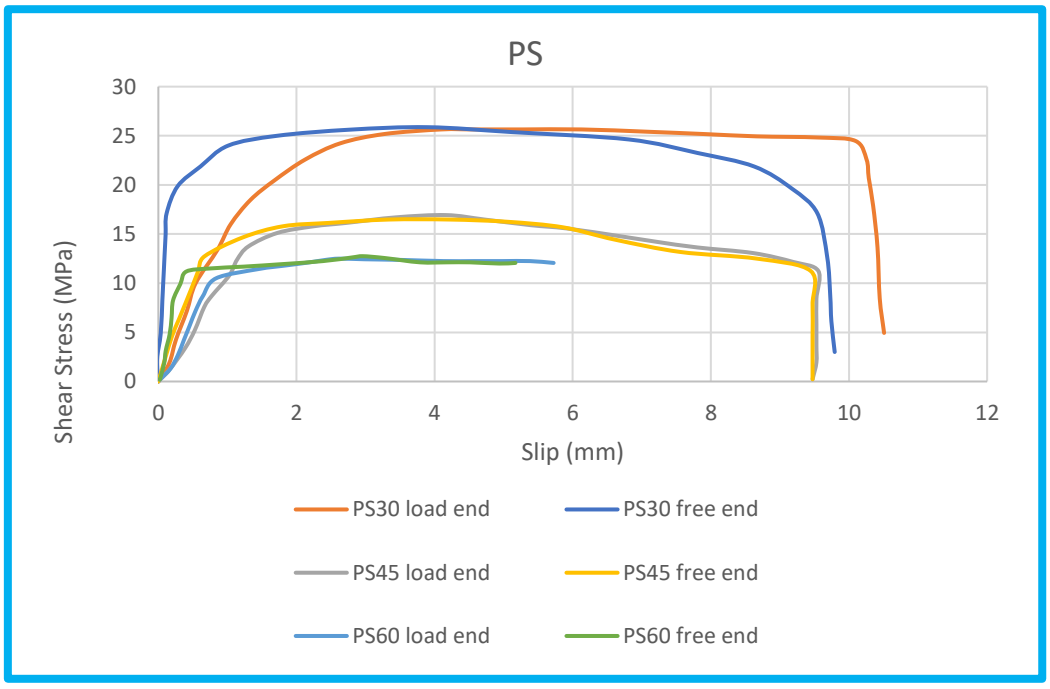

Figure (4-48): Shear Slip Curve for Steel Bars

Chapter Five

CHAPTER FIVE

CONCLUSIONS AND RECOMMENDATIONS

5.1 Conclusions

In this chapter, conclusions are presented for the experimental results.

1. GFRP reinforced beams have a greater ultimate load capacity than steel reinforced beams with the same reinforcing ratios.
2. It was determined that GFRP composites could be used in construction. Given its various benefits, such as being noncorrosive, low in weight, and high strength, it may be used as a substitute to the traditional reinforcing material, steel, to create sustainable buildings.
3. described the cracking characteristics of GFRP RC members. Due to the lower elastic modulus, the crack widths in GFRP RC members were significantly larger than those in steel bar RC members. However, it was also shown that with larger reinforcement ratios, the crack width was reduced due to a more effective absorption of the energy produced when the concrete cracked.
4. Because of the low modulus of elasticity of GFRP, the main factor controlling the design of a reinforced concrete beam with GFRP is the service requirements for cracks and deflection.
5. The deflection and crack width are indications of a possible rupture before the failure of the beam, GFRP bars may be a good alternative to steel reinforcement.
6. Considering the results depicted by the load deflections curves, beams with a GFRP bars appears to have linear curves this is because that

GFRP exhibits brittle behavior as opposed to the elastic and plastic behavior of the steel bars.

7. Because GFRP bars have a low elastic modulus, their flexural strength is higher than that of steel beams.
8. Despite having the same reinforcement ratio, steel-reinforced slabs have a higher ultimate load capacity than GFRP-reinforced slabs.
9. The slabs with a high percentage of reinforcement tested in this paper show brittle punching shear failure, while the slabs with a low percentage of reinforcement show flexural failure.
10. Sudden failure in slab that contain GFRP reinforcement and low reinforcement ratio due to it is brittle nature.
11. The punching shear ability, flexural strength, and deflection are greatly affected by the type of reinforcement in the slab.
12. Punching shear strength was predicted very conservatively by ACI 440. 1R-15 [2].
13. Although the GFRP bar's surface is helically ribbed, which should improve its adhesion to concrete and provide resistance, specimens PG failed due to bar pull-out, indicating weak bonding, whereas specimens PS failed due to bar cutting, indicating excellent bonding between ribbed steel bar and concrete.
14. The price of GFRP bars is more economical than steel bars.

5.2 Recommendations:

For upcoming works, the following recommendations are suggested:

1. It is recommended that additional research incorporate several types of reinforcement, such as CFRP and Basalt Fibre Reinforced Polymers bars, as the current study only examined one type of FRP reinforcement, GFRP bars.
2. The compressive and tensile strengths of concrete can be improved by adding improvers to the concrete mixture. It is recommended to study the FRP-reinforced concrete behavior containing additives to improve its strength.
3. Since GFRP bars are able to survive a lot of applied load and also help prevent corrosion and the high maintenance costs that come with it, it is important to spread awareness of the usage of GFRP bars as reinforcing materials.
4. It would be prudent to look into how different GFRP reinforced bar diameters affect flat slab behavior for punching shear capacity.
5. The effect of the punching shear capacity and how it reacts with other factors including effective depth, concrete strength, column size, and reinforcement ratio.

References

REFERENCES

1. TUF-BAR. (2018). TUF-BAR | Fiberglass Rebar. Retrieved August 28, 2018, from https://www.tuf-bar.com/application/
2. ACI-440 Committee. (2015). Guide for the design and construction of structural concrete reinforced with fiber-reinforced polymer (FRP) bars (ACI 440. 1R-15). *Farmington Hills, Michigan: American Concrete Institute*.
3. Nanni, A., De Luca, A., & Zadeh, H. J. Reinforced concrete with FRP bars: Mechanics and design. 2014.
4. Ahmad, S. (2003). Reinforcement corrosion in concrete structures, its monitoring and service life prediction—a review. *Cement and concrete composites*, *25*(4-5), 459-471.
5. Ahmed, E. A., Benmokrane, B., & Sansfaçon, M. (2017). Case study: Design, construction, and performance of the La Chancelière parking garage's concrete flat slabs reinforced with GFRP bars. Journal of Composites for Construction, 21(1), 6001-6013.
6. Brothers, H. (2011). Glass Fiber Reinforced Polymer (GFRP) Rebar—Aslan 100 Series FIBERGLASS REBAR.
7. https://www.dailysabah.com/business/2019/04/11/world-media-on-istanbul-airport-everything-about-it-is-huge
8. Nanni, A. (2000, March). FRP reinforcement for bridge structures. In *Proceedings, Structural Engineering Conference, The University of Kansas, Lawrence, KS* (Vol. 5).

9. Sun, R., Perera, R., Gu, J., & Wang, Y. (2021). A Simplified Approach for Evaluating the Flexural Response of Concrete Beams Reinforced with FRP Bars. *Frontiers in Materials*, *8*, 765058.
10. Hollaway, L. C. (2010). A review of the present and future utilisation of FRP composites in the civil infrastructure with reference to their important in-service properties. *Construction and building materials*, *24*(12), 2419-2445.
11. Benmokrane, B., Theriault, M., Masmoudi, R., & Rizkalla, S. (1997). Effect of reinforcement ratio on concrete members reinforced with FRP bars. *Society for the Advancement of Material and Process Engineering (USA)*, 87-98.
12. Rahmatian, A. (2014). *Static and Fatigue Behavior of FRP-Reinforced Concrete Beams and an SHM System with Fiber Optic Sensors under Different Weathering Conditions* (Doctoral dissertation, Concordia University).
13. Ashour, A. F. (2006). Flexural and shear capacities of concrete beams reinforced with GFRP bars. *Construction and Building Materials*, *20*(10), 1005-1015.
14. Lau, D., & Pam, H. J. (2010). Experimental study of hybrid FRP reinforced concrete beams. *Engineering Structures*, *32*(12), 3857-3865.
15. Kalpana, V. G., & Subramanian, K. (2011). Behavior of concrete beams reinforced with GFRP BARS. *Journal of reinforced plastics and composites*, *30*(23), 1915-1922.
16. Barris, C., Torres, L., Baena, M., Pilakoutas, K., & Guadagnini, M. (2012). Serviceability limit state of FRP RC beams. *Advances in Structural Engineering*, *15*(4), 653-663.

17. Shanour, A. S., Mahmoud, A. A., Adam, M. A., & Said, M. (2014). Experimental investigation of concrete beams reinforced with GFRP bars. *Journal Impact Factor*, *5*(11), 154-164.
18. Kheni, H. L., Satasiya, A. P., Balar, K. P., & Khokhar, P. R. (2016). GFRP Bars as a Substitution in Structure. *Global Research and Development Journal for Engineering*, *035*, 193–196.
19. Chidananda, S. H., & Khadiranaikar, R. B. (2017). Flexural behaviour of concrete beams reinforced with gfrp rebars. *International Journal of Advance Research, Ideas and Innovations in Technology*, *3*(5), 119-128.
20. Saleh, Z., Goldston, M., Remennikov, A. M., & Sheikh, M. N. (2019). Flexural design of GFRP bar reinforced concrete beams: An appraisal of code recommendations. *Journal of Building Engineering*, *25*, 100794.
21. Moolaei, S., Sharbatdar, M. K., & Kheyroddin, A. (2021). Experimental evaluation of flexural behavior of HPFRCC beams reinforced with hybrid steel and GFRP bars. *Composite Structures*, *275*, 114503.
22. Putri, D. T. (2021, October). Flexural Capacity of Concrete Beam Reinforced with GFRP Bars. In *Journal of Physics: Conference Series* (Vol. 2049, No. 1, p. 012075). IOP Publishing.
23. Aiello, M. A., & Ombres, L. (2000). A general method for deflections evaluation of fiber reinforced polymer (FRP) reinforced concrete members. *Journal of Composites for Constructions-2003*.
24. Achillides, Z., & Pilakoutas, K. (2004). Bond behavior of fiber reinforced polymer bars under direct pullout conditions. *Journal of Composites for construction*, *8*(2), 173-181.
25. Carvalho, E. P., Ferreira, E. G., Cunha, J. C. D., Rodrigues, C. D. S., & Maia, N. D. S. (2017). Experimental investigation of steel-concrete bond

for thin reinforcing bars. *Latin American Journal of Solids and Structures*, *14*, 1932-1951.

26. Sena-Cruz, J., Pereira, E. N. B., Freitas, N., Pereira, E., & Soares, S. R. R. (2018). Bond behaviour between GFRP rods and concrete produced with seawater: experimental research.
27. Gao, K., Li, Z., Zhang, J., Tu, J., & Li, X. (2019). Experimental research on bond behavior between GFRP bars and stirrups-confined concrete. *Applied Sciences*, *9*(7), 1340.
28. Solyom, S., & Balázs, G. L. (2020). Bond of FRP bars with different surface characteristics. *Construction and Building Materials*, *264*, 119839.
29. Hassan, M., Ahmed, E., & Benmokrane, B. (2013). Punching-shear strength of normal and high-strength two-way concrete slabs reinforced with GFRP bars. *Journal of composites for construction*, *17*(6), 04013003.
30. Dulude, C., Hassan, M., Ahmed, E. A., & Benmokrane, B. (2013). Punching shear behavior of flat slabs reinforced with glass fiber-reinforced polymer bars. *ACI Structural Journal*, *110*(5), 723.
31. Kara, I. F., & Sinani, B. (2016). Prediction of Punching Shear Capacity of Two-Ways FRP Reinforced Concrete Slabs.
32. Ahmed, E. A., Benmokrane, B., & Sansfaçon, M. (2017). Case study: Design, construction, and performance of the La Chancelière parking garage's concrete flat slabs reinforced with GFRP bars. *Journal of Composites for Construction*, *21*(1), 6001-6013.
33. Mohamed, O. A., & Khattab, R. (2017, October). Review of punching shear behaviour of flat slabs reinforced with FRP bars. In *IOP*

Conference Series: Materials Science and Engineering (Vol. 245, No. 3, p. 032064). IOP Publishing.

34. Ju, M., Park, K., & Park, C. (2018). Punching shear behavior of two-way concrete slabs reinforced with glass-fiber-reinforced polymer (GFRP) bars. *Polymers*, *10*(8), 893.
35. Iraqi Specification Standards "Portland Cement IQS No. (5)," Central Agency for Standardization and Quality Control, Planning Council, Baghdad, IRAQ, 1984 (in Arabic).
36. Iraqi Specification Standards "Aggregate from Natural Sources for Concrete and Construction IQS No. (45)," Central Agency for Standardization and Quality Control, Planning Council, Baghdad, IRAQ, 1984 (in Arabic).
37. ASTM A615, "Standard Specification for Deformed and Plain Carbon-Steel Bars for Concrete Reinforcement (ASTM A615-09)". West Conshohocken, PA: ASTM International, 2009.
38. BS 1881: Part 116, "Method for Determination of Compressive Strength of Concrete Cubes,'' British Standards Institution, 1989.
39. ASTM C78-10, "Standard test method for flexural strength of concrete (using simple beam with third-point loading)," in American society for testing and materials, pp. 19428-2959, 2010.
40. ASTM C496-11, "Standard Test Method for Splitting Tensile Strength of Cylindrical Concrete Specimens," ASTM International, West Conshohocken, PA, 2011, DOI: 10.1520/C0496_C0496M-11."
41. ACI, A. (2013). 440.3 R-13: Guide Test Methods for Fiber-Reinforced Polymers (FRPs) for Reinforcing or Strengthening Concrete Structures. *American Concrete Institute, Farmington Hills, USA*.
42. BS8110-1: 1997, "Structural Use of Concrete," British Standard, 1997.

43. ACI Committee 318. "Building Code Requirements for Structural Concrete (ACI 318-19): An ACI Standard: Commentary on Building Code Requirements for Structural Concrete (ACI 318R-19): an ACI Report." American Concrete Institute, 2019.
44. Russell, J. S. (Ed.). (2003). *Perspectives in Civil Engineering: Commemorating the 150th Anniversary of the American Society of Civil Engineers*. ASCE Publications.
45. Russell, J. S. (Ed.). (2003). *Perspectives in Civil Engineering: Commemorating the 150th Anniversary of the American Society of Civil Engineers*. ASCE Publications.
46. Muthuswamy, K. R., & Thirugnanam, G. S. (2014). *Structural behaviour of hybrid fibre reinforced concrete exterior Beam-Column joint subjected to cyclic loading*. International journal of civil and structural engineering, 4(3), 262.
47. Focacci, F., Nanni, A., & Bakis, C. E. (2000). Local bond-slip relationship for FRP reinforcement in concrete. *Journal of composites for construction*, *4*(1), 24-31.
48. Vint, L. (2012). *Investigation of bond properties of glass fibre reinforced polymer (GFRP) bars in concrete under direct tension* (Doctoral dissertation).
49. Cairns, J., & Abdullah, R. B. (1996). Bond strength of black and epoxy-coated reinforcement-a theoretical approach. *Materials Journal*, *93*(4), 362-369.

Appendix A

Appendix A

Design of Elements

All elements were design according to ACI-Code.

A.1 Flexural-critical beam BS4

The beam consists of four bars of Ø6 mm as flexural reinforcement at depth (d = 176 mm) and 2Ø6 mm as top reinforcement at depth (d'= 24 mm). The width of the cross section (b = 150 mm) and the height (h = 200 mm). The shear span was reinforced with Ø6mm@100mm. The yield strength for rebars (f_y) is equals to 514 MPa for longitudinal reinforcement. The target concrete compressive strength (f_c') is equals to 30 MPa.

• Checking flexural capacity of the section

$$\rho = \frac{As}{bd} = \frac{4 * 26.4}{150 * 176} = 0.004$$

$$\beta 1 = 0.85$$

$$\rho_{max} = 0.85\beta 1 \frac{f_c'}{f_y} \frac{\varepsilon u}{\varepsilon u + 0.004} = 0.85^2 \frac{30}{514} \frac{0.003}{0.003 + 0.004} = 0.0181$$

$$\therefore \ \rho < \rho_{max} \qquad single\ reinforced\ section\ analysis$$

$$\rho_t = 0.85\beta 1 \frac{f_c'}{f_y} \frac{\varepsilon u}{\varepsilon u + 0.005} = 0.85^2 \frac{30}{514} \frac{0.003}{0.003 + 0.005} = 0.0158$$

$$\therefore \ \rho < \rho_t \qquad tension\ controlled\ beam$$

$$a = \frac{As f_y}{0.85\, f_c'\, b} = \frac{4 * 26.4 * 514}{0.85 * 30 * 150} = 14.19\ mm$$

$$Mn = As\ f_y \left(d - \frac{a}{2}\right) = 4 * 26.4 * 514 * 10^{-6} \left(176 - \frac{14.19}{2}\right)$$

$$= 9.14 kN.mm$$

$$Mext = Mn$$

$$\frac{PL}{6} = 9.1$$

$$P = \frac{9.1 * 6}{1.2} = 45.5\ kN$$

• Checking shear capacity of the section

$$V_c = 0.17\sqrt{f_c'}bd = 0.17 * \sqrt{30} * 10^{-3} * 150 * 176 = 24.58\ kN$$

$$V_s = \frac{A_v f_y d}{s} = \frac{(2 * 26.4) * 514 * 10^{-3} * 176}{100} = 47.76\ kN$$

$$V_n = V_c + V_s = 24.58 + 47.76 = 72.34\ kN$$

$$Vext = V_n$$

$$0.5\ P = 72.34$$

$$P = 144.68\ kN$$

∴ Shear failure load > Flexural failure load

∴ Flexural tension failure controls

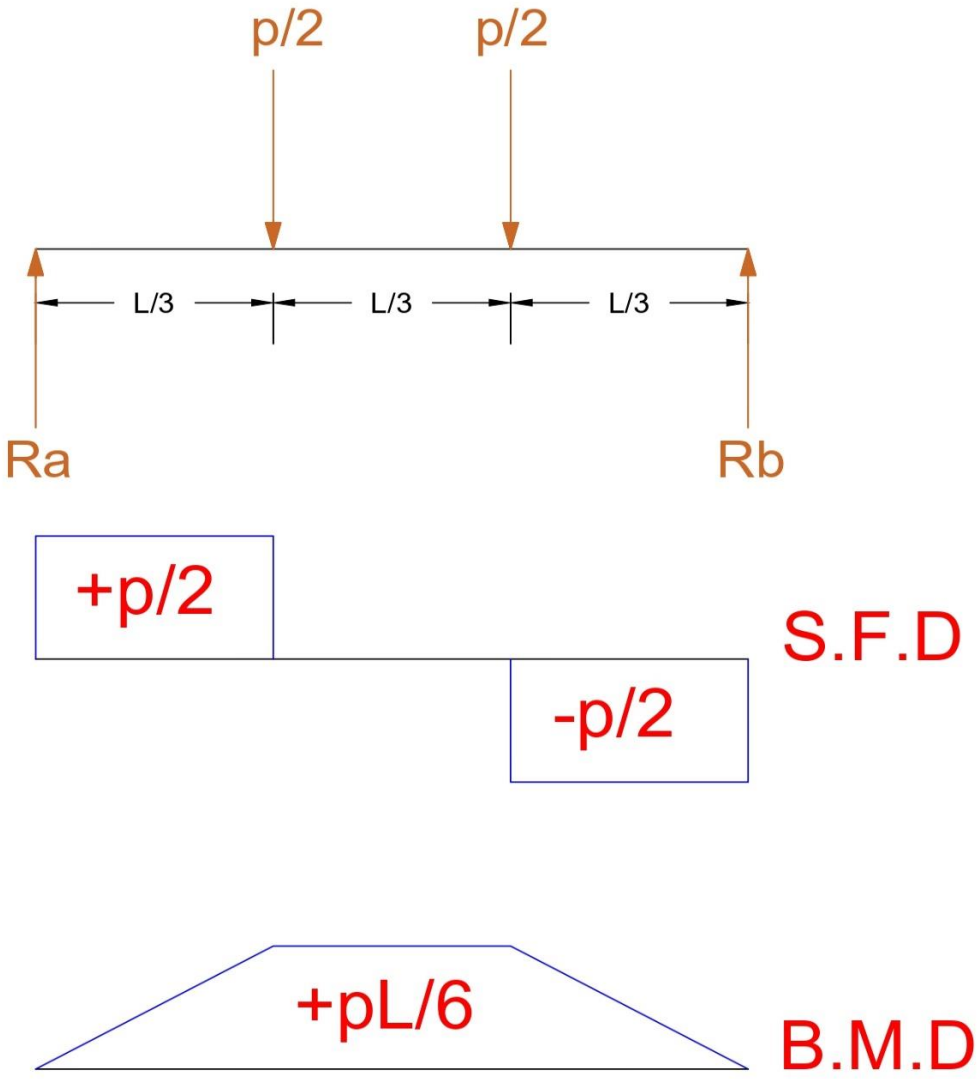

Figure A-1: Shear and bending moment diagrams for beams of both groups.

A.2 Flexural-critical beam BG4

The beam consists of four bars of Ø6 mm as flexural reinforcement at depth (d = 176 mm) and 2Ø6 mm as top reinforcement at depth (d'= 24 mm). The width of the cross section (b = 150 mm) and the height (h = 200 mm). The shear span was reinforced with Ø6mm@100mm. The tensile strength for GFRP rebars (f_{fu}) is equals to 896 MPa for longitudinal reinforcement and the yield strength for steel rebars (f_y) is equals to 514 MPa for shear reinforcement. The target concrete compressive strength (f_c') is equals to 30 MPa.

• Checking flexural capacity of the section

$$\rho_f = \frac{A_f}{bd} = \frac{4 * 31.67}{150 * 176} = 0.0048$$

$$\rho_{fb} = 0.85\beta_1 \frac{f_c'}{f_{fu}} \frac{E_f \varepsilon_{cu}}{E_f \varepsilon_{cu} + f_{fu}} = 0.85^2 \frac{30}{896} \frac{46000 * 0.003}{46000 * 0.003 + 896} = 0.0032$$

$$\therefore \rho_f > 1.4\rho_{fb}$$

$$f_f = \left(\sqrt{\frac{\left(E_f \varepsilon_{cu}\right)^2}{4} + \frac{0.85\beta_1 f_c'}{\rho_f} E_f \varepsilon_{cu}} - 0.5 E_f \varepsilon_{cu} \right) \leq f_{fu}$$

$$E_f \varepsilon_{cu} = 46000 * 0.003 = 138\ MPa$$

$$f_f = \left(\sqrt{\frac{(138)^2}{4} + \frac{0.85 * 0.85 * 30}{0.0048} * 138} - 0.5 * 138 \right) = 723.41\ MPa$$

$$a = \frac{A_f f_f}{0.85 f_c' b} = \frac{(4 * 31.67) * 723.41}{0.85 * 30 * 150} = 23.96\ mm$$

$$M_n = A_f f_f \left(d - \frac{a}{2}\right) = (4 * 31.67) * 723.41 * 10^{-6} * \left(176 - \frac{23.96}{2}\right)$$

$$= 15.03\ kN.mm$$

$$Mext = Mn$$

$$\frac{PL}{6} = 15.03$$

$$P = \frac{15.03 * 6}{1.2} = 75.15\ kN$$

• Checking shear capacity of the section

$$V_c = 0.17\sqrt{f_c'}bd = 0.17 * \sqrt{30} * 10^{-3} * 150 * 176 = 24.58\ kN$$

$$V_s = \frac{A_v f_y d}{s} = \frac{(2 * 26.4) * 514 * 10^{-3} * 176}{100} = 47.76\ kN$$

$$V_n = V_c + V_s = 24.58 + 47.76 = 72.34\ kN$$

$$Vext = V_n$$

$$0.5\ P = 72.34$$

$$P = 144.68\ kN$$

∴ Shear failure load > Flexural failure load

∴ Flexural tension failure controls

A.3 Flexural-critical beam BG2

The beam consists of two bars of Ø6 mm as flexural reinforcement at depth (d = 176 mm) and 2Ø6 mm as top reinforcement at depth (d'= 24 mm). The width of the cross section (b = 150 mm) and the height (h = 200 mm). The shear span was reinforced with Ø6mm@100mm. The tensile strength for GFRP rebars (f_{fu}) is equals to 896 MPa for longitudinal reinforcement and the yield strength for steel rebars (f_y) is equals to 514 MPa for shear reinforcement. The target concrete compressive strength (f_c') is equals to 30 MPa.

- **Checking flexural capacity of the section**

$$\rho_f = \frac{A_f}{bd} = \frac{2 * 31.67}{150 * 176} = 0.0024$$

$$\rho_{fb} = 0.85\beta_1 \frac{f_c'}{f_{fu}} \frac{E_f \varepsilon_{cu}}{E_f \varepsilon_{cu} + f_{fu}} = 0.85^2 \frac{30}{896} \frac{46000 * 0.003}{46000 * 0.003 + 896} = 0.0032$$

$$\therefore \rho_f < \rho_{fb}$$

$$\varepsilon_{fu} = \frac{f_{fu}}{E_f} = \frac{896}{46000} = 0.0195$$

$$c_b = \left(\frac{\varepsilon_{cu}}{\varepsilon_{cu} + \varepsilon_{fu}}\right) d = \left(\frac{0.003}{0.003 + 0.0195}\right) * 176 = 23.47\ mm$$

$$M_n = A_f f_{fu} \left(d - \frac{\beta_1 c_b}{2}\right) = (2 * 31.67) * 896 * 10^{-6} \left(176 - \frac{0.85 * 23.47}{2}\right)$$

$$= 9.42\ kN.mm$$

$$Mext = Mn$$

$$\frac{PL}{6} = 9.42$$

$$P = \frac{9.42 * 6}{1.2} = 47.1\ kN$$

- **Checking shear capacity of the section**

$V_c = 0.17\sqrt{f_c'}bd = 0.17 * \sqrt{30} * 10^{-3} * 150 * 176 = 24.58\ kN$

$V_s = \frac{A_v f_y d}{s} = \frac{(2 * 26.4) * 514 * 10^{-3} * 176}{100} = 47.76\ kN$

$V_n = V_c + V_s = 24.58 + 47.76 = 72.34\ kN$

$Vext = V_n$

$0.5\ P = 72.34$

$P = 144.68\ kN$

∴ Shear failure load > Flexural failure load

∴ Flexural tension failure controls

A.4 Design of Slab SS7: -

By using ACI 318M-19:

Material and section properties:

$As = 7Ø6 = 7 * 26.4 = 184.8\, mm^2$

$f_c' = 30\, MPa$, $t = 70$ mm

$f_y = 514\, MPa$, $d = 70 - 15 - 6 = 49\, mm$

$b = 1000\, mm$, $B = 100\, mm$

- **Check Flexural: -**

$$\rho = \frac{As}{bd} = \frac{7 * 26.4}{1000 * 49} = 3.77 * 10^{-3}$$

$$Mn = \rho b d^2 f_y \left(1 - 0.59\rho \frac{f_y}{f_c'}\right)$$

$$= 3.77 * 10^{-3} * 1000 * 49^2 * 514 * 10^{-6} \left(1 - 0.59 * 3.77 * 10^{-3} \frac{514}{30}\right)$$

$$= 4.48\, kN.mm$$

$$P = 8Mn$$

$$P = 8 * 4.48 = 35.84\, kN$$

- **Check punching shear: -**

$$b_\circ = (B + d) * 4 = (100 + 49) * 4 = 596\, mm$$

$$V_c = \frac{\sqrt{f_c'}}{3} b_\circ\, d = \frac{\sqrt{30}}{3} * 10^{-3} * 596 * 49 = 53.32\, kN$$

∴ Punching Shear failure load > Flexural failure load

∴ Flexural tension failure controls

A.5 Design of Slab SS14: -

By using ACI 318M-19:

Material and section properties:

$As = 14Ø6 = 14 * 26.4 = 369.6\ mm^2$

$f_c' = 30\ MPa$, $t = 70$ mm

$f_y = 514\ MPa$, $d = 70 - 15 - 6 = 49\ mm$

$b = 1000\ mm$, $B = 100\ mm$

- **Check Flexural Capacity of The Section: -**

$$\rho = \frac{As}{bd} = \frac{369.6}{1000 * 49} = 7.54 * 10^{-3}$$

$$Mn = \rho b d^2 f_y \left(1 - 0.59\rho \frac{f_y}{f_c'}\right)$$

$$= 7.54 * 10^{-3} * 1000 * 49^2 * 514 * 10^{-6} \left(1 - 0.59 * 7.54 * 10^{-3} \frac{514}{30}\right)$$

$$= 8.6\ kN.mm$$

$P = 8Mn$

$P = 8 * 8.6 = 68.8\ kN$

- **Check punching shear: -**

$b_\circ = (B + d) * 4 = (100 + 49) * 4 = 596\ mm$

$$V_c = \frac{\sqrt{f_c'}}{3} b_\circ\, d = \frac{\sqrt{30}}{3} * 10^{-3} * 596 * 49 = 53.32\ kN$$

∴ Punching Shear failure load < Flexural failure load

∴ Punching Shear failure controls

A.6 Design of Slab SG7: -

By using ACI 440-15:

Material and section properties:

$As = 7Ø6 = 7 * 31.67 = 221.7mm^2$

$f_c' = 30\ MPa$, $t = 70$ mm

$f_y = 514\ MPa$, $d = 70 - 15 - 6 = 49\ mm$

$b = 1000\ mm$, $B = 100\ mm$

- **Checking Flexural Capacity of The Section**

$$\rho_f = \frac{A_f}{bd} = \frac{221.7}{1000 * 49} = 0.00452$$

$$\rho_{fb} = 0.85\beta_1 \frac{f_c'}{f_{fu}} \frac{E_f \varepsilon_{cu}}{E_f \varepsilon_{cu} + f_{fu}} = 0.85^2 \frac{30}{896} \frac{46000 * 0.003}{46000 * 0.003 + 896}$$

$$= 0.0032$$

$$\therefore \rho_f > 1.4\rho_{fb}$$

$$f_f = \left(\sqrt{\frac{\left(E_f \varepsilon_{cu}\right)^2}{4} + \frac{0.85\beta_1 f_c'}{\rho_f} E_f \varepsilon_{cu}} - 0.5 E_f \varepsilon_{cu} \right) \leq f_{fu}$$

$$E_f \varepsilon_{cu} = 46000 * 0.003 = 138\ MPa$$

$$f_f = \left(\sqrt{\frac{(138)^2}{4} + \frac{0.85 * 0.85 * 30}{0.00452} * 138} - 0.5 * 138 \right) = 747.41\ MPa$$

$$a = \frac{A_f f_f}{0.85 f_c' b} = \frac{221.7 * 747.41}{0.85 * 30 * 1000} = 6.5\ mm$$

$$M_n = A_f f_f \left(d - \frac{a}{2}\right) = 221.7 * 747.41 * 10^{-6} * \left(49 - \frac{6.5}{2}\right)$$

$$= 7.58\ kN.mm$$

$$Mext = Mn$$

$$\frac{P}{8} = 7.58$$

$$P = 8 * 7.58 = 60.64\ kN$$

- **Check punching shear: -**

$$n = \frac{E_f}{E_C} = \frac{46000}{4700\sqrt{30}} = 1.79$$

$$n\rho_f = 1.79 * 0.00452 = 8.1 * 10^{-3}$$

$$k = \sqrt{(n\rho_f)^2 + 2n\rho_f} - n\rho_f$$

$$= \sqrt{(8.1 * 10^{-3})^2 + 2(8.1 * 10^{-3})} - 8.1 * 10^{-3} = 0.119$$

$$b_\circ = (B + d) * 4 = (100 + 49) * 4 = 596\ mm$$

$$V_c = \frac{4\ k}{5}\sqrt{f_c'}b_\circ\ d = \frac{4 * 0.119}{5}\sqrt{30} * 10^{-3} * 596 * 49 = 15.23\ kN$$

∴ Punching Shear failure load < Flexural failure load

∴ Punching Shear failure controls

A.7 Design of Slab SG14: -

By using ACI 440-15:

Material and section properties:

$As = 14Ø6 = 14 * 31.67 = 443.38\, mm^2$

$f_c' = 30\, MPa$, $t = 70$ mm

$f_y = 514\, MPa$, $d = 70 - 15 - 6 = 49\, mm$

$b = 1000\, mm$, $B = 100\, mm$

- **Checking Flexural Capacity of The Section**

$$\rho_f = \frac{A_f}{bd} = \frac{443.38}{1000 * 49} = 0.009$$

$$\rho_{fb} = 0.85\beta_1 \frac{f_c'}{f_{fu}} \frac{E_f \varepsilon_{cu}}{E_f \varepsilon_{cu} + f_{fu}} = 0.85^2 \frac{30}{896} \frac{46000 * 0.003}{46000 * 0.003 + 896} = 0.0032$$

$\therefore \rho_f > 1.4\rho_{fb}$

$$f_f = \left(\sqrt{\frac{\left(E_f \varepsilon_{cu}\right)^2}{4} + \frac{0.85\beta_1 f_c'}{\rho_f} E_f \varepsilon_{cu}} - 0.5 E_f \varepsilon_{cu} \right) \leq f_{fu}$$

$E_f \varepsilon_{cu} = 46000 * 0.003 = 138\, MPa$

$$f_f = \left(\sqrt{\frac{(138)^2}{4} + \frac{0.85 * 0.85 * 30}{0.009} * 138} - 0.5 * 138 \right) = 511.6\, MPa$$

$$a = \frac{A_f f_f}{0.85 f_c' b} = \frac{443.38 * 511.6}{0.85 * 30 * 1000} = 8.9\, mm$$

$$M_n = A_f f_f \left(d - \frac{a}{2}\right) = 443.38 * 511.6 * 10^{-6} * \left(49 - \frac{8.9}{2}\right) = 10.1\, kN.mm$$

$Mext = Mn$

$\frac{P}{8} = 10.1$ $P = 8 * 10.1 = 80.8\, kN$

- **Check punching shear: -**

$$n = \frac{E_f}{E_C} = \frac{46000}{4700\sqrt{30}} = 1.79$$

$$n\rho_f = 1.79 * 0.009 = 0.0161$$

$$k = \sqrt{(n\rho_f)^2 + 2n\rho_f} - n\rho_f = \sqrt{(0.0161)^2 + 2(0.0161)} - 0.0161 = 0.164$$

$$b_\circ = (B + d) * 4 = (100 + 49) * 4 = 596\ mm$$

$$V_c = \frac{4\ k}{5}\sqrt{f_c'}b_\circ\ d = \frac{4 * 0.164}{5}\sqrt{30} * 10^{-3} * 596 * 49 = 20.99\ kN$$

$\therefore$ Punching Shear failure load < Flexural failure load

$\therefore$ Punching Shear failure controls

Appendix B

Appendix B

Datasheets of Material

B.1 Data sheet of Glass Fiber Reinforced Polymer (GFRP)provided by the manufacturer

高耐久性玻璃纤维筋（High Durability of GFRP Bar）

使用高耐久性树脂为主要基体材料，具有优异的耐腐蚀特性，是解决钢筋锈蚀的最佳方案之一，可应用于化工厂、盐雾环境、桥面铺装等工程中。筋材耐腐蚀性达到加拿大ISIS认证说明书所定义的最高等级D1级耐久性要求。

We chose the high durability resin and have researched the high durability GFRP bar. It has the property of excellent corrosion resistance and passed the highest level (D1) of the ISIS certified.

产品型号 Type No.	大小 Size	公称直径 Nominal Diameter (mm)	公称横截面积 Nominal Area (mm^2)	极限抗拉力 Utimate Tensile Load (KN)	保证抗拉强度 Guaranteed Tensile Strength (MPa)	弹性模量 Modulus of Elasticity (GPa)	单位重量 Weight (g/m)	剪切强度 Transverse Shear Strength (MPa)
B100-6	2	6	31.67	28	896	46	77.4	
B100-10	3	10	71.26	59	827	46	159	
B100-13	4	13	126.7	96	758	46	281.3	
B100-16	5	16	197.9	143	724	46	427.1	
B100-19	6	19	285	197	690	46	607.2	
B100-22	7	22	387.9	254	655	46	809.6	150
B100-25	8	25	506.7	314	620	46	1046.2	
B100-29	9	29	641.3	376	588	46	1413.7	
B100-32	10	32	791.7	437	551	46	1711.4	
B100-35	11	35	958.1	462	482	46	1934.6	
B100-38	12	38	1160	520	448	46	2455.4	
B100-41	13	41	1338	554	413	46	2872.1	

B.2 Data sheet of epoxy provided by the manufacturer

BUILDING TRUST

PRODUCT DATA SHEET

Sikadur®-330

HIGH-MODULUS, HIGH-STRENGTH, IMPREGNATING RESIN

PRODUCT DESCRIPTION

Sikadur®-330 is a two-component , solvent-free, moisture-tolerant, high strength, high modulus structural epoxy adhesive.

USES

Sikadur®-330 may only be used by experienced professionals.
For use as an impregnating resin with the SikaWrap® Hex 106G, 113C, 117C, 230C and 430G Structural Strengthening Systems.

CHARACTERISTICS / ADVANTAGES

- Long pot life.
- Long open time.
- Easy to mix.
- Tolerant of moisture before, during and after cure.
- High strength, high modulus adhesive.
- Excellent adhesion to concrete, masonry, metals, wood and most structural materials.
- Fully compatible and developed specifically for the SikaWrap® Systems.
- High temperature resistance.
- High abrasion and shock resistance.
- Solvent-free, VOC compliant.

PRODUCT INFORMATION

Packaging	3.2 gal. (12 L) kit / (2) two 1.25 gal. (4.7 L) Component A pails, (2) two 0.35 gal. (1.3 L) Component B pails
Color	Light gray
Shelf Life	2 years in original, unopened container
Storage Conditions	Store dry at 40–95 °F (4–35 °C). Condition material to 65–75 °F (18–24 °C) before using.
Consistency	Non-sag paste

TECHNICAL INFORMATION

Compressive Strength		**60 °F (16 °C)**	**73 °F (23 °C)**	**90 °F (32 °C)**	(ASTM D-695) 50 % R.H.
	8 hour	-	-	8,000 psi (55.2 MPa)	
	1 day	8,100 psi (55.8 MPa)	10,700 psi (73.7 MPa)	10,600 psi (73.1 MPa)	
	3 day	11,200 psi (77.2 MPa)	11,100 psi (76.5 MPa)	11,000 psi (75.8 MPa)	
	7 day	11,600 psi (80.0 MPa)	11,200 psi (77.2 MPa)	11,800 psi (81.3 MPa)	
	14 day	12,400 psi (85.5 MPa)	11,800 psi (81.3 MPa)	11,900 psi (82.0 MPa)	
Flexural Strength	8,800 psi (60.6 MPa) (7 days)				(ASTM D-790) 73 °F (23 °C) 50 % R.H.
Modulus of Elasticity in Flexure	5.06 x 105 psi (3,489 MPa) (7 days)				(ASTM D-790) 73 °F (23 °C) 50 % R.H.
Tensile Strength	4,900 psi (33.8 MPa) (7 days)				(ASTM D-638) 73 °F (23 °C) 50 % R.H.
Elongation at Break	1.2 % (7 days)				(ASTM D-638) 73 °F (23 °C) 50 % R.H.
Heat Deflection Temperature	120 °F (50 °C) (7 days)				(ASTM D-648) [fiber stress loading=264 psi (1.8 MPa)]

APPLICATION INFORMATION

Mixing Ratio	Component 'A' : Component 'B' = 4 : 1 by weight
Coverage	First coat: 40-50 ft^2/gal.; Additional coats: 100 ft^2/gal.; Final coat: 160 ft^2/gal.
Pot Life	57 minutes (325 ml)
Cure Time	**Tack Free Time:** 4–5 hours

APPLICATION INSTRUCTIONS

SUBSTRATE PREPARATION

The concrete surface should be prepared to a minimum concrete surface profile (CSP-3) as defined by the ICRI-surface-profile chips. Localized out-of-plane variations, including form lines, should not exceed 1/32 in. (1 mm). Substrate must be clean, sound, and free of surface moisture. Remove dust, laitance, grease, oils, curing compounds, waxes, impregnations, foreign particles, coatings and disintegrated materials by mechanical means (i.e. sandblasting). For best results, substrate should be dry. However, a saturated surface dry condition is acceptable.

MIXING

Pre-mix each component. Mix entire unit, do not batch. Pour contents of part B to part A. Mix thoroughly for 5 minutes with a 1/2 inch "Jiffy" mixer mounted on a rotary drill and set at a slow speed (400–600 rpm) until uniformly blended. Mix only that quantity that can be used within its pot life.

APPLICATION METHOD / TOOLS

Dry Lay-Up: When installing a SikaWrap® Hex fabric in the dry lay-up process apply the mixed Sikadur®-330 epoxy resin directly onto the substrate at a rate of 40–50 ft.2/gal. (0.95–1.18 m^2/L). Coverage rate will depend on the actual surface profile. This equates to a thickness of approximately 32–40 mils. Carefully place the fabric into

the applied resin with gloved hands and smooth out. Work out any irregularities or air pockets with a plastic laminating roller. Let the resin squeeze out between the rovings of the fabric. If more than one layer of fabric is required, apply additional Sikadur®-330 at a rate of 100 ft²/gal. (2.37 m2/L) and repeat as described above. This equates to a thickness of approximately 16 mils. Add a final layer of Sikadur®-330 onto the exposed surface at a rate of 160 ft²/gal. (3.79 m²/L). This equates to a thickness of approximately 10 mils.

Wet Lay-Up: When installing a SikaWrap® Hex fabric vertically or overhead in the wet lay-up process, mixed Sikadur®-330 can be applied to the substrate as a primer/tack coat to prevent the impregnated fabric from sliding down the concrete. Due to its mixed viscosity, do not use Sikadur®-330 with an automatic fabric saturating device. Consult the SikaWrap® Hex fabric technical data sheet for information on saturating/impregnating fabric in a wet lay-up installation.

CLEANING OF TOOLS

Clean all equipment immediately with Sika® Colma Cleaner. Cured material can only be removed mechanically.

LIMITATIONS

- Minimum age of concrete is 21–28 days, depending on curing and drying conditions.
- All repairs required to achieve a level surface must be performed prior to application.
- Do not apply or cure Sikadur®-330 in direct sunlight.
- Minimum substrate temperature 40 °F (4 °C). Maximum application temperature 95 °C (35 °C)
- Do not thin with solvents.
- Material is a vapor barrier after cure.
- Do not encapsulate saturated concrete in areas of freezing and thawing.
- Color of Sikadur®-330 may alter due to variations in lighting and/or UV exposure.
- Due to its mixed viscosity, do not use Sikadur®-330 with an automatic saturating device. Fabric must be saturated/impregnated manually when the wet lay-up process is used.
- At low temperatures and/or high relative humidity, a slight oily residue (blush) may form on the surface of the cured epoxy. If an additional layer of fabric, or a coating is to be applied onto the cured epoxy. This residue must first be removed to ensure adequate bond. The residue can be removed with either a solvent wipe (e.g. MEK) or with water and detergent. In both cases, the surface should be wiped dry prior to application of the next layer or coating.
- Not an aesthetic product. Color may alter due to variations in lighting and/or UV exposure.

BASIS OF PRODUCT DATA

Results may differ based upon statistical variations depending upon mixing methods and equipment, temperature, application methods, test methods, actual site conditions and curing conditions.

OTHER RESTRICTIONS

See Legal Disclaimer.

ENVIRONMENTAL, HEALTH AND SAFETY

For further information and advice regarding transportation, handling, storage and disposal of chemical products, user should refer to the actual Safety Data Sheets containing physical, environmental, toxicological and other safety related data. User must read the current actual Safety Data Sheets before using any products. In case of an emergency, call CHEMTREC at 1-800-424-9300, International 703-527-3887.

LEGAL DISCLAIMER

- **KEEP CONTAINER TIGHTLY CLOSED**
- **KEEP OUT OF REACH OF CHILDREN**
- **NOT FOR INTERNAL CONSUMPTION**
- **FOR INDUSTRIAL USE ONLY**
- **FOR PROFESSIONAL USE ONLY**

Prior to each use of any product of Sika Corporation, its subsidiaries or affiliates ("SIKA"), the user must always read and follow the warnings and instructions on the product's most current product label, Product Data Sheet and Safety Data Sheet which are available at usa.sika.com or by calling SIKA's Technical Service Department at 1-800-933-7452. Nothing contained in any SIKA literature or materials relieves the user of the obligation to read and follow the warnings and instructions for each SIKA product as set forth in the current product label, Product Data Sheet and Safety Data Sheet prior to use of the SIKA product.

SIKA warrants this product for one year from date of installation to be free from manufacturing defects and to meet the technical properties on the current Product Data Sheet if used as directed within the product's shelf life. User determines suitability of product for intended use and assumes all risks. User's and/or buyer's sole remedy shall be limited to the purchase price or replacement of this product exclusive of any labor costs. **NO OTHER WARRANTIES EXPRESS OR IMPLIED SHALL APPLY INCLUDING ANY WARRANTY OF MERCHANTABILITY OR FITNESS FOR A PARTICULAR PURPOSE. SIKA SHALL NOT BE LIABLE UNDER ANY LEGAL THEORY FOR SPECIAL OR CONSEQUENTIAL DAMAGES. SIKA SHALL NOT BE RESPONSIBLE FOR THE USE OF THIS PRODUCT IN A MANNER TO INFRINGE ON ANY PATENT OR ANY OTHER INTELLECTUAL PROPERTY RIGHTS HELD BY OTHERS.**

Sale of SIKA products are subject to the Terms and Conditions of Sale which are available at: https://usa.sika.com/en/group/SikaCorp/termsandconditions.html or by calling 1-800-933-7452.

Sika Corporation
201 Polito Avenue
Lyndhurst, NJ 07071
Phone: +1•800•933•7452
Fax: +1•201•933•6225
usa.sika.com

Sika Mexicana S.A. de C.V.
Carretera Libre Celaya Km. 8.5
Fracc. Industrial Balvanera
Corregidora, Queretaro
C.P. 76920
Phone: 52 442 2385800
Fax: 52 442 2250537

B.3 Stress Strain for Steel Bar

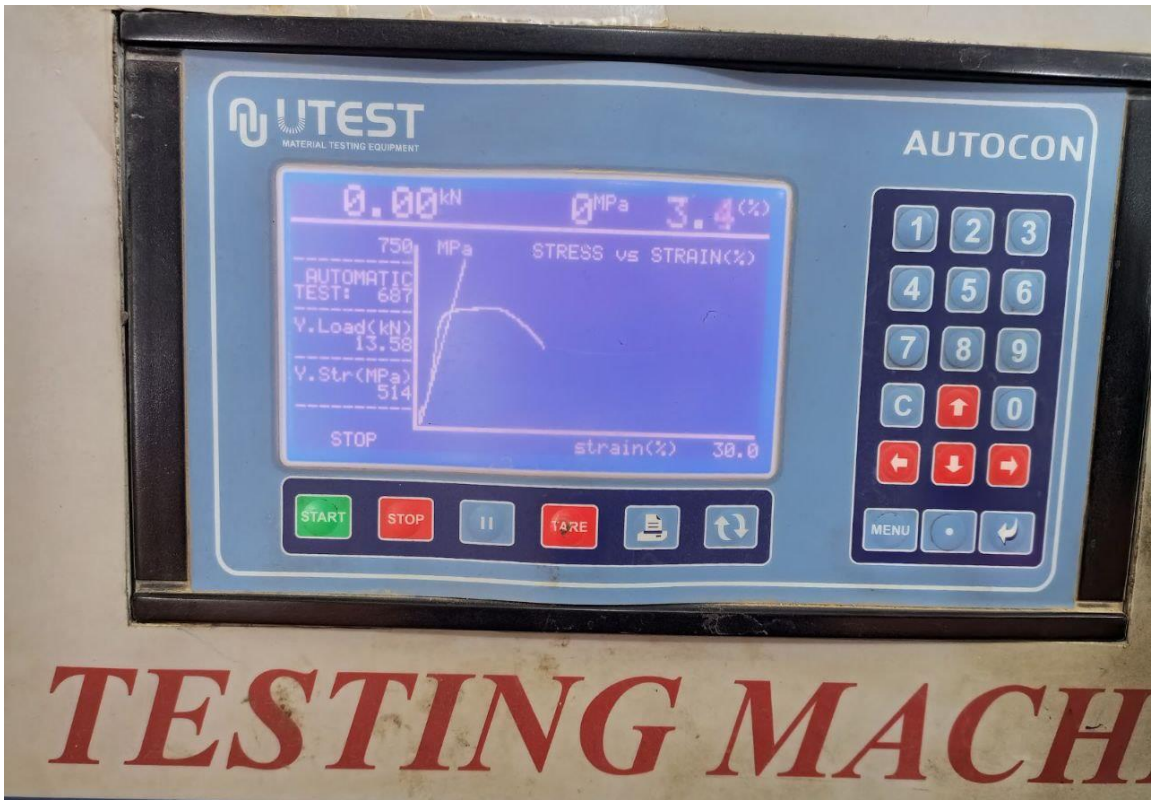

الخلاصة

تآكل حديد التسليح هو السبب الأكثر شيوعًا لتدهور هيكل الخرسانة المسلحة. كبديل لحديد التسليح الفولاذي، تم استخدام البوليمر المقوى بالألياف الزجاجية (GFRP). بدلاً من حديد التسليح الفولاذي. لديها قوة عالية وخفيفة الوزن ومقاومة للتآكل. مع أداء ميكانيكي جيد. اشتمل البرنامج التجريبي على العديد من الاختبارات التجريبية حيث تم تصنيف العينات الخرسانية إلى مجموعتين من أنواع مختلفة من العناصر للاعتاب وتم اختبار السقوف ذات الاتجاهين. أيضا ، الخواص الميكانيكية للتسليح البديل ، ثلاث اعتاب تحت نظام تحميل من أربع نقاط. تم أيضًا وضع أربع عينات من السقوف ثنائية الاتجاه واختبارها حتى فشلت تحت التحميل المتحد المركز. بالإضافة إلى ذلك ، تمت دراسة انسحاب هنا عن طريق اختبار ست عينات ، ثلاثة منها لقضبان حديد التسليح وثلاثة لقضبان GFRP. تم تقوية مجموعة الاعتاب بواسطة حديد التسليح وقضبان GFRP بشكل منفصل في هذه المجموعة تم دراسة سلوك التسليح البديل تحت تأثير سلوك القص والانحناء. جميع الاعتاب لها مقطع عرضي مستطيل 150 × 200 مم ، وكان المسافة بين المساند 1200 مم. لتجنب فشل القص ، تم استخدام ركائب فولاذية بكمية مناسبة Ø6 @ 100mm ، واستخدمت قضبان اسمية 6 مم كتعزيز علوي. كانت المعايير الرئيسية التي تم فحصها هي نوع وكمية التسليح. تظهر النتائج أن فشل الانثناء يحدث من تمزق الشد للقضبان في القسم الأوسط أو تحت نقطة التحميل. أشارت البيانات إلى أن الاعتاب الخرسانية المسلحة ذات قضبان GFRP تمتلك هطول أكثر من الاعتاب الخرسانية المسلحة بقضبان الحديد وأن عرض شقوق الاعتاب الخرسانية المسلحة بGFRP أكبر من عرض الشقوق للاعتاب الخرسانية المسلحة بالحديد. مجموعة السقوف تتضمن 4 سقوف الأول والثاني يتكون من 7Ø6 في اتجاهين من GFRP والحديد بنسبة تسليح 4.5٪ و 3.8٪ على التوالي من GFRP والحديد. يتكون السقوف الثالث والرابع من Ø6 14 من GFRP والحديد بنسبة تسليح 9٪ و 7.5٪ على التوالي GFRP والحديد. كانت المعايي الرئيسية التي تمت دراستها هي نوع التسليح ، وتأثير المباعدة بين تسليح الانحناء على السقوف المسطحة. كانت العينات مربعةالبعد الصافي 1000 مم وسمك 70 مم ، وتم استخدام اسناد بسيط لجميع العينات التي تعمل على الجوانب الأربعة. وفقًا لأنماط الفشل ، تفشل الألواح ذات نسبة التسليح العالية عن طريق قص التثقيب ، في حين تفشل السقوف ذات نسبة التسليح المنخفضة بسبب فشل الانحناء ، عند المقارنة بين السقوف المسلحة بالحديد وقضبان GFRP التي فشلت بسبب قص التثقيب وفشل الانحناء ، زادت مقاومة سقوف المسلحة بالحديد بنسبة 34٪ و 30٪ على التوالي.

مجموعة الربط تتضمن GFRP فقط ومكعبات فولاذية فقط. كانت المعايير الرئيسية التي تم فحصها في المكعبات المسحوبة هي شريط GFRP وقضيب فولاذي وطول التضمين (5 ، 7.5 ، و 10 أضعاف قطر القضيب). كانت الأبعاد الهندسية لمكعب السحب 200 × 200 × 200 ملم. تم استخدام التفاف حلزوني لاختبار نسيج السطح لقضبان GFRP للانسحاب. كان الشريط متمركزًا في المكعب الخرساني. العينات التي احتوت على قضبان GFRP فشلت بسبب سحب القضيب من المكعب الخرساني بسبب الانزلاق بين شريط GFRP والخرسانة. هذا نتيجة ضعف الترابط بين شريط GFRP والخرسانة. العينات المحتوية على قضبان حديدية فشلت بسبب قطع القضبان ، في أماكن مختلفة. نقطة القطع هي النقطة التي يلتقي فيها حديد التسليح والخرسانة ، أو نهاية المكعب الخرساني ، أو نقطة التقاء ذراع الإمساك بالقضيب. هذا نتيجة الربط الجيد للقضبان الفولاذية والخرسانة.

جمهورية العراق
وزارة التعليم العالي والبحث العلمي
جامعة بابل
كلية الهندسة
قسم الهندسة المدنية

دراسة مقارنة للأداء الإنشائي بين قضبان الحديد و قضبان البوليمر المقوى بالألياف الزجاجية في عناصر الخرسانة المسلحة

رسالة

مقدمة الى كلية الهندسة - جامعة بابل

كجزء من متطلبات نيل درجة الماجستير في الهندسة / الهندسة المدنية / انشاءات

من قبل

زهراء لؤي عزيز شُبّر

اشراف

الاستاذ الدكتور هيثم حسن متعب الدعمي

2023م **1444هـ**